Fakultät für Maschinenwesen

Studies on safety and performance of metallic fuel bearing minor actinides in a nuclear fast reactor

Luca Capriotti

Vollständiger Abdruck der von der
Fakultät für Maschinenwesen
der Technischen Universität München zur Erlangung des akademischen Grades
eines Doktor – Ingenieurs (Dr.-Ing.)
genehmigten Dissertation.

Vorsitzende/-r: Prof. Dr. Rudolf Neu

Prüfende/-r der Dissertation:

1. Prof. Rafael Macian Juan, Ph.D.
2. Prof. Dr. Thomas Fanghänel

Die Dissertation wurde am 16.04.2020 bei der Technischen Universität München
eingereicht und durch die
Fakultät für Maschinenwesen am 21.10.2020 angenommen.

Acknowledgements

The opportunity to have been involved in an international project collaborating with people coming from all over the world has been an incredible and exceptional journey. I am grateful to the European Commission and Technical University of Munich to have made this possible.

I would like to thank the former and present director of the ex Institute for Transuranium Elements (ITU), now part of the Directorate for Nuclear Safety and Security, Joint Research Center, Prof. Dr. Thomas Fanghänel and Dr. Maria Betti for giving me the possibility to perform this research project in the institute. I would like to acknowledge Prof. Dr. Rafael Macián-Juan for accepting me as Ph.D. candidate at the Technische Universität München and for all the academic advices.

I would like to express deep gratitude to Dr. Vincenzo Rondinella, Head of the Safety of Irradiated Materials Unit (now Head of Department of Nuclear Decommissioning) for introducing me to the fascinating world of nuclear fuel performance and post irradiation examination. He gave me unlimited supervision and mentorship during these years and extremely strong support also in the most difficult time along the way.

I warm thank Dr. Stephane Bremier for all his scientific support on this PhD project, for all I learnt on microanalysis and his infinite patience and guidance in the correction of this manuscript.

I would like to acknowledge the contribution of Dr. Dimitrios Papaiannou and the support in the daily hot cells work and of my japanese colleagues (Dr. Ogata-san, Dr. Inagaki-san and Dr. Ohta-san) for sharing their knowledge and experience on metallic fuel.

I would also like to thank all the ITU staff, in particular:

- Dr. R. Caciuffo, Dr. R. Eloirdi, Dr. P. Poml, Mr. Pagliosa, Mr. Bouexiere, Dr. Raison and the microscopy group (Dr. Wiss, Mr. Cremer, Mr. Ernstberger) for their scientific support and help with the metallic fuel archive materials analysis.
- Gianni, Gegé, Ramil, Ralf, Jerome and Rachid, for being always available in the hot cells. I acknowledge the alpha-gamma group.

I would thank all the awesome people, who have lived and worked beside me during my time as PhD student: the "Italian Group", Dario, Elisa, Fidelma, Fabiola, Sara, Elena, Lorenzo, Simona, Valentina, Francesco and Zap; Johnny (and the Stovchen) and Sandrine, Sylvain, Emily, Brandon, Laura, Vaclav, Tsveti, Oliver, Roland, Kevin for all the nice moment together.

Immense and forever gratitude goes to my parents, if I arrived where I am now is thanks to their teaching and their values which they transmitted me, but mostly for their unconditional love.

Finally I left for last the recognition of the incredible person with whom I lived every single moment of this work and this journey. Fidelma has been always my safe harbour, ready to listen all my concerns but also support and encourage me in everything. I feel blessed to have you always with me.

Thank you all !

Contents

Acronyms

AE	Absorbed Electron
AFC	Advance Fuel Campaign
ANL	Argonne National Laboratory
ATR	Advanced Testing Reactor
BOI	Beginning of Irradiation
BSE	Back – Scattered Electron
CEA	Commissariat à l´Énergie Atomique et aux Energies Alternatives
CRIEPI	Central Research Institute of Electric Power Industry
DFR	Dounreay Fast Reactor
EBR-I/-II	Experimental (Fast) Breeder Reactor
EC	European Commission
EDX	Energy Dispersive X-ray Spectroscopy
EOI	End of Irradiation
EPMA	Electron Probe Micro Analysis
FCC	Face Center Cubic
FCCI	Fuel Cladding Chemical Interaction
FCMI	Fuel Cladding Mechanical Interaction
FFTF	Fast Flux Test Facility
FUTURIX-FTA	FUels for Transmutation of transuranium elements in Phenix / Fortes Teneurs en Actinides
GDMS	Glow Discharge Mass Spectrometer
GIF	Generation IV International Forum
IAEA	International Atomic Energy Agency
IFR	Integral Fast Reactor
INL	Idaho National Laboratory
ITU	Institute for Transuranium Elements
JRC	Joint Research Center
KAERI	Korea Atomic Energy Research Institute
LWR	Light Water Reactor
MA	Minor Actinides
MOX	Mixed Uranium – Plutonium OXides

NEA	Nuclear Energy Agency
OECD	Organisation for Economic Co-operation and Development
OM	Optical Microscopy
PIE	Post Irradiation Examination
P&T	Partitioning and Transmutation
R&D	Research and Development
RE	Rare Earths
SE	Secondary Electron
SEM	Scanning Electron Microscopy
SFR	Sodium Fast Reactor
TRU/s	Transuranic Elements
USA	United States of America
WDS	Wavelength Dispersive Spectroscopy
XRD	X – Ray Diffraction

List of Figures

List of Tables

Abstract

Closed nuclear fuel cycles, based on separation from spent fuel and subsequent recycling of Pu, U as fuel, and transmutation of Minor Actinides (MA) Np, Am, Cm, are developed as an option to ensure sustainable low-carbon energy supplies while minimizing the long-term radiotoxicity of the resulting high level waste. Metal fuel for fast reactor is a good candidate to achieve this goal for several reasons, e.g. higher densities of fissile and fertile materials than any other fuel forms and higher breeding ratio. Concerning the transmutation of MA, metal-fuelled fast reactors provide higher transmutation rate due to harder neutron spectrum. Because of the favourable features mentioned above, the development of MA-bearing metal fuel has been pioneered in the United States and considered in Europe. More recently, Japan and the Republic of Korea have implemented programs to investigate this option.

The METAPHIX project is a collaboration between the Central Research Institute of Electric Power Industry (Japan) and the European Commission, Joint Research Centre Karlsruhe (Germany) with the support of the Commissariat a l'Energie Atomique et aux Energies Alternatives (CEA, France); it investigates safety and performance of a closed fuel cycle option based on fast reactor metal alloy fuels containing MA. The aim of the project is to study the behaviour of this type of fuel and demonstrate the transmutation of MA under irradiation.

Nine Na-bonded fuel pins loaded with four U-19Pu-10Zr-based alloy compounds were prepared at JRC-Karlsruhe. Two compounds contained MA (Np, Am, Cm) in addition to rare earths (RE: Y, Ce, Nd, Gd) , reproducing the output of pyrometallurgical reprocessing of LWR spent fuel. The fuel was irradiated in the PHENIX reactor in France until May 2008, achieving burnup levels of ~2.5 at.%, ~7.0 at.% and ~10.0 at.%.

The present research work is dedicated to understanding the behaviour in pile of this complex fuel system taking advantage of advanced characterization techniques, in particular optical microscopy, scanning electron microscopy (SEM), electron

probe micro analysis (EPMA). Additionally, a series of measurements on un-irradiated archive fuel samples was performed in order to complement the Post-Irradiation Examination (PIE) work and the old as-synthesized data. Very few studies have been performed on such alloys and this project is unique due to the addition of Cm and the variety of alloys irradiated (2MA-2RE, 5MA-5RE, 5MA, basic alloy).

The characterization of as-prepared metallic alloy U-19Pu-10Zr-2MA-2RE was performed using EPMA and XRD. The fuel matrix is composed mainly of U-Pu-Zr-Np and reveals two different phases where the concentration of U and Zr vary inversely. The crystalline structure was identified by XRD as a mix of U-Pu ζ and δ – UZr2 phases. Am is found alloyed in the matrix in small concentrations whereas the majority is found in secondary phases that are present throughout the fuel radius and contain RE as well. These features associated with the presence of MA do not change dramatically the microstructure and crystalline structure in comparison with the basic alloy, thus inferring similar fuel properties.

The behaviour under irradiation of metallic fuel with MA and/or RE is analyzed and compared with the basic U-19Pu-10Zr alloy. The redistribution of the main fuel elements is a phenomenon mainly driven by temperature and chemical gradient of the different species, and is affected only to a limited extent by the addition of MA and RE; on one hand, Am and Cm and RE are not included in the matrix and precipitate as segregated phases; on the other hand Np behaves like U and Pu. There are no relevant differences in microstructure comparing Np-bearing U-Pu-Zr and the basic ternary alloy of METAPHIX. During irradiation Am, Cm and RE precipitates combine with noble metals and fission products as well. Compared with the basic alloy, two different (RE, Am)-rich phases are present, one associated with noble metals (Pd and Rh) and one without. The precipitates that includes both noble metals and rare earth elements have phase compositions corresponding to RE7(Pd,Rh)3, similarly to what observed in the basic alloy fuel and in literature. It is worth mentioning that Pd and Am have a peculiar behaviour at the radial

periphery of the fuel ingot in contrast with the redistribution of other major RE like Nd and Ce.

Concerning fuel cladding chemical interaction (FCCI), PIE revealed a different phase configuration on the inner cladding side at both 2.5 at.% burnup and at 6.9 at.% burnup. This configuration, characterized by intergranular "attack", is only detected in the presence of MA, independently from the presence of RE. Quantitative analysis identified that this penetration is mainly due to Sm and Am. Nd and Ce are also present in small amounts in the intergranular attack phase. This behaviour is reported in this work for the first time.

Keywords: Metallic Nuclear Fuel, Minor Actinides, Rare Earth, Transmutation, Post Irradiation Examination, Nuclear Fuel Performance

Chapter 1

Introduction

In the era of concern about climate change, nuclear energy can play an important role due to its low CO_2 emissions, high power density and reliability.
Nowadays, nuclear reactors around the world produce circa 11% of the global electricity, with USA, France and China generating the largest output.
The current nuclear reactors fleet designed and operated successfully for the last 60 years face some challenges such as lack of public acceptance (also connected to the legacy of Fukushima and Chernobyl accidents), adaptation to long term operation, and implementation of waste management solutions.
In order to overcome these challenges and meet future energy needs, it is essential that nuclear power generation pursues maintaining or improving the goals of sustainability, safety and reliability, economic competitiveness and proliferation resistance [1].

GIF, created in 2000 by 9 countries and today counting 13 members [1], considers those goals and international collaboration essential to advance nuclear energy into its next generation of systems deployable after 2030. In 2002 GIF selected six systems, from nearly 100 concepts, as Generation IV systems (a detailed description of the selected systems is available in reference [1]):

- Gas-cooled fast reactor (GFR)
- Lead-cooled fast reactor (LFR)
- Molten salt reactor (MSR)
- Sodium-cooled fast reactor (SFR)
- Supercritical-water cooled reactor (SCWR)
- Vey-high-temperature reactor (VHTR)

Closing the nuclear fuel cycle is an important component for achieving the sustainability goal. A closed fuel cycle is based on the reprocessing and partitioning of spent nuclear fuel and on the management of each separated fraction with the most optimized strategy [2-4].

Spent nuclear fuel from existing commercial nuclear reactors is a major concern for the public due to long term radiotoxicity (mainly from some fission products and actinides), heat load issues (mainly from fission products for "young" spent fuel) and proliferation risk (mainly from fissile Pu isotopes). Fig. 1.1 shows the decay heat of spent fuel irradiated at 50 GWd/t. It is evident that the fission products govern the heat load generated in the existing spent fuel whereas actinides will contribute for the majority of the heat generated on the long term, in particular after emplacement in a geologic repository. Reducing this heat source production, for example of a factor 3 can reduce the needed repository gallery length by a factor of 3 and its footprint by a factor of 9 [2].

P&T of some or all relevant elements of the spent nuclear fuel, is a technically viable strategy to reduce the long-term radiotoxicity and close the nuclear fuel cycle. Many recent studies have demonstrated that the impact of P&T on geological disposal concepts could be significant in term of reducing the disposal footprint, the hazardous radioactive materials and the uncertainties associated with the different scenarios in which man can come into contact with the disposed waste [2].

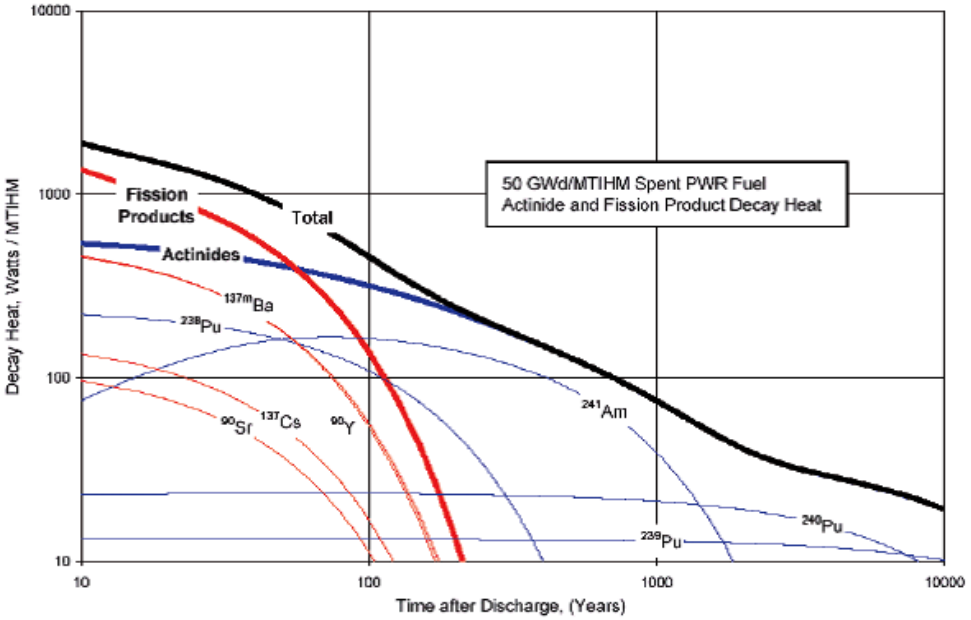

Fig. 1.1. Decay heat of LWR spent fuel irradiated to 50 GWd/t [5].

Concerning the long term radiotoxicity, if P&T is employed, especially for Pu, Am and Cm, it will be possible to reduce the time required for the radiotoxicity to reach the level of natural U by 2 orders of magnitude, as described in fig. 1.2 (dotted red lines options).

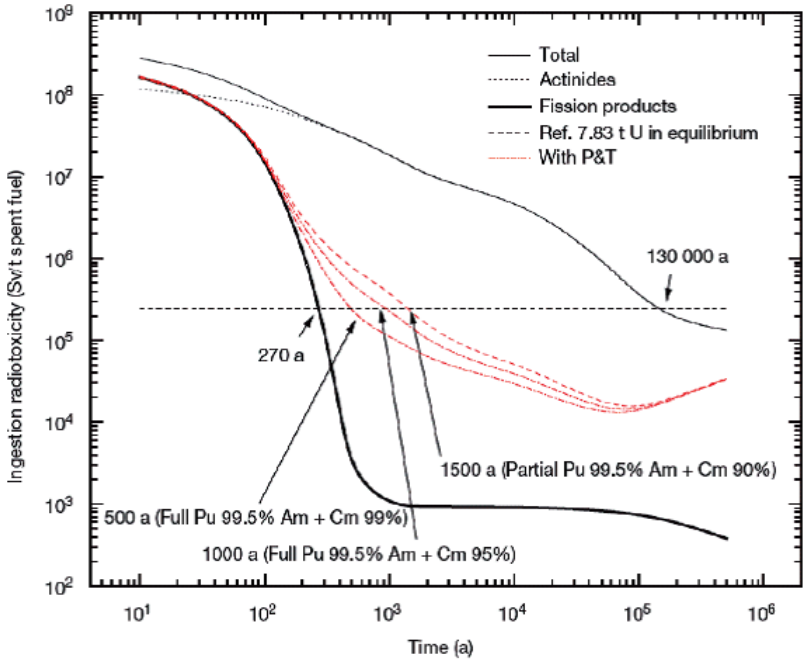

Fig. 1.2. The impact of removing transuranics from the high level waste on ingestion radiotoxicity as a function of time [5].

P&T schemes have been proposed for a variety of reactors (thermal and fast spectrum) and fuel cycle options; however, the best transmutation performance is obtained in a fast neutron reactor.

Fast reactors bring several advantages compared to thermal reactors in term of transmutation of actinides. Hereafter the main reasons are reported from an OECD/NEA report [6]:

- A favourable neutron balance, which allows introducing MA of any type and in significant amounts, without perturbing the reference performances of the corresponding core without MA.

- A neutron spectrum which allows fissions to dominate captures for all TRUs. This feature allows limiting the build-up of higher mass nuclei, e.g. the build-up of Cf-252 during TRU multi-recycle.

- The flexibility to burn or breed fuel, or to be iso-generator (a system that has a zero net production of TRU constituents in the fuel).

- The possibility to benefit from the favourable characteristics indicated above, whatever the Pu vector, the type of fuel (oxide, metal, nitride, carbide) and the type of coolant (sodium, heavy liquid metal, gas).

However, there are several limitations of the amount of MA that can be added to a fast reactor system; deterioration of neutronic characteristics of the reactor core, such as Doppler coefficient or coolant void temperature coefficient, have to be taken into account. Concerning the reprocessing of the fuel, it has to be performed remotely and in a shielded environment due to high radioactive component. Finally, in terms of fuel safety performance, He generation might enhance fuel swelling and pin over-pressurisation [5, 6].

Two main schemes have been considered and tested to recycle and transmute MA in fast reactor; (i) homogenous mode in which the MA are integrated in the standard fuel assemblies, and (ii) heterogeneous mode in which the MA are concentrated in specific fuel targets in the periphery of the core (fig. 1.3). The homogenous mode, in which the MA contents is kept below 5 wt.%, is already a robust developed route, demonstrated by several experimental programmes, e.g. the pioneeristic SUPERFACT [7]. However, a full scale pin bundle or assembly demonstration is still missing to complete the demonstration that the addition of MA will not affect safety and economic performance. The heterogeneous mode is a more complex endeavour to develop targets with much higher MA contents. Decay heat and radioactivity of these targets make the handling and fabrication more complex and

problematic. The main pro and contra of these 2 schemes are summarized in the table 1.1 below.

Table 1.1 Homogenous and Heterogeneous mode comparison

Homogenous mode	Heterogeneous mode
Fuel fabrication is easier but impacts all fuel fabrication streams.	Fabrication more complex but is concentrated on a limited mass flux.
Fuel behaviour under irradiation is quite close to the typical standard fuel.	Fuel behaviour under irradiation is quite different from the standard fuel.
No flexibility is possible between production of electricity and long-lived wastes mission.	Due to a large production of Cm and He released, targets design must be validated.
Some impact on core reactivity coefficient limits content of MA to about a few wt.%.	No impact on main reactor core parameters but higher thermal load of spent fuels.
A higher mass flux of sub-assemblies with MA has to be managed within the fuel cycle compared to heterogeneous mode.	Due to lower neutron fluxes, the MA inventories are quite higher than in the homogeneous mode.

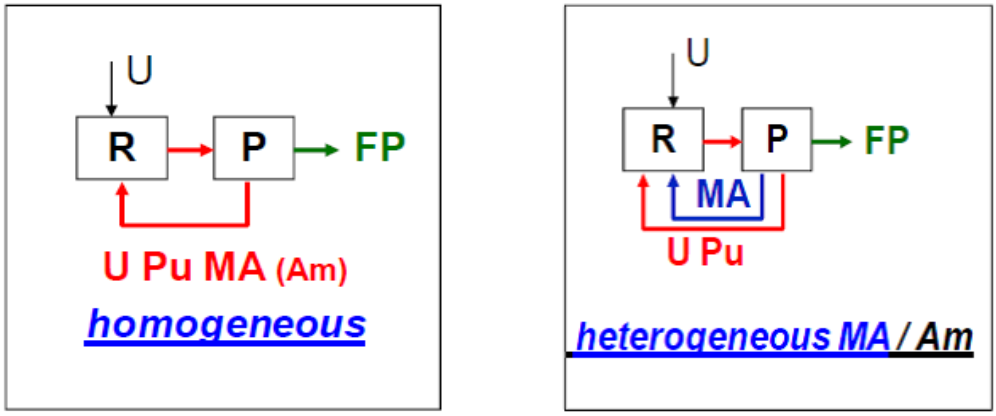

Fig. 1.3. Schematic representation of the 2 different methods to recycle and transmute MA. In the figures R stand for Recycling and P for Partitioning, while FP is Fission Product.

1.1 Metallic fuel

Metallic fuel alloy U-based has been studied and used since the beginning of the nuclear civil era as nuclear fuel, even before developing the oxide nuclear fuel technology. Metallic fuels are ideal for fast reactors because of higher densities of fissile and fertile materials compared to other fuel forms which provide higher

reactor core performance, such as higher breeding ratio and result in lower fissile inventory [8].

Considering the physical properties, higher thermal conductivity of the metallic alloy produces favourable coupling between the fuel pin and the coolant; however the low melting point of U or U-Pu alloys (compared to oxides) makes necessary the incorporation of Zr in the fabrication of metallic fuel alloys. Table 1.2 reports some important properties for metallic fuel (U-Pu-Zr) in comparison with other 3 fuel forms, oxide, nitride and carbide, mostly studied around the world.

Concerning the transmutation of minor actinides, metal-fuelled fast reactors provide higher transmutation rate due to harder neutron spectrum [9, 10]. Lastly, metallic fuel is easily recycled and, if coupled with pyroprocessing, provides also a stronger proliferation resistance route.

Table 1.2. Comparison of a few properties of various types of SFR fuel (Pu/(U+Pu) = 20%) [7]

	(U,Pu)O_2	*(U,Pu)N*	*(U,Pu)C*	*UPuZr*
Density (g cm^{-3})	11	14.3	13.6	15.6
Heavy atom density (g cm^{-3})	9.7	13.5	12.9	14
Melting temperature				
Liquidus (°C)	2775	2780	2480	1160
Solidus (°C)	2740	2720	2325	
Thermal conductivity at 1000 °C[a] (W m^{-1} K^{-1})	2.9	19.8	19.6	35
Thermal expansion from 20 to 1000 °C (10^{-6} °C^{-1})	12.6	10	12.4	16.5

[a]500 °C for UPuZr

1.1.1 Review of the literature on metallic fuel

Metallic fuel was selected to fuel many of the first reactors in USA such as EBR-I and EBR-II, FERMI-I and in the UK the DFR, and the MAGNOX commercial reactors (metallic uranium in thermal spectrum) [8].

Early metallic fuel performance was limited to a few atom percent burnup because the increase of FCMI caused by gas swelling brought to failure many fuel pins. The game changer technology solution was to reduce the fuel smear density (smear density: defined as the cross sectional area ratio of the fuel slug to the cladding inside) at 75%, so to effectively promote fission gas release before fuel-cladding contact. At the time the fuel is contacting the cladding, an interconnected porosity is

formed and around 70-80% of the fission gases are released into the plenum, resulting in a weak fuel mass that cannot exert significant mechanical force [11, 12]. Under irradiation U-Pu-Zr system undergoes redistribution of the main elements (U, Pu, Zr) from early stages of irradiation and different microstructure morphologies are also present (restructuring) along the fuel radius and with different compositions phases. Restructuring is strongly depending on irradiation temperature: when the fuel central temperature is higher than 650 °C for alloy U-19Pu-10Zr, a higher composition Zr phase formed in the centre of the fuel characterized with large fission gas bubbles [11, 12].

Extensive metal fuel irradiation tests were conducted in the USA during the IFR program [13, 14]. EBR-II operational and fuel qualification program included the irradiation of over 30000 Mark-II driver fuel pins (U-Fs, Fs: Fissium, 2.46Mo, 1.96Ru, 0.28Rh, 0.19Pd, 0.1Zr and 0.01Nb), 13000 Mark-III/IIIA/IV (U-10Zr) driver fuel pins and 600 U-Pu-Zr fuel pins from 1964 to 1994.

Mark-II was qualified for 8 at.% burnup. Mark-IIIA was qualified for 10 at.% due to swelling of the 316 stainless steel. Experimental test with U-Pu-Zr and U-Zr with cladding 316SS, D9, HT9 reached burnup of 15 to >19 at.% without cladding breach.

In the FFTF, full length metallic pins were tested with the purpose to effectively qualify U-Zr (1050 U-10Zr pin above 14 at.%; 37 U-Pu-Zr above 9 at.%) for FFTF core conversion.

During the IFR program, the safety performance of metallic fuel was assessed as well. In-pile transient tests [15] and out-of-pile heating tests [16, 17] were conducted and demonstrated the inherent safety performance of metal-fuelled core in the events of loss of coolant flow without scram and loss of heat sink without scram. Metal fuel is characterized by "benign run" properties in the occurrence of cladding breach due to its good compatibility with sodium.

The reprocessing and fuel re-fabrication of metal fuels have already been demonstrated in the past at ANL west (now INL). About 560 fuel subassemblies were processed by pyro-metallurgical process, called "melt refining," then fuel slugs were re-fabricated by injection casting from the recovered fuel [18]. The

simultaneous recovery of MA with plutonium is possible with the electrometallurgical process facilities.

1.1.2 Metallic fuel state of the art and MA addition

The design of a metallic fuel pin includes the fuel section (e.g. 1m long approximately), a gas plenum and the cladding, typically made of austenitic or ferritic-martensitic steel (fig. 1.4). The basic fuel alloy is U-Pu with Zr in fractions between 10-30 wt.%. The initial gap between fuel and cladding is wider compared to oxide fuel pin design, for the reason pointed out in the previous paragraph (accommodate swelling and fission gas release). The initial gap is filled with sodium (Na-bonding) to enhance the thermal conductivity [8, 11].

In the context of minor actinides transmutation, up to 5 wt.% MA is incorporated in the alloy (homogenous transmutation core design as discussed in previous paragraph) [7].

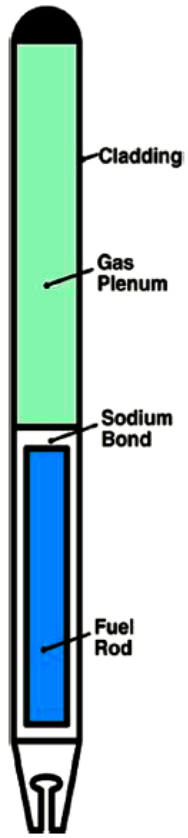

Fig. 1.4. Schematic of a metallic, sodium bonded, fast reactor fuel pin [11]

The first irradiation of MA-bearing metal fuel was conducted in the X501 test assembly in EBR-II up to 7.6 at.% burnup [19-21]. Preliminary post irradiation examinations revealed that the macroscopic behaviour in pile is similar to the basic alloy metallic fuel.

Because of the favourable features mentioned above, the development of MA-bearing metal fuel has been pioneered in the United States. More recently, Japan and the Republic of Korea have implemented programmes to investigate this option. A series of irradiation tests on non-fertile and low-fertile alloys, designated as AFC-1 [22-24], has been conducted in the ATR at the INL. Non-fertile and low-fertile alloys similar to the AFC-1 test alloys have been irradiated at Phénix as a part of the international FUTURIX-FTA program [25, 26]. For the more recent AFC-2 irradiation test series at INL [27, 28], MA-bearing U-Pu-Zr based alloys are to be irradiated. Characterisation of MA-bearing metal fuel alloys has also been performed at INL as well as the development of fuel fabrication technology [29-31]. Research and development activities at the KAERI cover the characterisation of U-Zr-Ce alloys, which are used as surrogates for U-Pu-Zr-MA-RE alloys, the fabrication of TRU-bearing metal fuel, and the development of lined cladding for metal fuel [32].

Carmack et al. [11] summarised the current focus areas of MA-bearing metal fuel research and development, some of them are reported hereafter:

- Metal fuel properties must not be seriously degraded by the addition of the MA compared to the U-Pu-Zr system performance.
- Demonstration of an acceptable (limited) level of FCCI with fuel that includes rare earth impurities and MA fuel constituents over the lifetime of the fuel up to its burnup limit, e.g. ~20 at.%.
- Assuming that fuel (resistance to) melting and FCCI characteristics are acceptable; behaviour of MA-bearing fuel in power transients and run beyond

cladding breach should also be acceptable. Performance modelling and perhaps proof testing of these assumptions may be required.

- Burnup limitation extensions greater than 23 at.% can be anticipated with current ferritic/martensitic steel cladding and up to 30 at.% may be achievable with increased high-temperature cladding strength and performance.

1.2 METAPHIX: concept and goals of the project

The METAPHIX project (which includes the main scope of the present thesis work) is a collaboration between the CRIEPI (Japan) and the EC-JRC Karlsruhe site (formerly known as ITU) with the support of CEA (France).

The main purpose of the project is to study the safety and feasibility of a closed nuclear fuel cycle deploying fast reactor minor actinides containing metal fuel.

The project includes different phases: the synthesis and characterization (JRC-ITU, early '90s), irradiation (Phénix reactor, France, 2003-2008), PIE and pyroprocessing (JRC-Karlsruhe, ongoing) [33-39].

Nine Na-bonded fuel pins loaded with four U-Pu-Zr-based alloy compounds were fabricated using arc-melting technology in an argon glove box. Two compounds contained RE (Y, Ce, Nd, Gd) in addition to MA, reproducing the output of pyrometallurgical reprocessing of LWR spent fuel. The composition of the alloys and the methods of fabrication will be treated in more details in Chapter 2.

The fuel pins irradiated reached 3 different burn-up (2.5 at.%, 7 at.% and 10 at.%).

In order to study the behaviour of the metallic fuel in pile, PIE are performed at JRC-Karlsruhe. Two groups of examinations are applied, non-destructive (gamma spectroscopy, profilometry) on the entire fuel pin and destructive on specific sections cut from the fuel pin (optical microscopy, SEM, EPMA, radiochemical analysis, etc.). Complete non-destructive examinations were performed on all fuel pins at each burnup. Optical microscopy and chemical analysis were carried out on specimens from low and medium burn-up pins.

1.3 Thesis synopsis

The scope of this research work is to try and answer some of the open questions related to the behaviour and performance under irradiation of metallic fuel with the addition of MA and RE, such as: confirming that the behaviour in pile of metallic fuel does not change dramatically adding MA and RE to the system and how the FCCI is affected by them.

The manuscript is composed of 6 chapters. The present Chapter 1 highlights metallic fuel characteristics in fast reactor, provides a literature review of the most important experience with this fuel type and introduces the METAPHIX project. The METAPHIX project is described in more details in Chapter 2, while Chapter 3 is focused onto the different experimental techniques employed in this work. The characterization of the as-prepared metallic fuel pin with addition of MA is the topic of Chapter 4. Finally, Chapter 5 is dedicated to the description of the behaviour in pile of this innovative fuel. The manuscript is concluded with remarks and description of potential future work in Chapter 6.

1.4 References

[1] Technology roadmap update for generation IV nuclear energy systems, GIF 2014.

[2] Potential benefits and impacts of advanced nuclear fuel cycles with actinide partitioning and transmutation, OECD/NEA, ISBN 978-92-64-99165-1, 2011

[3] D. Haas, P.D.W. Bottomley, G.G.M. Cojazzi, J.-P. Glatz, P. Hahner, R. Hurst, R.J.M. Konings, V.V. Rondinella, J. Somers, Research on sustainable fast neutron reactors, in: Proc. Int. Conf. On Future Nuclear Systems GLOBAL '09, Sept. 6-11, ANS, Paris, France, 2009 paper 9037.

[4] Management of Spent Nuclear Fuel and its Waste, JRC-EASAC, 2014.

[5] Status of minor actinides fuel development, IAEA nuclear energy series, No. NF-T-4.6, 2009.

[6] Homogeneous versus heterogeneous Recycling of Transuranics in Fast Nuclear Reactors, OECD/NEA, ISBN 978-92-64-99177-4, 2012.

[7] Actinide-Bearing Fuels and Transmutation Targets, S. Pillon in: R.J.M. Konings (Ed.), Comprehensive Nuclear Materials, vol. 3, Elsevier, Amsterdam, 2012, pp. 109-141.

[8] Metal Fuel, T. Ogata in: R.J.M. Konings (Ed.), Comprehensive Nuclear Materials, vol. 3, Elsevier, Amsterdam, 2012, pp. 1-40.

[9] T. Inoue, et al., "Development of Partitioning and Transmutation Technology for Long-Lived Nuclides," Nucl. Technol., 93 (1991) 206.

[10] T. Yokoo, et al, "Core performance of fast reactors for actinide recycling using metal, nitride, and oxide fuels", Nucl. Technol., 116 (1996) 173.

[11] W.J. Carmack, D.L. Porter, Y.I. Chang, S.L. Hayes, M.K. Meyer, D.E. Burkes, C.B. Lee, T. Mizuno, F. Delarge and J. Somers, "Metallic Fuels for Advanced Reactors", J. Nucl. Mater., 392 (2009) 139.

[12] G.L. Hofman and L.C. Walters, ‘Metallic Fast Reactor Fuels,’ Materials Science and Technology, A Comprehensive Treatment, R.W. Cain, P. Haasen, and E.J. Kramer, Eds., in Nuclear Materials, Vol. 10A, Part 1, B. R. T. Fros, Ed., VCH Verlagsgesellschaft (1994).

[13] Y.I. Chang, "The Integral Fast Reactor", Nucl. Technol., 88 (1989) 129.

[14] C. E. Till and Y. I. Chang, "Progress and Status of the Integral Fast Reactor (IFR) Fuel Cycle Development", Proc. Int. Conf. Fast Reactor and Related Fuel Cycles, Kyoto, Japan, Oct. 28 - Nov. 1, (1991).

[15] T.H. Bauer, A.E. Wright, W.R. Robinson, J.W. Holland and E.A. Rhodes, "Behaviour of Modern Metallic Fuel in TREAT Transient Overpower Tests", Nucl. Technol., 92 (1990) 325.

[16] A.B. Cohen, H. Tsai and L.A. Neimark, "Fuel/Cladding Compatibility in U-19Pu-10Zr/HT9-Clad Fuel at Elevated Temperatures", J. Nucl. Mater., 204 (1993) 244.

[17] Y.Y. Liu, H. Tsai, M.C. Billone, J.W. Holland and J.M. Kramer, "Behaviour of EBR-II Mk-V-Type Fuel Elements in Simulated Loss-of-Flow Tests", J. Nucl. Mat., 204 (1993) 194.

[18] C.E. Stevenson, "The EBR-II Fuel Cycle Story", American Nuclear Society, La Grange Park, Illinois (1987).

[19] M.K. Meyer, S.L. Hayes, W.J. Carmack and H. Tsai, "The EBR-II X501 Minor Actinide Burning Experiment", INL/EXT-08-13835, Idaho National Laboratory (2008).

[20] M.K. Meyer, S.L. Hayes, W.J. Carmack and H. Tsai, "The EBR-II X501 Minor Actinide Burning Experiment", J. Nucl. Mater., 392 (2009) 176.

[21] Y.S. Kim, G.L. Hofman and A.M. Yacout, "Migration of Minor Actinides in Fast Reactor Metallic Fuel", J. Nucl. Mater., 392 (2009) 164.

[22] B.A. Hilton, S.L. Hayes, M.K. Meyer, D.C. Crawford, G.S. Chang and R. Ambrosek, "The AFC-1AE and AFC-1F Irradiation Tests of Metallic and Nitride Fuels for Actinide Transmutation", Global 2003, New Orleans, Louisiana, Nov. 16-20 (2003).

[23] B.A. Hilton, D.L. Porter and S.L. Hayes, "AFC-1 Transmutation Fuels Post-Irradiation Hot Cell Examination 4 to 8at% Final Report - Irradiation Experiments AFC-1B, AFC-1F and AFC-1AE", INL/EXT-05-00785 Rev.1, Idaho National Laboratory (2006).

[24] B.A. Hilton, D.L. Porter and S.L. Hayes, "Post irradiation Examination of AFCI Metallic Transmutation Fuels at 8at%", Trans. ANS, 98 (2008) 773.

[25] L. Donnet, F. Jorion, N. Drin, S.L. Hayes, J.R. Kennedy, K. Pasamehmetoglu, S.L. Voit, D. Haas and A. Fernandez, "The FUTURIX-FTA Experiment in Phenix: Status of Fuel Fabrication", Global 2005, Tsukuba, Japan, Oct. 9-13 (2005).

[26] P. Jaecki, S. Pillon, D. Warrin, S.L. Hayes, J.R. Kennedy, K. Pasamehmetoglu, S.L. Voit, D. Haas, A. Fernandez and Y. Arai, "Update on the FUTURIX-FTA Experiment in Phenix," Global 2005, Tsukuba, Japan, Oct. 9-13 (2005).

[27] H.J. MacLean and S.L. Hayes, "Irradiation of Metallic and Oxide Fuels for Actinide Transmutation in the ATR", Global 2007, Boise, Idaho, Sep. 9-13 (2007).

[28] S.L. Hayes, "Irradiation of Metallic Fuels With Rare Earth Additions for Actinide Transmutation in the Advanced Test Reactor - Experiment Description for AFC-2A and AFC-2B", INL/EXT-06-11707 Rev. 2 Idaho National Laboratory (2007).

[29] D. E. Janney and J. R. Kennedy, "As-cast microstructure in U-Pu-Zr alloy fuel pin with 5-8 wt.% minor actinides and 0-1.5 wt.% rare-earth elements", Mat Charact. 61 (2010) 1194.

[30] D. E. Burkes, J. R. Kennedy, T. Hartmann, C. A. Papesch, D. D. Keiser Jr., "Phase characteristics of a number of U–Pu–Am–Np–Zr metallic alloys for use as fast reactor fuels", J. Nuc. Mater. 396 (2010) 49.

[31] D. E. Janney, J. R. Kennedy, J.W. Madden, T.P. O'Holleran, "Crystal structure of high-Zr inclusions in an alloy containing U, Pu, Np, Am, Zr and rare-earth elements", J. Nuc. Mater. 448 (2014) 109.

[32] H. J. Ryu, B.O. Lee, S. J. Oh, J. H. Kim, C. B. Lee, "Performance of FCCI barrier foils for U–Zr–X metallic fuel", J. Nuc. Mater. 392 (2009) 206.

[33] M. Kurata, I. Inoue, L. Koch, J-C. Spirlet, C. Sari and J-F. Babelot, "Development of Transmutation Technology of Long-Lived Nuclides - Properties of the Alloy Concluding MA and RE -", CRIEPI Report T92005, Central Research Institute of Electric Power Industry (1992) in Japanese.

[34] M. Kurata, A. Sasahara, T. Inoue, M. Betti, J.-F. Babelot, J.-C. Spirlet, and L. Koch, “Fabrication of U-Pu-Zr Metallic Fuel Containing Minor Actinides”, Proc. Int. Conf. Future Nuclear Systems, Challenge Towards Second Nuclear Era with Advanced Fuel Cycles (Global ’97) vol. 2 (1997) 1384.

[35] H. Ohta, T. Yokoo, T. Ogata, T. Inoue, M. Ougier, J.P. Glatz, B. Fontaine and L. Breton, "Irradiation Experiment on Fast Reactor Metal Fuels Containing Minor Actinides up to 7at.% Burnup", Global 2007, Boise, Idaho, Sep. 9-13 (2007).

[36] L. Breton, E. Garces, S. Desjardins, B. Fontaine, T. Martella, L. Loubet, H. Ohta, T. Yokoo, M. Ougier and J. P. Glatz, “METAPHIX-1 Non-Destructive PIE in the Irradiated Elements Cell of PHENIX”, Global 2007, Boise, Idaho, Sep. 9-13 (2007).

[37] T. Ogata, K. Nakamura and H. Ohta, "Progress in Metal Fuel Development at CRIEPI", Trans. ANS, 98 (2008) 977

[38] H. Ohta, T. Ogata, T. Yokoo, M. Ougier, J.-P. Glatz, B. Fontaine and L. Breton, “Low-burnup Irradiation Behaviour of Fast Reactor Metal Fuels Containing Minor Actinides” ,Nucl. Technol. 165 (2009) 96.

[39] H. Ohta, T. Ogata, T. Yokoo, T. Koyama, D. Papaioannou, J-P. Glatz and V. Rondinella, "Post-Irradiation Examinations on Fast Reactor Metal Fuels Containing Minor Actinides - Fission Gas Release and Metallography of ~2.5at% Burnup Fuels -", Global 2009, Paris, France, Sep. 6-11 (2009).

Chapter 2

The METAPHIX project

As mentioned in chapter 1, the METAPHIX project is composed of a sequence of phases (e.g. preparation of alloys, irradiation experiment, PIE) that will be discussed in more details in this chapter.

2.1. Metallic fuel alloys preparation and characterization

Four different metallic alloys were prepared in a double containment argon glove box in JRC-Karlsruhe in 1994 [1]. Table 2.1 lists the average composition of the fuels. Two compounds contained RE (Y, Ce, Nd, Gd) in addition to MA (Am, Np, Cm), reproducing the output of pyrometallurgical reprocessing of LWR spent fuel. The total level of impurities, measured by GDMS, was less than 0.3 wt.% [1].

Table 2.1. Average composition (in wt.%) of the metallic fuel pins

	U-Pu-Zr	U-Pu-Zr 2MA-2RE	U-Pu-Zr 5MA	U-Pu-Zr 5MA-5RE
U	71.00	66.85	66.30	63.50
Pu	18.93	19.80	19.35	19.75
Zr	10.19	9.46	8.97	8.19
MA	0.03	2.08	4.74	4.78
Np		1.23	2.97	3.04
Am	0.03	0.67	1.45	1.52
Cm		0.18	0.32	0.31
RE	-	1.73	-	3.40
Y		0.12		0.31
Ce		0.20		0.45
Nd		1.25		2.30
Gd		0.16		0.32

The different alloys were prepared by arc-melting using a Y_2O_3 crucible. The alloys were produced as pins with diameter of 4.9 mm and cut into rodlets of 20 and 50 mm, as shown in fig. 2.1.

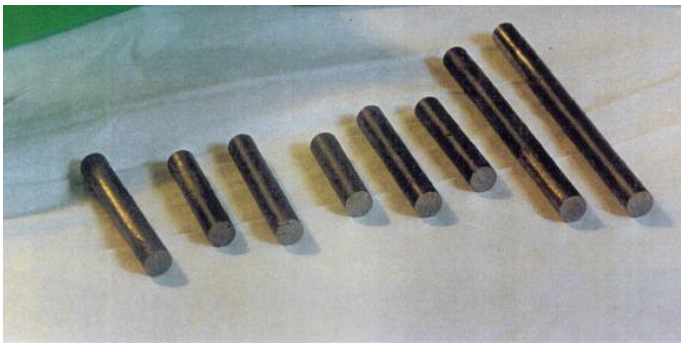

Fig. 2.1. As-prepared metallic alloy

Fig. 2.2 reports the preparation flow diagram of the different RE/MA-containing metallic alloys. For the UPuZr and UPuZrMA, U-Pu or U-Pu-MA alloys were first melted and then mixed with molten Zr. For the compounds with RE, some difficulties were encountered to achieve the desired homogeneity by simple arc melting, because of the low miscibility of RE in U-Pu-Zr-MA alloys. To improve the homogeneity, the U-Pu-Zr-MA and RE were pulverized into powders and mixed mechanically before melting [1, 2]. In order to minimize the volatilization of Am metal, the melting and casting of the fuel alloys were carried out under an overpressure of Ar.

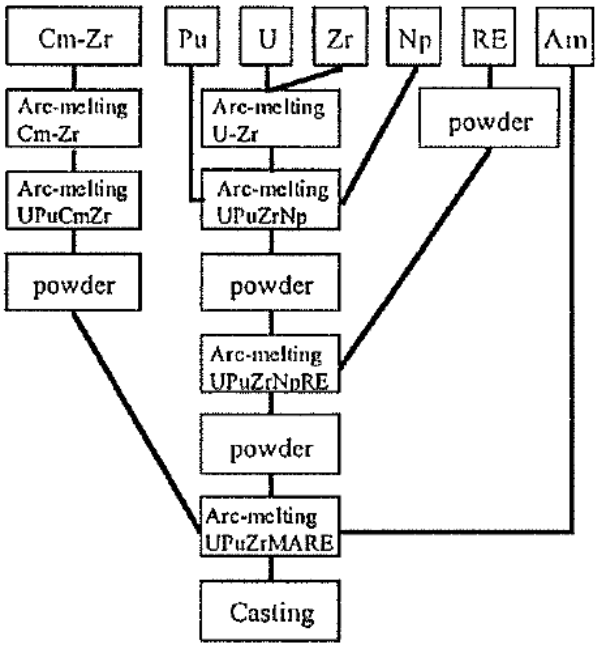

Fig. 2.2. Preparation flow diagram of the different metallic fuel alloys [1]

The results of the composition analysis indicated that the U-Pu-Zr basic alloy prepared by simple arc melting was less uniform compared with the MA-containing alloys prepared through the multiple steps process. For the alloys containing RE, local composition variations were observed, possibly because of RE-rich phases precipitates [3].

The characterization of the metallic alloys was carried out with different experimental techniques to understand the effects of the addition of MA and/or RE on the basic alloy on the microstructure, phase transition temperatures and thermal conductivity [4].

Additional characterization techniques such as melting point determination and mechanical properties measurements were also applied [4].

2.1.1 Microstructure of the different metallic alloys

Fig. 2.3 shows an optical microscopy macrograph of an as-polished UPuZr+2MA+2RE sample in which several precipitates of different sizes (dark grey) are visible [5].

In fig. 2.4 a higher magnification micrograph of the cross-section of the sample shown fig. 2.3 provides a closer look which allows observation of the different sizes and shapes of precipitates in the sample.

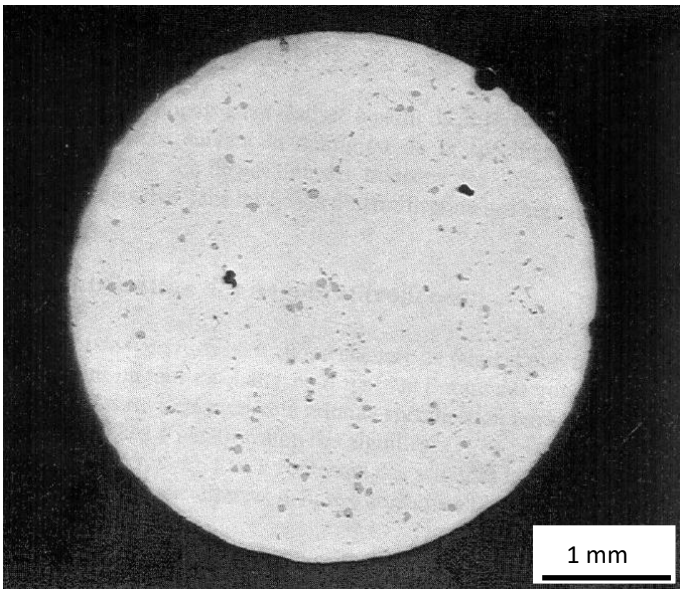

Fig. 2.3. Optical macrograph of a sample of UPuZr+2MA+2RE

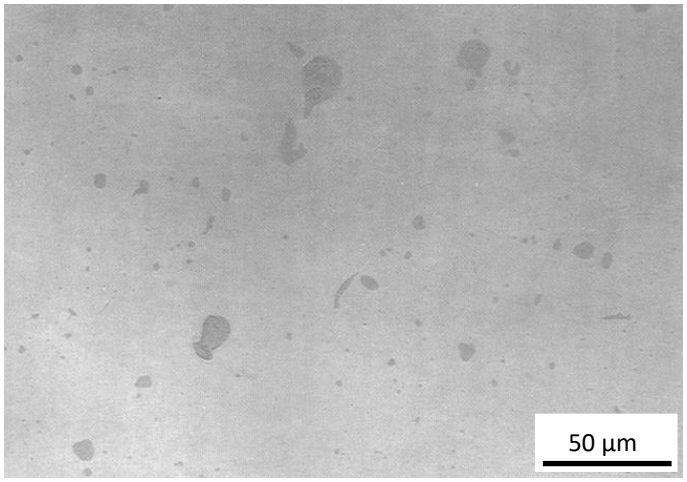

Fig 2.4. Detail of precipitates from fig. 2.3

In fig. 2.5 EPMA X-ray qualitative maps of a sample of UPuZr+5MA+5RE show the qualitative distribution of precipitates in which MA are present together with RE [5]. The dedicated X-ray map for Np shows that this element is present mainly in the fuel matrix.

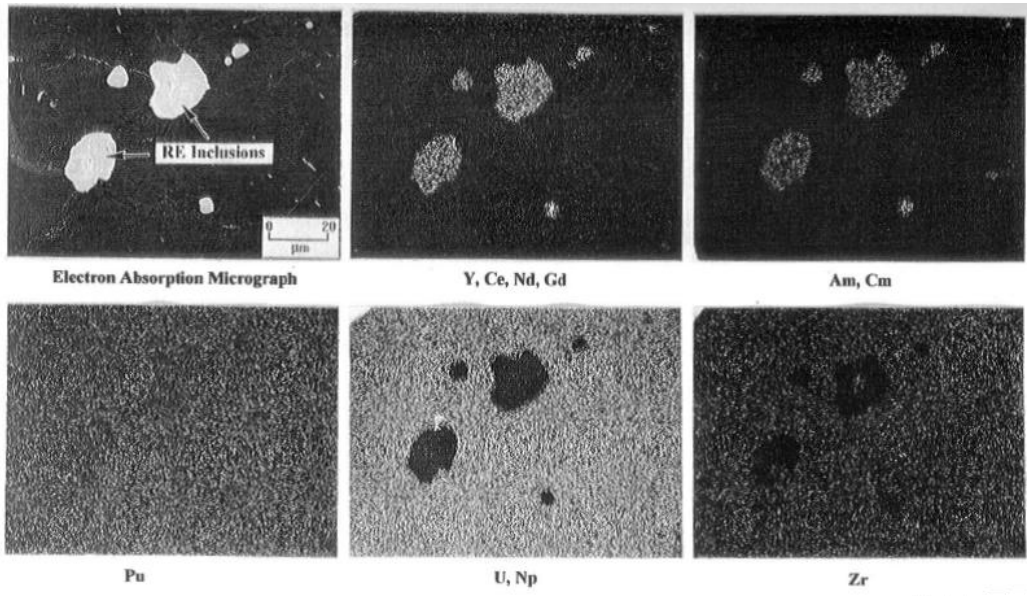

Fig 2.5. EPMA absorbed electron image and X-ray qualitative maps of a sample of UPuZr+5MA+5RE showing the details of the distribution of MA-RE precipitates.

Fig. 2.6 shows EPMA absorbed electron images of two different samples of UPuZr + 5MA. The microstructure of the alloy without RE reveals a more complex configuration with two secondary phases, dendritic and acicular, inferred to contain different amounts of MA [5].

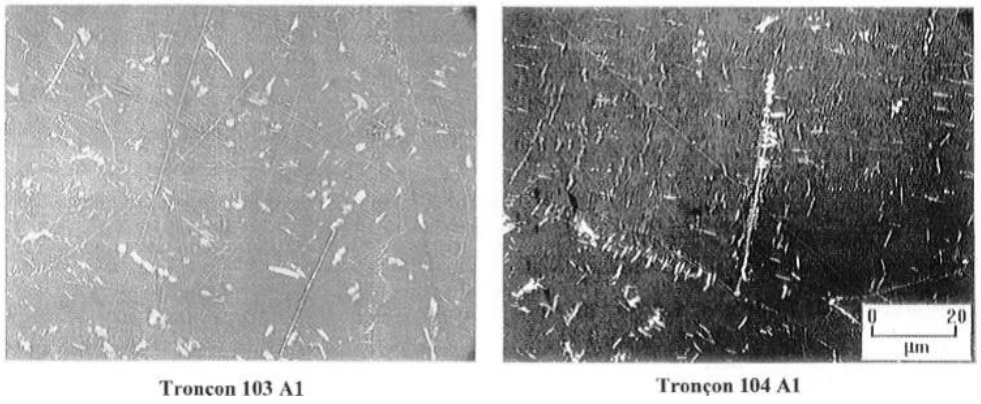

Fig. 2.6. UPuZr+5MA, EPMA absorbed electron image.

Annealing tests were also performed to understand the behaviour of the different precipitates at high temperatures. The tests were carried out on two alloys: UPuZr +

2MA+2RE and UPuZr + 5MA+5RE, at 773 K, 873 K, 973 K, 1023 K for 3.5 - 100 hours followed by rapid (1 second) quenching in water [4].

In order to assess the microstructure evolution with temperature, after annealing optical microscopy and EPMA were performed. Figs. 2.7 and 2.8 illustrate the metallography of annealed and etched alloys. The dark precipitates are enriched in RE and Am and are dispersed homogeneously. Ohta et al. [4] estimated also the nature of the different observed phases. At 773 K and 873 K the microstructure presents two phases, respectively ζ+δ and ζ+γ . At 973 K and 1023 K a single γ phase precipitates at the grain boundaries.

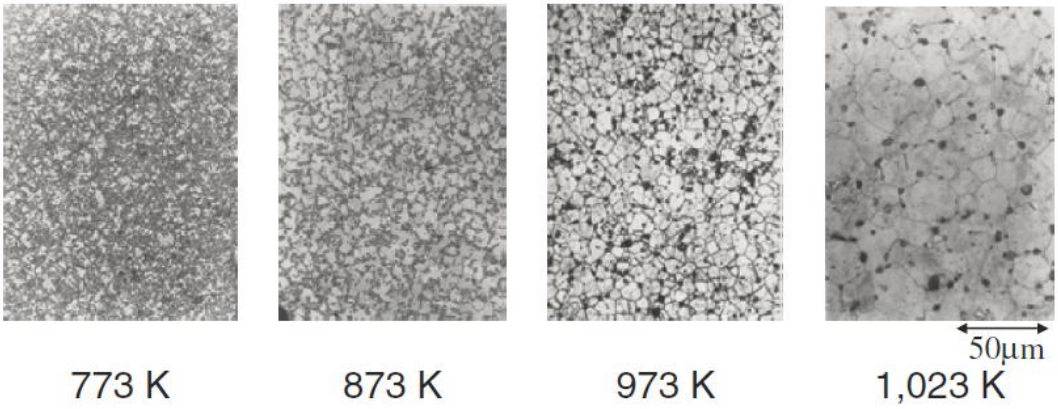

Fig. 2.7. Optical microscopy photographs of annealed and etched metallic fuel alloy with 2MA+2RE [6]

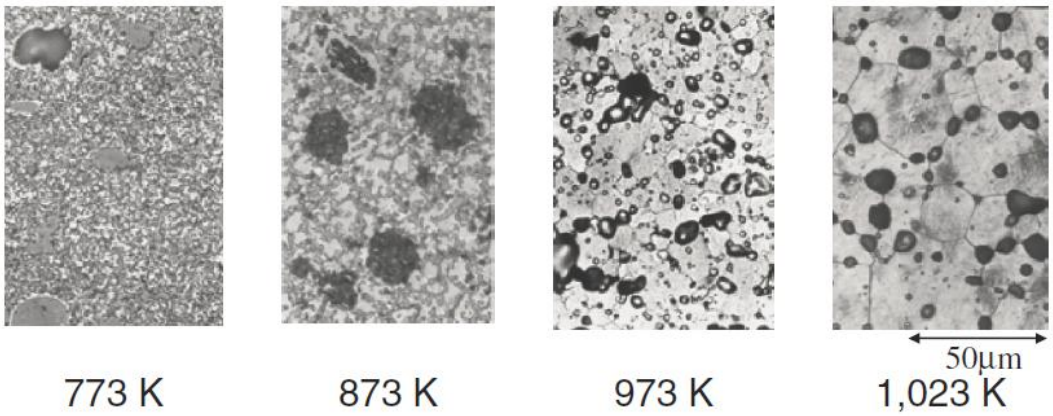

Fig 2.8. Optical microscopy photographs of annealed and etched metallic fuel alloy with 5MA+5RE [4]

2.1.2 Thermophysical properties

Thermophysical properties such as phase transition temperatures and thermal conductivity were measured for the different metallic alloys in order to evaluate the effect of the addition of MA and RE [4].

In order to analyse the phase transition temperatures, dilatometry was applied to 3 different alloy compositions: UPuZr+2MA+2RE (CR11), UPuZr+5MA+5RE (CR12) and UPuZr (CR13)[1] [4].

From the dilatometry curves reported in [4] and shown here in fig. 2.9, 2 distinct phase transition temperatures at approx. 853 (ζ+δ ↔ζ+γ) and 903 K (ζ+ γ ↔γ) are observed for the samples independently from their composition. These results indicate that the wt.% of MA and RE added does not have an effect on the phase change temperatures. This is in line with temperatures transition reported in literature [7-8].

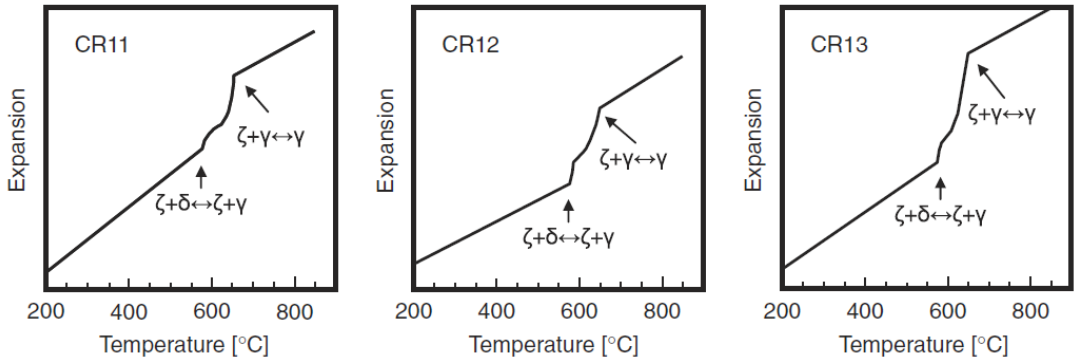

Fig. 2.9. Dilatometry curves for UPuZr+2MA+2RE (CR11), UPuZr+5MA+5RE (CR12) and UPuZr (CR13). The two phase changes are highlighted by arrows in the plots.

Concerning the thermal conductivity measurements, samples from 5MA+5RE and basic alloy were measured by a comparative method with pure iron as a reference material [4]. Fig. 2.10 reports the measured data, which indicate that the influence of MA and RE addition on the thermal conductivity is not significant.

[1] CR11, CR12, CR13 are the laboratory name / labels of the different alloys also found in fig. 2.9

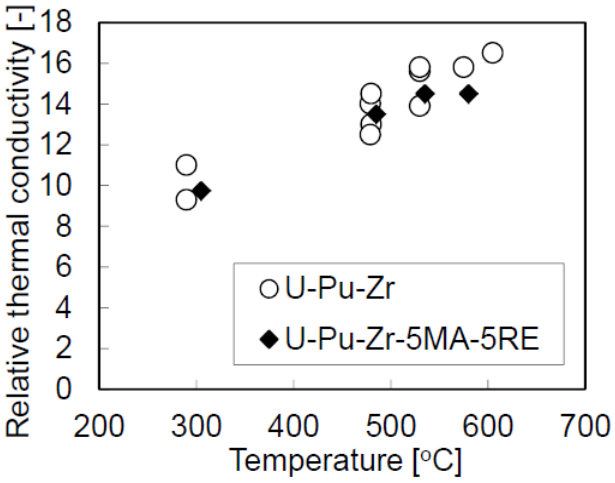

Fig. 2.10. Thermal conductivity of UPuZr and UPuZr+5MA+5RE alloys

2.2 Irradiation experiment

The different fuel alloy ingots were stacked in 3 different fuel pins (#1, #2, #3) with a total active fuel length of 485 mm. They were irradiated in a capsule together with sixteen oxide fuel driver pins in the Phenix reactor, France, from 2003 to 2008. A schematic view of the 3 different fuel pins and of the experimental capsule in the reactor are shown in fig. 2.11 and fig. 2.12, respectively. Table 2.2 reports the detailed axial configuration with the composition of the different ingots loaded in the fuel pins.

The cladding utilized was the 15-15Ti [9], the gap was filled with sodium to enhance the thermal conductivity and the plenum length was 464 mm. The main characteristics of the metallic fuel pins are reported in table 2.3.

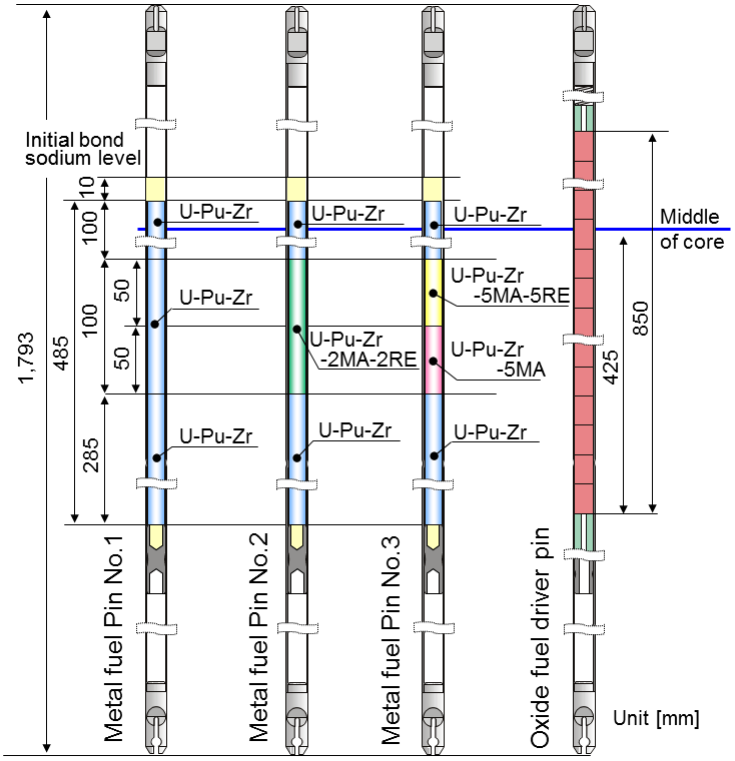

Fig. 2.11. Schematic view of the 3 different fuel pins.

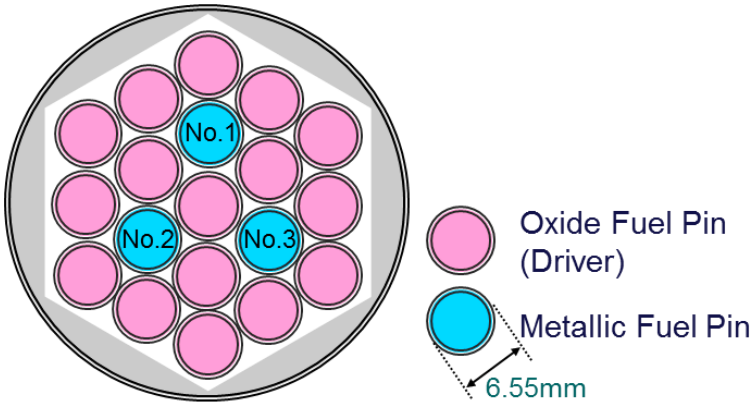

Fig. 2.12. Schematic view of the experimental capsule in the Phenix reactor

Table 2.2. Detailed compositions of metal fuel alloys in pins #1, #2 and #3

Ingot	Pin #1	Pin #2	Pin #3	
A	$U_{71}Pu_{19}Zr_{10}$	$U_{71}Pu_{19}Zr_{10}$	$U_{71}Pu_{19}Zr_{10}$	
B	$U_{71}Pu_{19}Zr_{10}$	$U_{67}Pu_{19}Zr_{10}MA_2RE_2$	top half	$U_{61}Pu_{19}Zr_{10}MA_5RE_5$
			bottom half	$U_{66}Pu_{19}Zr_{10}MA_5$
C	$U_{71}Pu_{19}Zr_{10}$	$U_{71}Pu_{19}Zr_{10}$	$U_{71}Pu_{19}Zr_{10}$	
Remark	*All ingots consisted of the same fuel compositions*	*Ingots A and C consisted of the same fuel compositions* *MA_2: $Np_{1.2}\ Am_{0.6}\ Cm_{0.2}$* *$RE_2$: $Nd_{1.4}\ Y_{0.2}\ Ce_{0.2}\ Gd_{0.2}$*	*Ingots A and C consisted of the same fuel compositions* *Ingot B is divided in two parts: with RE and without RE. Both parts contain MA.* *MA_5: $Np_3\ Am_{1.6}\ Cm_{0.4}$* *RE_5: $Nd_{3.5}\ Y_{0.5}\ Ce_{0.5}\ Gd_{0.5}$*	

Table 2.3. Characteristics of the metallic fuel pins [4]

Pin length	1793 mm
Outer cladding diameter	6.55 mm
Cladding thickness	0.45 mm
(active) Fuel stack length	485 mm
Fuel pin diameter	4.9 mm
Initial fuel-cladding gap	0.375 mm
Fuel smear density	75.2 %TD*
Sodium level above fuel	~10 mm
Plenum length	464 mm

*Theoretical Density

The irradiation experiment started ~9 years after the fabrication of the fuel pins. Three irradiation capsules were prepared and irradiated to three different peak burnups ~2.5at.% (METAPHIX-1), ~7at.% (METAPHIX-2), ~10at.% (METAPHIX-3). The irradiation history, burnups, linear heat power were evaluated from the reactor operation by CEA and are schematically described in table 2.4.

Table 2.4. Details of the irradiation history for the 3 different irradiation capsules.

	METAPHIX-1	METAPHIX-2	METAPHIX-3
Irradiation period [EFPD]	119.96	356.63	584.09
Peak linear heat power [1] [W/cm]			
Max during irradiation[2]	323	313	275
Min during irradiation[3]	273	252	204
Cladding peak temperature[1] [°C]			
Max during irradiation[2]	555	541	495
Min during irradiation[3]	554	522	480
Discharged peak burnup[1] [at.%]	2.5-2.7	6.6-7.2	9.3-10.2
Fast neutron fluence [dpa]	17	48	73

[1] Maximum value for the fuel pins;
[2] Beginning of the second irradiation cycle;
[3] End of irradiation

2.2.1 Temperature distribution during irradiation

The axial temperature profiles (fig. 2.13) were calculated using ALFUS code [10] at the BOI and EOI, for the 3 different burnups and for the fuel centre and periphery [11]. Uncertainty on the calculation was estimated to be around 10% due to fabrication tolerance and irradiation swelling [11]. The temperature distributions described here will be extensively used in chapter 5 to assess the different phases present in the metallic fuel and to analyse the quantitative data of the different concentration measured by EPMA.

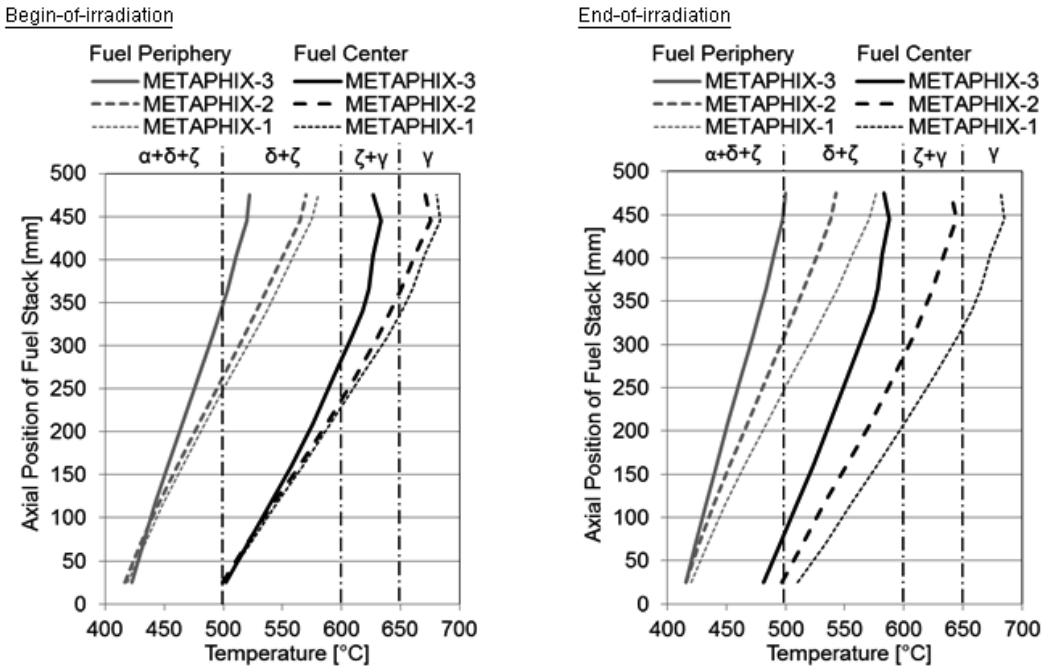

Fig. 2.13. Axial temperature distribution profiles for METAPHIX-1, -2, -3. The temperatures were calculated by ALFUS code for BOI and EOI, for fuel periphery and fuel centre.

2.3 References

[1] M. Kurata, A. Sasahara, T. Inoue, M. Betti, J.-F. Babelot, J.-C. Spirlet, L. Koch, Fabrication of U-Pu-Zr Metallic Fuel Containing Minor Actinides, Proc. Int. Conf. Future Nuclear Systems, Global ’97 (1999) 1384-1389

[2] J.-P. Glatz, T. Koyama, Demonstration of Minor Actinide Recycling with Metal Fuel (I) overview of the METAPHIX – PYRO Project, Proc. GLOBAL 2015, 1757-1763

[3] H.Ohta, T. Ogata, S. Van Winckel, D. Papaioannou, V.V. Rondinella, "Minor actinide transmutation in fast reactor metal fuels irradiated for 120 and 360 equivalent full-power days, J. Nucl. Science and Tech., 53, 968-980 (2016)

[4] H. Ohta, T. Ogata, D. Papaioannou , M. Kurata, T. Koyama, J.-P. Glatz and V.V. Rondinella, “Development of fast reactor metal fuels containing minor actinides,” J. Nucl. Sci. Technol., 48, 654-661 (2011).

[5] J. Rebizant, J.C. Spirlet, F. Wastin, "Rapport de fabrication des combustibles metalliques", Commission Europeenne, Centre Commun de Recherche, Institut Europeen des Transuraniens Recherche sur le Actinides, Technical note K0298193, 1998 (French)

[6] H. Ohta, T. Ogata, K. Nakamura, T. Koyama, "Development of minor actinide transmutation by CRIEPI", IEMPT 2010, San Francisco CA, USA

[7] D.R. O’Boyle, A.E. Dwight, in: Proc. Fourth Int. Conf. on Pu and Other Actinides, Santa Fe, NM, 1970, p. 720.

[8] Ogata T. Metal Fuel. In: Konings R.J.M., (ed.) Comprehensive Nuclear Materials, volume 3, pp. 1-40, (2012), Amsterdam: Elsevier.

[9] J.L. Seran et al., "Behaviour under neutron irradiation of the 15-15Ti and EM10 steels used as standard materials of the Phenix fuel subassembly", Proc. 15th Int. Symp. Effects of Radiation on Materials, Nashville, Tennessee, June 19-21, 1990, p. 1209, ASTM International (1992).

[10] T. Ogata, T. Yokoo, "Development and Validation of ALFUS: An Irradiation Behaviour Analysis Code for Metallic Fast Reactor Fuels", Nuclear Technology, Vol. 128, pp. 113-123, 1999

[11] H. Ohta, D. Papaioannou, T. Ogata, T. Yokoo, T. Koyama, V. Rondinella, J.-P. Glatz, "Post-irradiation Examinations on Fast Reactor Metal Fuels Containing Minor Actinides - Fission gas release and metallography of ~2.5at.% burnup fuels" Proc. Int. Conf. on Future Nuclear Systems GLOBAL '09, Sept. 6-11, 2009, Paris, France, ANS, paper 9241.

Chapter 3

Experimental techniques

This chapter will describe the methods adopted for preparing metallic fuel samples for destructive examination and the different experimental techniques exploited.

3.1 Sample preparation and method for preservation

Metallic fuel samples for destructive examinations of METAPHIX-1 & 2 pins were prepared taking into account the fuel alloy composition, irradiation temperature and burnup distribution. The cut samples and pin segments are stored under protective atmosphere in a autoclave as shown in fig. 3.1. The vessel is filled with high purity 99.9999% helium gas of in order to preserve the materials against oxidation by the atmosphere of the hot cells (N_2 + 2%O_2).

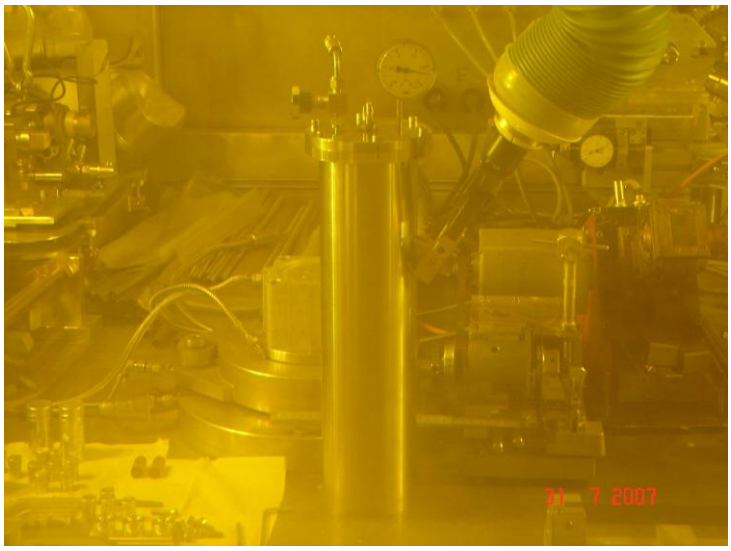

Fig. 3.1. Storage vessel for the metallic fuel alloy samples in hot cell.

The fuel pins were cut using a diamond saw without use of coolant or lubricant; after cutting, all the samples for microstructure observations, SEM and EPMA were embedded into resin. The embedding was performed under vacuum so that the resin could penetrate into the gaps or cracks of the samples. After embedding, the samples were stored in the high purity helium chamber.

3.1.1 Grinding and Polishing

The embedded samples were polished using an ethanol based diamond suspension (BioDiamond produced by Heraeus Kulzer GmbH). Ethanol was also added as lubricant during polishing. At the coarse polishing stages, suspensions with diamond abrading size of 40μm to 12μm were used. The abrading size was gradually reduced to 9μm, 6μm, and 3μm. Finally, the sample surface was polished with the finest, 1μm size abrading suspension. The types of polishing-cloth set on the rotation table were adapted to the abrading size. The polishing-cloths themselves do not contain any abrading substance (New Lam classic and New Lam MM produced by Heraeus Kulzer GmbH).

3.2 Optical Microscope

The fuel samples were examined using a Leica Telatom-3 optical microscope. The microscope is connected to the sample preparation cell by a shielded tunnel, and the sample is transported using a motorized cart. Images were collected at different magnitude (50X, 100X, 200X and 500X) for different grade of detail.

For each sample were produced:

- An overview optical macrograph of the whole cross section.
- An optical macrograph of the radius at 3 different angles (collage of 6 different images).
- Optical images recorded at intervals of r/r_0[1]=0.25 (taking r/r_0=0 as the centre).

[1] Definition of the system of reference for location across a generic fuel cross section, where r is the generic radial position and r_0 is the reference radius of the fuel cross section.

3.3 Scanning Electron Microscope (SEM)

The nuclearized SEM device for analysis of highly radioactive specimens at JRC-Karlsruhe is a JEOL JSM-6400. Electron images of magnification up to 5000 times can be obtained. The EDX device combined to the SEM equipment is a SAMx Numerix DXD-X10P. The detector is equipped with a lead collimator (length = 3cm, aperture diameter = 1.5mm). Owing to the background radiation from the sample and to mutual energy interferences on the actinides M lines, quantitative evaluation of EDX spectra is considered not sufficiently accurate. Additionally, the estimation of U, Pu and other MA composition using L peaks for actinides is difficult as they are affected by the interferences originating from X-ray emission caused by the internal conversion by the daughter atoms from the alpha-decaying actinides [1]. Consequently, the evaluated composition values strongly depend on which lines are used for the evaluation. Therefore, EDX results of actinide-containing compounds are presented here only to discuss the relative increase and decrease of each element between the different phases by comparing the corresponding X-ray spectra. The characteristic X-ray peaks of fuel constituents (U, Pu, Zr), of the RE elements (La, Ce, Pr, Nd, Sm, Gd), and of the other fission product elements of relatively high fission ratio (Y, Mo, Ru, Pd) are considered. In the vicinity of the fuel-cladding interface, cladding elements (Fe, Cr, Ni) are also taken into consideration. Fig. 3.2 and fig. 3.3 show relevant X-ray spectra. The former shows U, Pu and Zr peaks and is representative of fuel matrix, while the latter describes a RE precipitate phase where the different overlapping picks are visible.

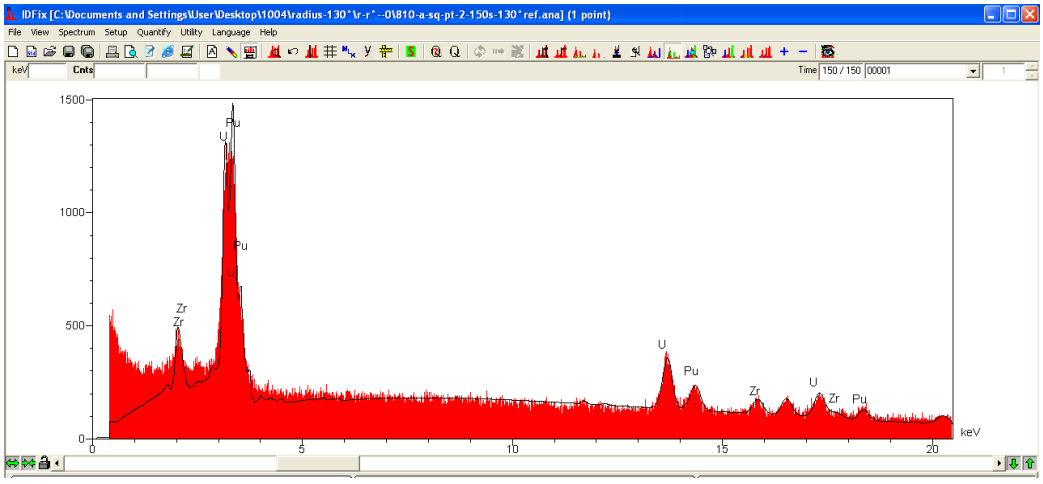

Fig. 3.2. Representative X-ray spectrum for fuel matrix phase for METAPHIX-1 showing the presence of U, Pu, Zr.

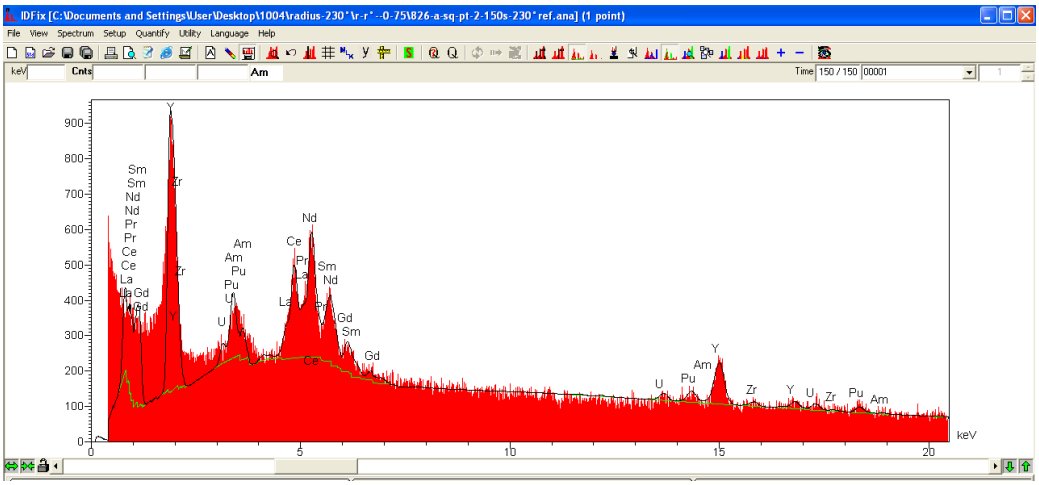

Fig. 3.3. Representative X-ray spectrum for RE phase precipitates for METAPHIX-1.

3.4 Electron Probe Micro Analysis (EPMA)

EPMA was performed using a state-of-the-art Cameca SX 100 R microprobe specially shielded with lead and tungsten to permit the analysis of irradiated nuclear fuel. The SX100 is equipped with four vertical spectrometers, two of which have quartz 1011 crystals installed for the analysis of actinides [2].

The shielded microprobe is located in a different location than the hot cells where the preparation of the sample is performed. Transporting of the sample to the microprobe laboratory while avoiding its oxidation is a major challenge. Successful

transport and introduction of the sample in the microprobe is achieved by keeping the sample under vacuum. A special version of the microprobe sample holder was designed for this purpose (Fig. 3.4). After sample preparation is completed, the specimen and the ring holding the reference materials are placed in the sample holder, and a dedicated cover put in place and sealed with a Viton o-ring. Finally, the container is vacuumed to 10^{-2} mbar, which ensures protection of the sample against oxidation during the transfer. Before the microprobe analysis is performed, the specimen is coated with a conducting film of aluminium approximately 20 nm thick to avoid charging effects.

a) **b)**

Fig. 3.4. Electron probe sample holder. (a): view of the top part of the sample holder with cover and Viton O-ring; (b): view from below of the modified sample holder showing the connection to the pumping system required to establish protective vacuum conditions against oxidation. Height: 34 mm. Cover diameter: 48 mm.

3.4.1 Quantitative analysis

Quantitative point analysis and mapping for the fuel and cladding components were carried out at an electron acceleration potential (E_0) of 25 keV and a beam current (I_b) of 250 nA. The dead time was fixed at 3µs. The matrix correction was made using the PAP [3] option in both the CAMECA PeakSight and Probe for EPMA® microanalysis programs. The conditions used for quantitative point analysis and the elemental mapping of all the elements analysed are summarised in table 3.1.

Spectral interferences

Spectral interferences (or peak overlaps) occur whenever the wavelength of the characteristic X-ray used for analysis is near to or coincides with the characteristic X-ray line of one or more matrix elements. This can lead to serious source of errors

in quantitative microanalysis [4]. Corrections for spectral interferences were performed using the databases for element X-ray lines from both the CAMECA PeakSight and Probe for EPMA® microanalysis programs. Table 3.1 lists the major interferences corrected.

3.4.2 Mapping

Extensive use of mapping was made during the analysis of fuel samples. This section describes the different modes of imaging used and the information obtained.

Electron images

Scanning electron micrographs prepared with SE, BSE or AE electron detectors provide information on compositional heterogeneity through the mechanism of atomic number contrast. Such images are used for characterising microstructures.

X-ray elemental mapping

Elemental images are obtained by displaying, for a given element, the characteristic X-ray signals derived from the spectrometers. The X-ray count rate is displayed in each pixel of the image as grey level and/or colour coded by use of image processing software packages. The information contained in the map is qualitative and is used to reveal the distribution or localisation of an element over an area of interest.

Compositional X-ray mapping

The quantification of element-specific X-ray maps requires the application of background and matrix corrections to obtain the true X-ray count in each pixel. After correction, each pixel has its own quantitative signature and the X-ray map consists of a matrix of grey levels.

3.4.3 X-ray spectra

An X-ray spectrum is a display of the intensity of X-rays as a function of the wavelength; it consists of a continuous bremsstrahlung spectrum on which are superimposed groups of sharp lines characteristic of the elements in the target. In this analysis, spectra were used for identifying the peak and background positions; this information is required for the quantitative analysis of each element, and to investigate the elements constituting the phases of interest.

3.5 X-ray diffraction for un irradiated measurement

XRD measurements were performed with a Bruker® D8 Advance diffractometer (Cu-Kα1 radiation) operated at 40 kV and 40 mA with a 2θ range of 10°–120° using 0.02° steps of 2 s of integration time per step. The material for the XRD measurement was a thin slice of the metallic alloy with shiny surface obtained by hand polishing for about 5 min (with sandpaper) [5].

Table 3.1. Conditions used for quantitative electron probe microanalysis.

Element	X-ray Line	Diffracting crystal	E_0 (KeV)	I (nA)	Standard	Interference corrections for
Fuel Components – Quantitative point analysis and mapping						
U	Mα	QTZ	25	250	UO_2	Pd
Pu	Mβ	QTZ	25	250	PuO_2	U, Zr, Fe
Zr	Lα	PET	25	250	ZrO_2	
Xe	Lα	QTZ	25	250	Sb	La
Am	Mα	QTZ	25	250	UO_2	U, Np, Pu
Np	Mα	QTZ	25	250	$NpAl_2$	U
Cm	Mβ	QTZ	25	250	UO_2	U, Pu, Ni
Cs	Lβ	LIF	25	250	Pollucite	La, Nd
Mo	Lα	PET	25	250	Mo	
Nd	Lα	LIF	25	250	$NdPo_4$	
Ru	Lα	PET	25	250	Ru	
Ce	Lα	QTZ	25	250	$CePo_4$	
Rh	Lα	PET	25	250	Rh	
Pd	Lβ	PET	25	250	Pd	
La	Lα	QTZ	25	250	$LaPO_4$	Nd, Cs
Pr	Lα	LIF	25	250	$PrPO_4$	Xe, La
Gd	Lα	LIF	25	250	Gd	La, Ce
Y	Lα	PET	25	250	YP_3O_9	
Sm	Lα	LIF	25	250	Sm	Ce, Nd
Cladding Components – Quantitative point analysis and mapping						
Ni	Kα	LIF	25	20	IRX glass	
Fe	Kα	LIF	25	20	Hematite	Ru
Cr	Kα	QTZ	25	20	Chromite	
Ti	Kα	PET	25	250	$SrTiO_3$	Pu
Mn	Kα	LIF	25	250	Mn	Cr, Pr

3.6 References

[1] T.Wiss, H.Thiele, B.Cremer and I.Ray, "Internal Conversion in Energy Dispersive X-ray Analysis of Actinide-Containing Materials", Microscopy and Microanalysis, 13, 196-203, (2007)

[2] C.T. Walker, “Electron probe microanalysis of irradiated nuclear fuel: an overview”, J. Anal. Atomic Spectrom., 14 (1999) 447-454.

[3] J.L. Pouchou and F. Pichoir, La recherche Aérospatiale 5 (1984) 167.

[4] J. Donovan; D. Asnyder and M. Rivers. An improved interference correction for trace element analysis. Microbeam Analysis, 2 (1993) 23-28

[5] L. Capriotti, P. Pöml, S. Bremier, D. Papaioannou, R. Eloirdi, T. Ogata, V. Rondinella, "Characterization of an as-prepared metallic nuclear fuel alloy containing minor actinides and rare earths", *in preparation*

Chapter 4

Un irradiated testing campaign

Characterization of the as-prepared metallic fuel alloy containing MA and RE is of paramount importance to understand the behaviour under irradiation of the fuel and to complement post irradiation examinations.
The investigations were carried out on samples of nominal composition U-19Pu-10Zr-2MA-2RE using EPMA and XRD. A detailed description of the different techniques can be found in chapter 3.

4.1 Materials

The details of the metallic fuel samples fabrication and some properties of the as fabricated fuels are reported in chapter 2.
Figure 4.1 shows the metallic fuel alloy archive material investigated in this chapter, protected in a quartz tube (fig. 4.1a) and after removal (fig. 4.1b) in November 2013. For visual comparison fig. 4.2 reports the metallic alloy at the time of preparation.

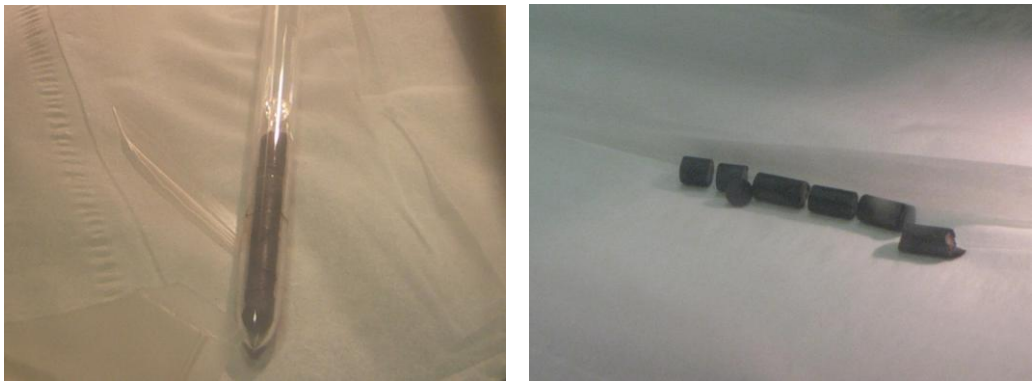

a) **b)**

Fig. 4.1. Fuel samples stored in a quartz tube and after removing them from the quartz tube.

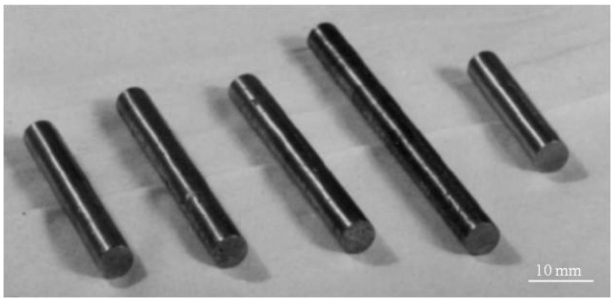

Fig. 4.2. Metallic alloy ingots at the time of preparation [2].

The characterisation of the un-irradiated metallic fuel alloys was performed twice. At the time of samples fabrication and in 2014 twenty years later. The sample composition in 2014 was recalculated using the free software Decay chain++ [4] for the alloy of composition U-19Pu-10Zr-2MA-2RE. The major changes in the composition appear to be the decay of Cm (46% reduction) and corresponding increase of Np, and the formation of He bubbles (Table 4.1).

Table 4.1. Specific composition values for Np, Am, Cm isotopes considering a mass of the alloy U-19Pu-10Zr-2MA-2RE at the time of preparation and after 20 years of storage.

Isotope	**Mass (g)**	
	0 y (1994)	**20 y (2014)**
93 Np237	1.229E+00	1.238E+00
95 Am243	3.936E-01	3.929E-01
93 Np239	0.000E+00	3.383E-07
95 Am241	2.740E-01	2.750E-01
96 Cm244	1.541E-01	7.137E-02
94 Pu241	1.583E-02	6.034E-03
96 Cm245	1.399E-02	1.397E-02
96 Cm246	1.128E-02	1.125E-02
94 Pu242	1.385E-03	1.449E-03
95 Am242 m	1.942E-03	1.760E-03
95 Am242	0.000E+00	2.273E-08
96 Cm242	0.000E+00	4.598E-06
96 Cm247	5.216E-04	5.216E-04
2 He4 Stable	0.000E+00	1.737E-03
Cm tot	1.799E-01	9.711E-02
Am tot	6.695E-01	6.696E-01

4.2 Measurements and results

4.2.1 XRD

In order to investigate the fine structure of the metallic alloy, XRD measurements were carried out. XRD spectra show a few broad peaks with a high background as shown in fig. 4.3. The broadening of the peaks is due to the intrinsic nature of the sample, not powder, but pellet slice, which is affected by surface texture and preferred orientation artefacts [5].

Literature reports that U-Pu-Zr alloys can consist of 4 different phases, mainly U-Pu ζ and δ – UZr_2 and a few percent of α-U and γ-U [5]. In fig. 4.3, the (2θ) positions of peaks observed by Burkes et al [5, 6] are reported for comparison. It can be concluded that the 2 spectra agree well regarding the main peak positions.

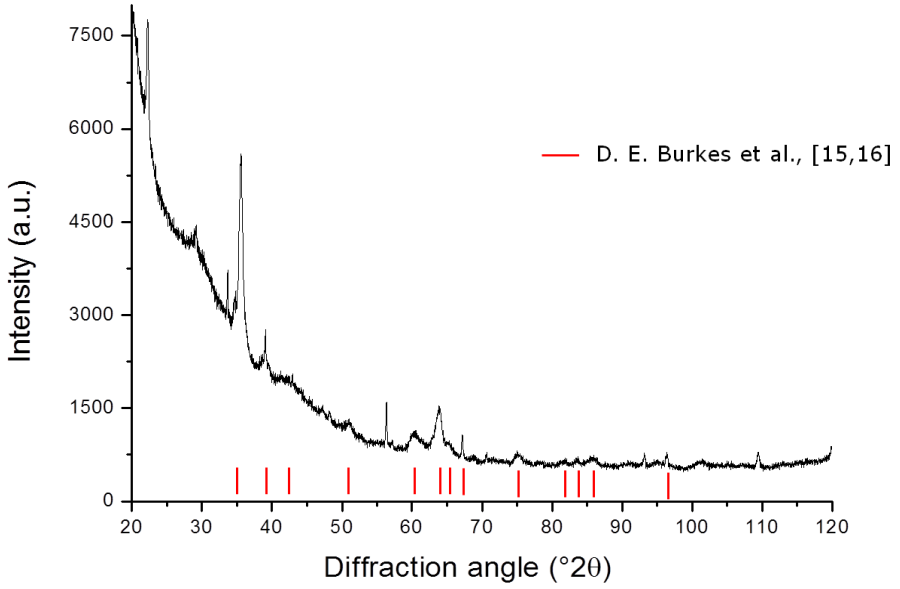

Fig. 4.3. XRD diffraction pattern of the U-Pu-Zr-2MA-2RE alloy. The peak positions of Burkes et al. [5, 6] are reported in red.

4.2.2 EPMA

A BSE image of the sample analysed by EPMA is visible in fig. 4.4. Regions containing heavy elements are lighter in colour, while light elements regions appear darker in colour. The fuel sample presents a complex configuration with a fuel matrix, secondary phases dispersed along the radius and pores appearing in black.

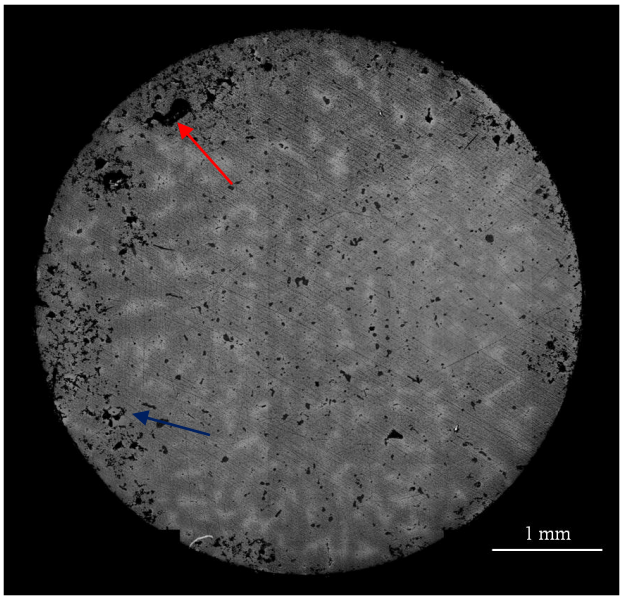

Fig. 4.4. BSE of the U-Pu-Zr-2MA-2RE sample. The red arrow identifies a big pore, while the blue arrow indicates the secondary phases (in dark grey).

Fuel matrix

The fuel matrix appears not homogenous with dark and light grey areas. This is related to the different contents of U and Zr, while Pu and Np are maintaining approximately the same concentration everywhere. Am is also present as reduced amount (0.4-0.5 wt.%) in both phases. The fuel matrix results in 2 phases, high Zr matrix (dark grey) and low Zr matrix (light grey). Table 4.2 reports the compositions of the 2 phases.

Table 4.2. Average composition of the two matrix phases ("low Zr matrix", "high Zr matrix") in wt.% . The oxidation of the sample was estimated around 5 wt. % averaged on the fuel sample.

	Low Zr	High Zr
U	67.00 ± 4.54	58.69 ± 3.36
Pu	7.22 ± 1.08	8.35 ± 1.30
Zr	5.10 ± 1.44	11.49 ± 1.74
Np	1.14 ± 0.07	1.05± 0.08
Am	0.38 ± 0.18	0.51 ± 0.15

Secondary phases

Secondary phases exhibit 2 distinct compositions, one enriched in Zr and one enriched in RE-(Am, Cm). An absorbed electron image of the sample is shown in figure 4.8. Regions containing heavy elements are darker in colour, while light elements regions appear lighter in colour. Zr-rich phases were found mainly at the periphery of the fuel sample as agglomeration of particles (fig. 4.5). Fig. 4.6, selected from the area highlighted in the red square of fig. 4.5b, reports qualitative false colour X-ray maps as an illustration of the two secondary phases. RE-(Am, Cm) precipitates are mainly constituted of Cm, Am, Nd, Gd, Ce. Np is mostly present in the matrix surrounding the different precipitates.

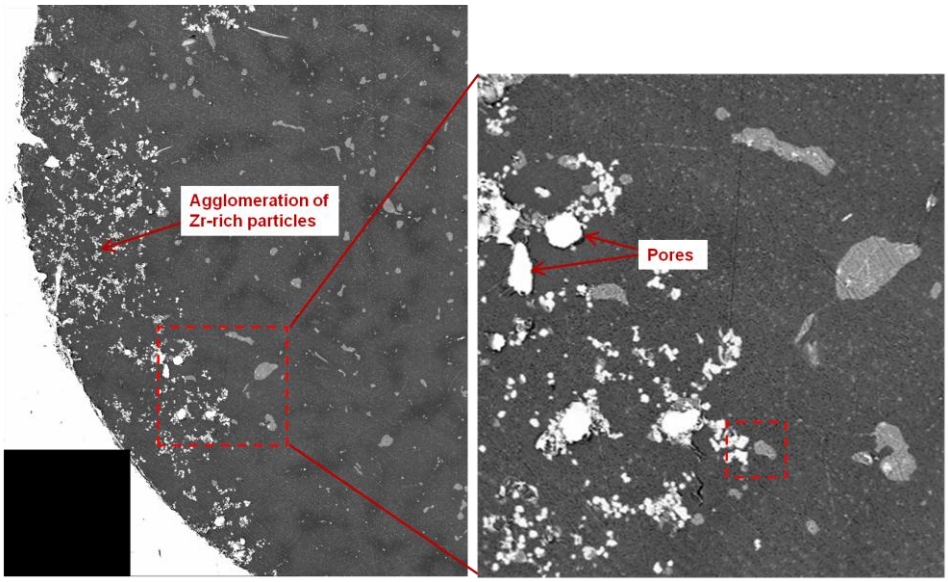

a) b)

Fig. 4.5. AE image (a) showing the periphery of the fuel sample (left bottom corner of figure. 4.4). Agglomeration of Zr-rich particles is visible together with several pores; (b) the position selected for collecting the X-ray maps shown in fig. 4.6 is shown in fig. 4.5b as a red square.

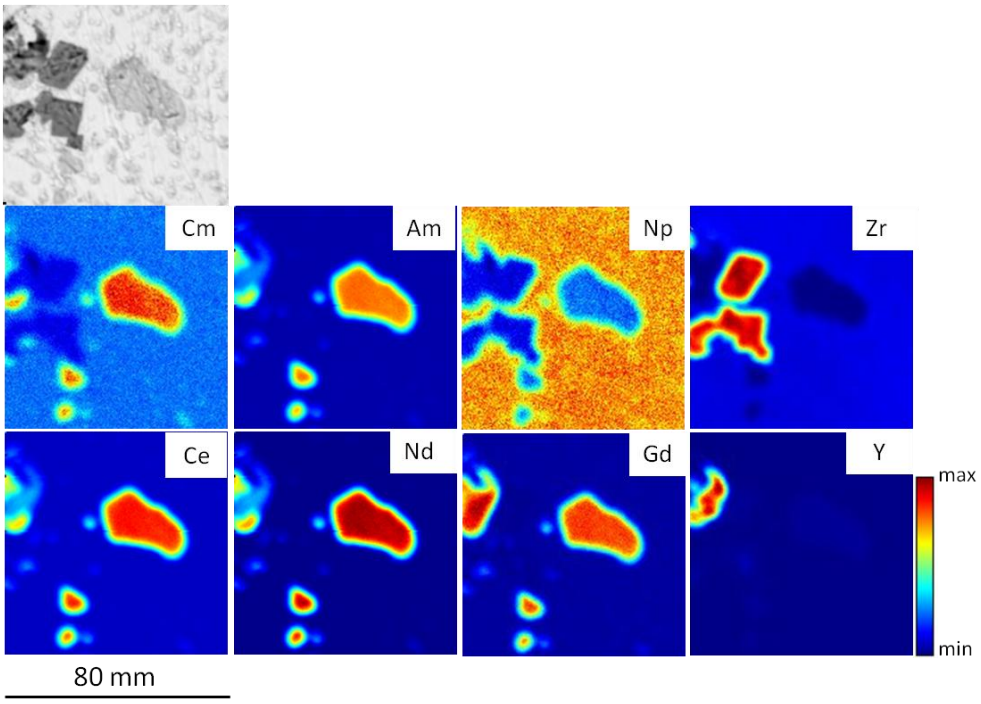

Fig. 4.6. BSE image and qualitative false colour X-ray maps for Zr-rich and RE-(Am, Cm) rich precipitates, r/r_0 = 0.75 (r/r_0= 1 periphery, r/r_0= 0 centre).

RE-(Am, Cm) rich phases were more homogenously distributed along the fuel radius than the Zr precipitates. Fig. 4.7 shows qualitative false colour X-ray maps taken from the central region of the fuel sample. The main elements observed in the second phase are the same as those identified in fig. 4.6. The different apparent concentration levels inside the precipitate can be attributed to the removal or deposition of material during the process of manual grinding and polishing.

The composition of the second phases was measured by quantitative point analysis. Table 4.3 reports the average compositions of the 2 different precipitates.

In the Zr-rich precipitates the only other element measured in concentrations of few wt.% is U; in the RE-(Am, Cm) phase, minor actinides Am, Cm are quantified as (6.88 ± 1.02) wt.% and (2.98 ± 0.40) wt.%, respectively. Among the initial constituents of the fuel, only Pu is measured up to 12 wt.%

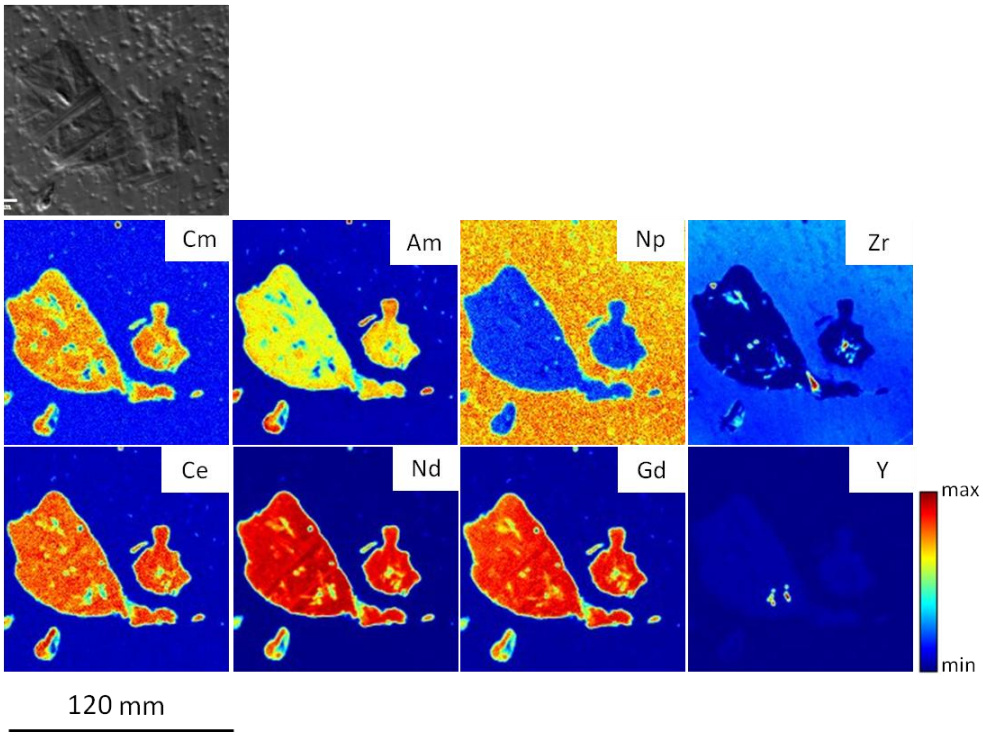

Fig. 4.7. BSE image and qualitative false colour X-ray maps of RE-(Am, Cm) rich precipitates, $r/r_0 = 0.30$ ($r/r_0 = 1$ periphery, 0 centre).

Table 4.3. Average compositions of Zr-rich and RE-(Am, Cm)-rich precipitates in wt.%. The oxidation of the sample was estimated around 5 wt. % averaged on the fuel sample.

El	Zr-rich	RE-MA
U	2.05 ± 0.69	0.50 ± 1.58
Pu	0.47 ± 0.25	12.34 ± 1.50
Zr	64.08 ± 2.89	0.38 ± 0.46
MA		
Np	-	0.12 ± 0.04
Am	-	6.88 ± 1.02
Cm	-	2.98 ± 0.40
RE		
Y	0.46 ± 0.27	1.37 ± 0.43
Ce	-	4.73 ± 0.44
Nd	0.19 ± 0.36	55.08 ± 3.77
Gd	0.13 ± 0.04	6.19 ± 0.44

The measurements of the Zr-rich phase resulted in a very low total concentration: ~70-75 wt.% including oxygen. However, from the analysis of X-ray spectra, no

others elements were detected. Considering the elements identified in this phase, it is very likely that the Zr count rate is underestimated. After careful verification of the standards and other relevant parameters for the quantification (dead time, overlap corrections) it was not possible to find an unequivocal explanation for this technical issue.

4.3. Discussion

4.3.1 Microstructure

The microstructure of the metallic alloy U-Pu-Zr-2MA-2RE is characterized by various features.

The fuel matrix is composed of U, Pu, Np and Zr, but it is not homogenous and presents two different compositions where U and Zr are enriched or depleted, respectively. This finding is in line with Janney et al. [7] who analysed different U-Pu-Zr alloys with various amounts of MA and RE.

Np behaves very similarly to Pu in the matrix and it is not found in any of the secondary phases.

Am is found mainly in the secondary phases alloyed with RE (between 6-8 wt.%) and is also found in the matrix up to 0.5 wt.%. Janney et al. [7, 8] also observed the presence of Am in the matrix (1-2 wt.%) as well as in RE-rich precipitates.

Cm is found only in the precipitates with RE and Am. Since Cm is chemically and thermodynamically in affinity with Am, Cm was expected to behave alike; however, direct comparison with other studies is not possible since the METAPHIX project is the only one containing this particular actinide.

Zr-rich particles are detected by EPMA mainly in the outer part of the fuel sample in agglomeration of particles where Zr is likely to react with the yttria crucible, as shown in fig. 4.5a. Zr-rich precipitates were already observed in other metallic fuel alloys with or without MA [7, 9]. Zr-rich inclusions were thought to be α-Zr stabilised by impurities such as O, C, or N in the feed during preparation [9, 10]. New electron diffraction data showed that the structure is FCC and the authors suggest a nanocrystalline formation of ZrO_2 [10].

The composition of the RE rich phase is well consistent with studies presented in the literature [7, 8]. In a recent work by Janney et al. [11], two different RE rich phases were reported. However it was asserted by the authors that one of the RE phase was the result of oxidation of the material during casting.

4.3.2 Phase determination

The determination of the different phases of the U-Pu-Zr matrix in the arc-melted fuel was possible using EPMA point analysis measurements.

Since there is no phase diagram examining the U-Pu-Zr-Np-Am system, the phase determination was performed only on the ternary U-Pu-Zr.

To reduce the two compositions to the main elements U, Pu, Zr, the same argumentation as in [5, 6] was taken as guideline. Considering minimal solubility between Am and U and since Np is soluble with both U and Pu, Am was added to U and Np was evenly divided between U and Pu.

Finally, the reduced compositions were U-20Pu-5Zr for the low and U-21Pu-12Zr for the high Zr matrixes respectively. Using the only U-Pu-Zr phase diagram extrapolated to room temperature published in the literature [5] and reported in fig.4.8, it is possible to finally determine the different phases present in the studied metallic alloy.

For both compositions the corresponding major phases are U-Pu ζ and $\delta - UZr_2$ in different amount. The high Zr-matrix (green dot in fig. 4.8) is a pure $\zeta+\delta$ phase, while the low Zr-matrix (red dot in fig. 4.8) also includes α-U.

This finding confirms what was speculated from the comparison between XRD diffraction pattern and literature [5, 6]. Furthermore, these results are in general agreement with the finding reported by other authors on metallic alloys containing MA and RE in different compositions [5-8].

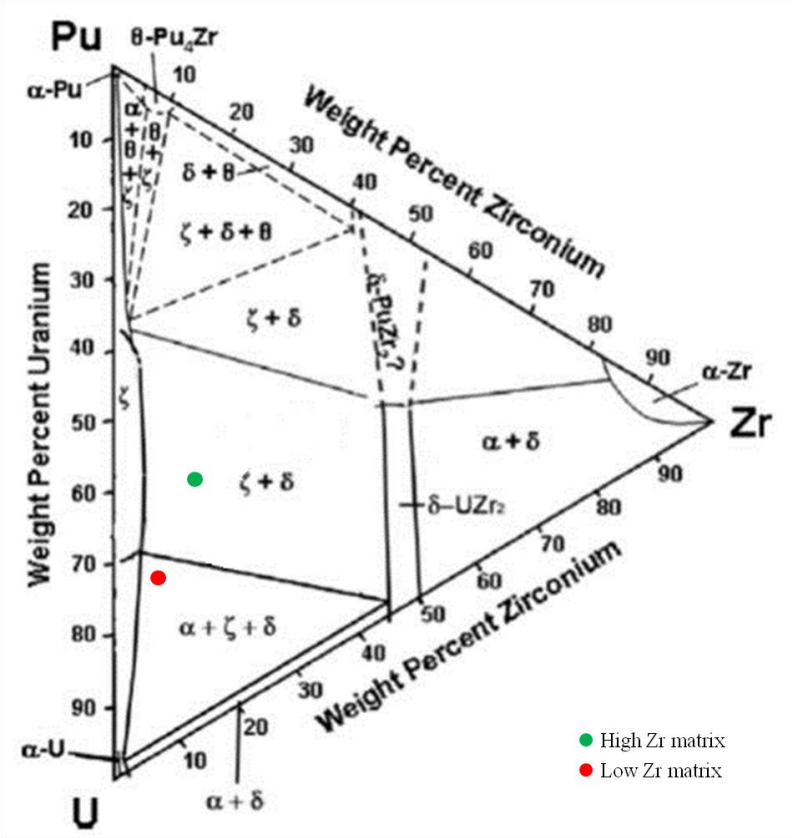

Fig. 4.8. U-Pu-Zr ternary phase diagram extrapolated to room temperature by Burkes et al. [5]. The coloured dots correspond to the compositions of the phases determined in this work for U-21Pu-12Zr (green dot) and U-20Pu-5Zr (red dot).

4.4 References

[1] M. Kurata, A. Sasahara, T. Inoue, M. Betti, J.-F. Babelot, J.-C. Spirlet, L. Koch, "Fabrication of U-Pu-Zr Metallic Fuel Containing Minor Actinides", Proc. Int. Conf. Future Nuclear Systems, Global '97 (1999) 1384-1389.

[2] J.-P. Glatz, T. Koyama, "Demonstration of Minor Actinide Recycling with Metal Fuel (I) Overview of the METAPHIX – PYRO Project", Proc. GLOBAL 2015, 1757-1763

[3] H. Ohta, T. Ogata, D. Papaioannou, V.V. Rondinella, M. Masson, J-L Paul, "Irradiation of Minor Actinide-Bearing Uranium-Plutonium-Zirconium Alloys up to ~2.5 at%, ~7 at.% and ~10 at.% Burnups", Nucl. Technol., 190, 36-51 (2015).

[4] Decay Chain++, Nucleonica web driven nuclear science, www.nucleonica.net

[5] D. E. Burkes, J. R. Kennedy, T. Hartmann, C. A. Papesch, Dennis D. Keiser Jr., "Phase characteristics of a number of U-Pu-Am-Np-Zr metallic alloys for use as fast reactor fuels", J. Nucl. Mater., 396 (2010) 49-56

[6] D. E. Burkes, J. R. Kennedy, T. Hartmann, C. A. Papesch, "Phase characteristics of a U-20Pu-3Am-2Np-15Zr metallic alloys containing rare earths", Nucl. Eng. Des., 239 (2009) 2747-2753

[7] D. E. Janney, J. R. Kennedy, "As-cast microstructures in U-Pu-Zr alloy fuel pins with 5-8 wt.% minor actinides and 0-1.5 wt.% rare-earth elements", Mater. Charact., 61 (2010) 1194-1202

[8] D. E. Janney, J. R. Kennedy, J. W. Madden, T. P. O'Holleran, "Am phases in the matrix of a U–Pu–Zr alloy with Np, Am, and rare-earth elements", J. Nucl. Mater, 456 (2015) 46–53

[9] C. L. Trybus, J. E. Sanecki, S. P. Henslee, "Casting of metallic fuel containing minor actinide additions", J. Nucl. Mater., 204 (1993) 50-55

[10] D. E. Janney, J. R. Kennedy, J. W. Madden, T.P. O'Holleran, "Crystal structure of high-Zr inclusions in an alloy containing U, Pu, Np, Am, Zr and rare-earths elements", J. Nucl. Mater., 448 (2014) 109-112

[11] D. E. Janney, J. W. Madden, T. P. O'Holleran, "High- and low Am RE inclusions phases in U-Np-Pu-Am-Zr alloy", J. Nucl. Mater., 458 (2015) 106-114

Chapter 5

Behaviour in pile of METAPHIX experiment

The behaviour under irradiation of metallic fuel is complex and characterized by many phenomena such as redistribution of main fuel elements, secondary phases and FCCI. Those phenomena are influenced by many factors, the most important being burnup, temperature radial profile and chemistry changes along the radius. The system grows in complexity when MA and/or RE are added during fabrication of the fuel.

Characteristics of irradiated metallic fuel (such as redistribution of main fuel constituents or fission gas swelling) have been studied for many years and are known [1]; other aspects (e.g. FCCI or the mechanisms responsible for secondary phases distribution) are not yet fully understood [1, 2]. Concerning MA and/or RE behaviour, very few studies are available [2].

In this chapter, the behaviour of metallic fuel with MA and/or RE is analyzed and compared with basic alloy focusing onto 3 main topics: redistribution of fuel constituents, secondary phases, and FCCI. These features are studied and characterized quantitatively mainly by EPMA, and investigated qualitatively by OM and SEM.

5.1. Redistribution of main fuel elements

A major feature of the behaviour in reactor of metallic fuel is the redistribution of the main fuel elements, namely U, Zr and Pu. This phenomenon has been observed and studied extensively [1-3] on metallic fuel systems like U-Zr, U-Pu-Zr and its main driving force was identified as the Soret thermochemical effect [1, 3]. Several computational efforts were made; however, a strong and complete model for simulating the performance of the metallic fuel is yet to be implemented [4-5].

Restructuring processes, indicated by various microstructure morphologies exhibiting different phase compositions, are also observed along the irradiated fuel radius,. Restructuring is strongly dependent on the irradiation temperature. When the fuel central temperature is higher than 923 K, alloy U-19Pu-10Zr forms a bcc γ phase and the cross section of the fuel pin exhibits a 3-ring structure. If the temperature condition to form γ phase is not met, a 2-ring structure is normally observed.

Fig. 5.1 shows the phase transition temperatures for U-Pu-Zr systems [2].

Redistribution and restructuring effects are also correlated; Porter [6] observed that the fuel restructuring precedes the constituent migration during the initial stage of irradiation.

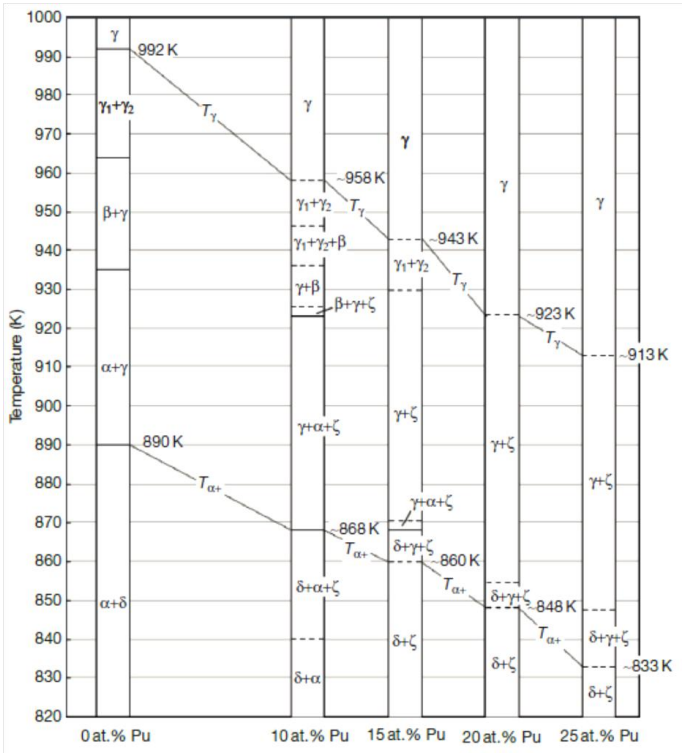

Fig. 5.1. Phase transition temperature of U-Zr and U-Pu-Zr alloys estimated from O´Boyle and Dwight [7], from [2].

Figs. 5.2 (cross section) and 5.3 (higher magnification of a radial profile) illustrate a 3 region metallic fuel cross section, exhibiting various degrees of porosity of a U-Pu-Zr metallic fuel containing 5 wt.% of MA and 5 wt.% of RE with burnup of 2.5

at.%. The central part (in fig. 5.2) appears to be separated from the rest of the fuel by a circular crack (or fuel-fuel gap) and large fission gas bubbles, characteristic of the high temperature phase (γ-phase), are visible. A BSE high magnification image of the gas bubbles is shown in fig. 5.4(a). Second phase precipitates are also visible in this region (fig. 5.4(b)) and are inferred to be agglomerates of MA and fission products [8]. The intermediate radius region is characterized by a dense phase, considered to be ζ-phase [2], together with relatively large voids (fig. 5.5(a)). In the periphery, a highly porous phase and a second phase are present (inferred to be rich in fission products and RE [8]), as shown in fig. 5.5(b).

Fig. 5.6 shows representative EDX radial profiles for the main constituents (U, Pu, Zr) of a fuel pin exhibiting a 3 regions redistribution [8]. Zr and U present inverse behaviour, with the former enriched in the center of the fuel and periphery.

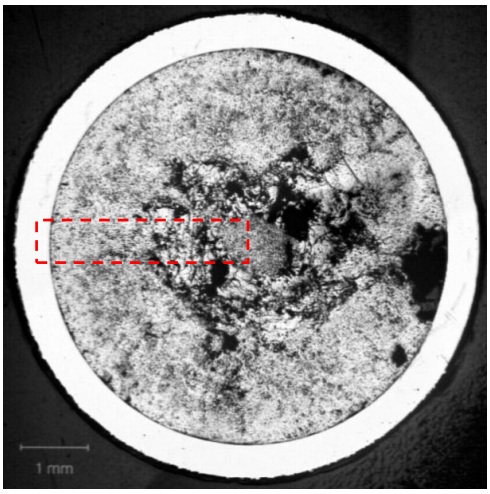

Fig. 5.2. Macrograph of a U-Pu-Zr metallic fuel containing 5 wt.% of MA and 5 wt.% of RE at 2.5 at.% burnup.

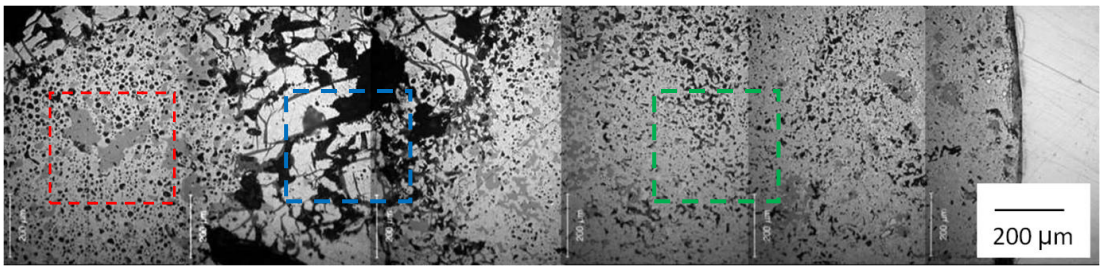

Fig. 5.3. Detailed radial profile from Fig. 5.2 (red dashed rectangle) of a U-Pu-Zr metallic fuel containing 5 wt.% of MA and 5 wt.% of RE.

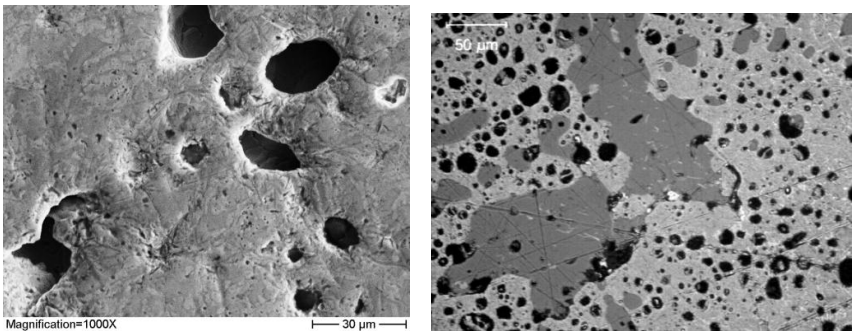

a) **b)**

Fig. 5.4. High magnification BSE of the central region of fig. 5.3. (red dashed rectangle) showing a) fission gas bubble; b) agglomerates of MA and fission products.

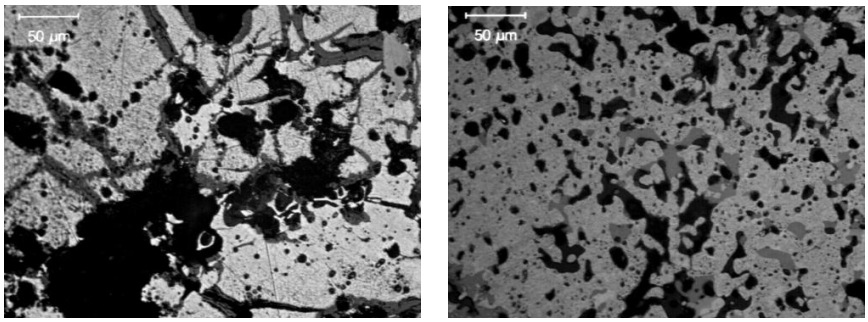

a) **b)**

Fig. 5.5. High magnification BSE of fig. 5.3. showing a) a dense phase in the intermediate radius region (blu dashed rectangle); b) high porosity and secondary phases in the periphery region (green dashed rectangle).

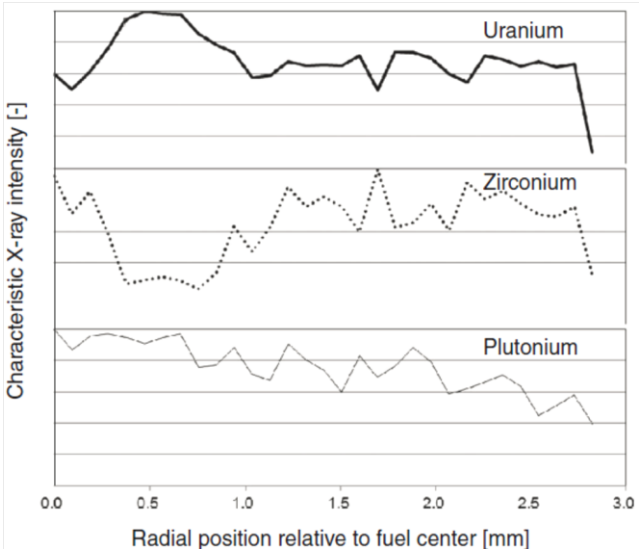

Fig. 5.6. Radial distribution of the characteristic X-ray intensity for the main fuel elements (U, Pu, Zr) measured by EDX for low burnup METAPHIX-1 [8].

Figs. 5.7 and 5.8 display a 2 regions microstructure fuel in which the fuel center temperature did not reach 923 K during irradiation, so the γ phase is not present. The central region appears as a dense phase with both intragranular and intergranular fine porosity where no precipitates are visible.

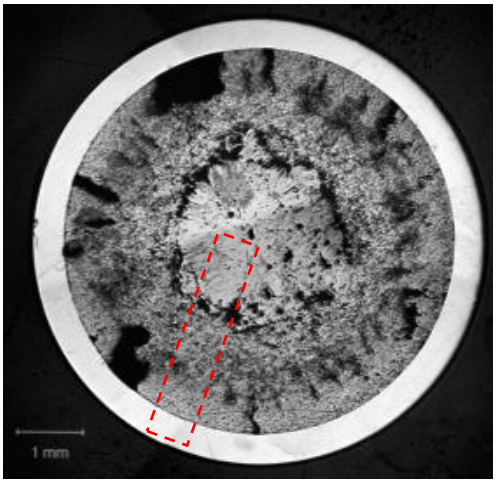

Fig. 5.7. Macrograph of a U-Pu-Zr metallic fuel at 2.5 at.% burnup.

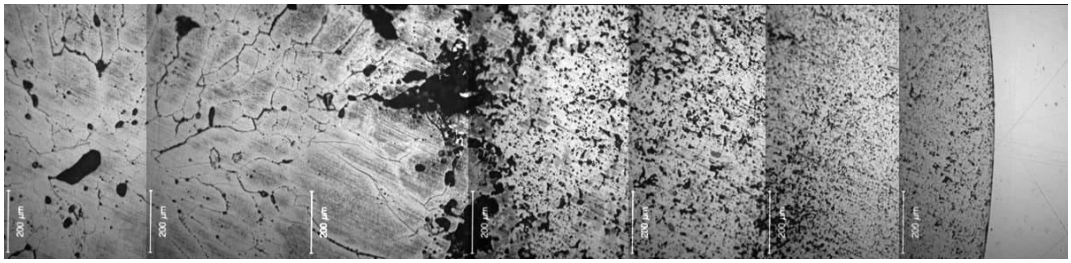

Fig. 5.8. Detailed radial profile from fig. 5.8 of a U-Pu-Zr metallic fuel at 2.5 at.% burnup.

To deepen the investigation using quantitative data, two metallic fuel samples (a basic metallic alloy, and a fuel pin containing additions of MA and RE) have been extensively investigated by EPMA. The results of the EPMA investigation and the related discussions are described in the next two sections.

5.1.1. Basic alloy U-Pu-Zr

EPMA was performed on a sample of U-19Pu-10Zr basic alloy from METAPHIX-2. Fig. 5.9 and 5.10 [9-10] show relevant macrographs illustrating the morphologies

observed. The sample was cut 480 mm from the bottom of the fuel stack; this location corresponds to the highest burnup, 6.9 at.%.

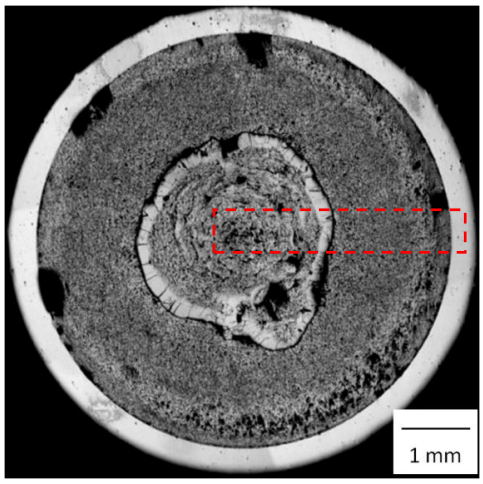

Fig. 5.9. Macrograph of a U-Pu-Zr metallic fuel sample at 6.9 at.% burnup.

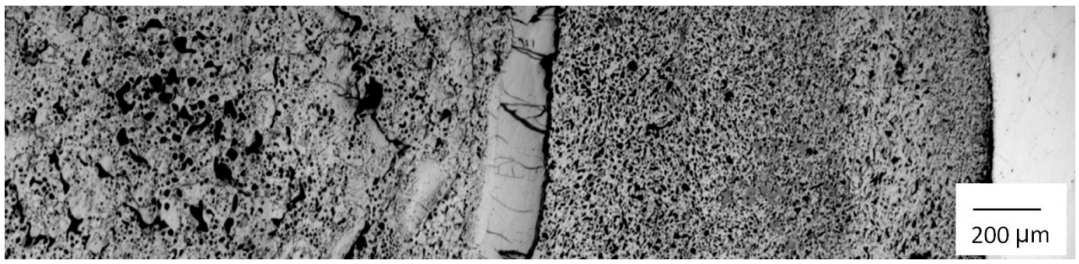

Fig. 5.10. Detailed radial profile from fig. 5.9 (red dashed rectangle) of a U-Pu-Zr metallic fuel sample at 6.9 at.% burnup.

The calculated end of irradiation temperatures are 923 K in the centre of the fuel and 803-823 K at the fuel-cladding interface, as reported in Chapter 2 section 2.2.1. EPMA has the capability to quantitatively measure the chemical composition of the fuel elements, fission products and precipitates (quantitative point analysis). The point analysis results correlated with published ternary phase diagrams such as U-Pu-Zr experimentally measured by O´Boyle and Dwight [7] and calculated by Kurata et al. [11], allowing the identification of the different phases in the fuel matrix. Fig. 5.11 reports an example of measured and calculated phase diagrams used in this study at 868 K.

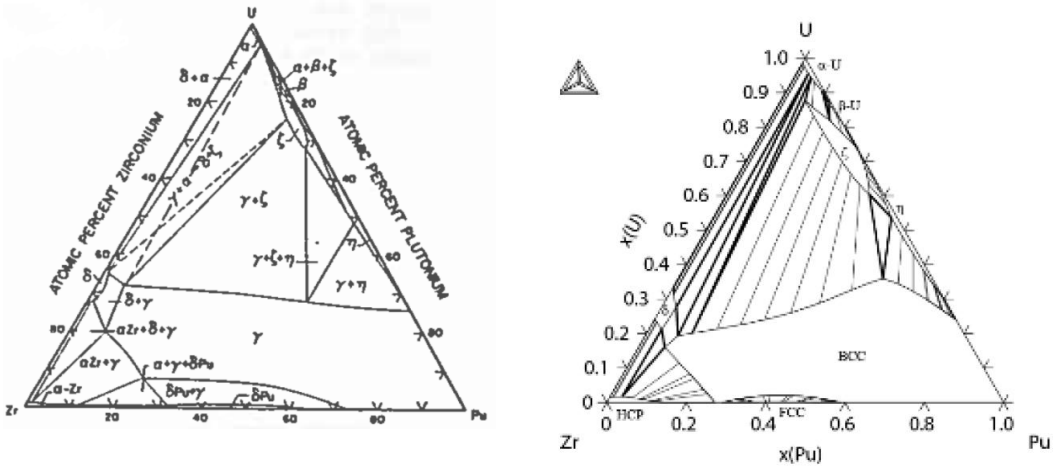

a) **b)**

Fig. 5.11. Examples of U-Pu-Zr ternary phase diagrams at 868 K; a) experimentally measured by O´Boyle and Dwight [7]; b) calculated by Kurata [11].

The distribution of the main fuel elements (U, Pu, Zr) was assessed by X-ray mapping. Fig. 5.12 shows the qualitative (re)distribution of U, Pu, Zr in the irradiated fuel. The 3 different regions are labelled 1, 2, 3 and indicated in the AE image for easier identification. In fig. 5.13 (a), (b), (c) the results of the quantitative concentration analysis for the three main fuel elements are plotted.

In the centre of the fuel (region 1 in fig. 5.12) an almost complete depletion of Zr is observed (also visible in fig. 5.13 (b)). Moreover, Pu and U (fig. 5.13 (a) and (c)) formed two heterogeneously distributed phases ("core phase I and II", respectively) with different U/Pu ratio (fig. 5.14). The almost complete depletion of Zr in this region is the main reason justifying the assumption that the temperature at the end of the irradiation was around 873 K; this is not in contradiction with the temperature profile calculated by ALFUS because it is within the 10% uncertainty affecting the irradiation parameters ([12] Ohta et al., 2009). Taking in consideration this aspect, the ternary phase diagram at 868 K from [11] identifies as β-U and ζ phases the core phase I and II, respectively.

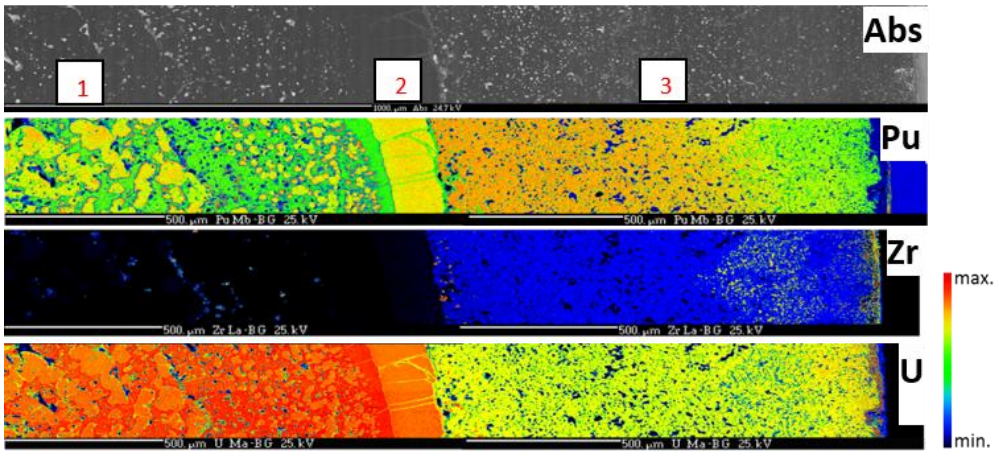

Fig. 5.12. Large area qualitative X-ray maps obtained by EPMA illustrating the redistribution of the main fuel elements (Pu, Zr, U) in a METAPHIX-2 U-Pu-Zr sample [9-10]. The different regions are labelled (1, 2, 3) in the AE image.

In the "dense phase" or "crust" stripe at mid-radius (region 2 in fig. 5.12), the Zr content is very low; this region consists of a single phase, identified as the ζ phase in the ternary diagram at 823 K. This dense phase is characterised by a very fine porosity (fig. 5.15) as described in [3].

From mid-radius to the periphery of the fuel (region 3 in fig. 5.12), the microstructure is very porous. U and Pu exhibit symmetric radial profiles; the Pu concentration is decreasing close to the periphery (fig. 5.13 (c)) and the Zr content in the fuel matrix is close to its nominal, as-fabricated value. A Zr-rich phase is also present in the outer radial region, as seen in fig. 5.11 (a) ("outer Zr-rich").

Taking in consideration the U-Pu-Zr phase diagrams at 823 K (close to mid-radius) and 773 K (radial periphery of fuel) from [7], the matrix fuel phases are estimated to be a mixture of ζ, δ and α-U; the appearance of the fuel in this region is quite heterogeneous. Characteristic of this fuel microstructure is the high degree of porosity and distorted configuration that is associated with a high content of α-phase U [1, 2].

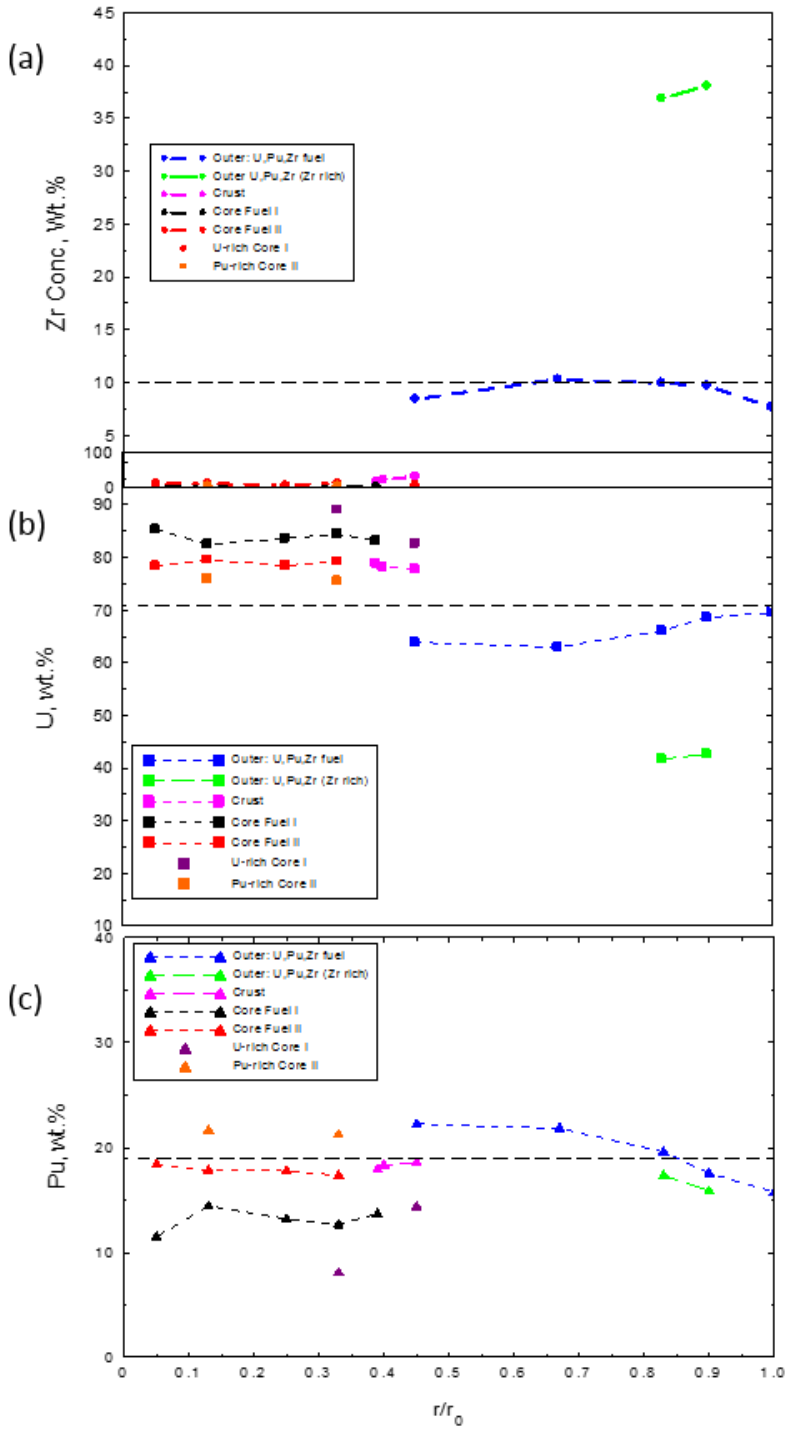

Fig. 5.13. Concentration and redistribution profiles of the main fuel elements along the radius of a METAPHIX-2 U-Pu-Zr sample: (a) Zr, (b) U (c) Pu [10, 13].

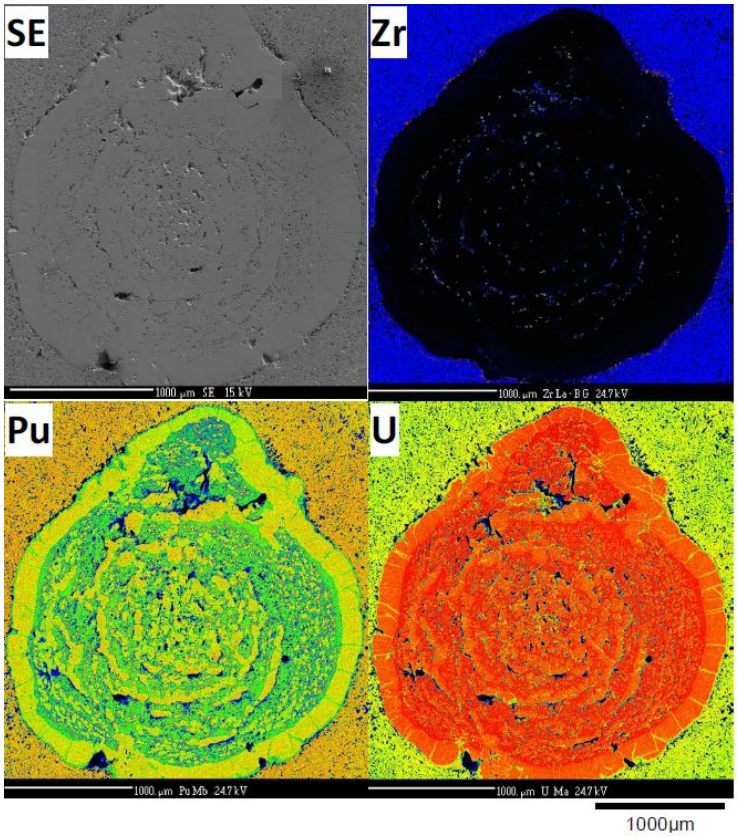

Fig. 5.14. SE image and large area qualitative X-ray mapping for Zr, Pu and U in the centre of the fuel sample.

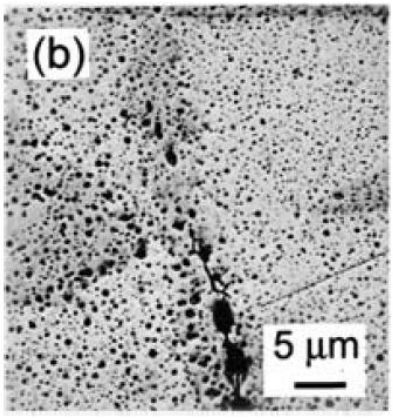

Fig. 5.15. SEM image illustrating the very fine porosity of the "dense phase"; image taken from ref. [3].

Table 5.1 describes schematically all fuel phases identified, their relative radius position and corresponding temperature, the range of composition for the fuel elements measured by point analysis and the corresponding fuel phases.

As a summary it is possible to draw of the following considerations.

Zr is totally depleted in the fuel centre and present with very few wt.% in the "crust" phase; however, assuming that no axial migration of Zr is expected in the fuel pin [14], the Zr inventory is balanced by the presence of the Zr-rich secondary phases or precipitates, which will be described in more details in section 5.2.

Concerning the different phases in the centre of the fuel, careful examination of the high magnification SE and X-ray images obtained in this region could suggest a γ phase morphology since the images reveal the presence of big pores and gas bubbles [1, 2]. However, quantitative composition analysis as described before is contradicting this conclusion. This apparent contradiction could be explained according to Porter's description [6]; he observed that the fuel restructuring precedes the constituent migration during the initial stage of irradiation. In the present case, at the beginning of the METAPHIX irradiation the conditions to form the ternary γ phase were met, hence the corresponding (and observed) morphology could be established. In later stages of the irradiation, changes in the temperature conditions enabled the relocation of Zr towards the outer regions of the fuel in precipitates or secondary phases, without affecting the morphology of the central region.

The effect of the Zr depletion in the central area of the fuel on the fuel integrity needs to be assessed with regards to risks of local occurrence of liquid phase or melting. To this aim, in order to assess the temperature that could be reached in the centre of the fuel, the 'worst case' situation was simulated. This worst case situation includes: outside temperature of 843 K; linear power of 313 W/cm [15]; a redistribution of Zr outside of the central area as observed in the sample after 6.9 at.% burnup; an outer fuel/fuel gap of 56 μm close to the crust region filled with Kr; 80% of the porosity at the periphery filled with Na. The porosity radial profile was taken from Ogata [4]. The thermal conductivities for the fuel, for Na and for the fission gas Kr were taken from Yun [16] and Lassmann [17] respectively. Under these conservative conditions the maximum temperature of the fuel in the central area was calculated to reach 1010 ± 70K [10]. The binary phase diagram for U-Pu (fig. 5.16) for a range of compositions between 80 and 85 at.% U [18] indicates that

the presence of liquid is observed only at temperatures higher than 1220K confirming that the conditions for melting were not fulfilled.

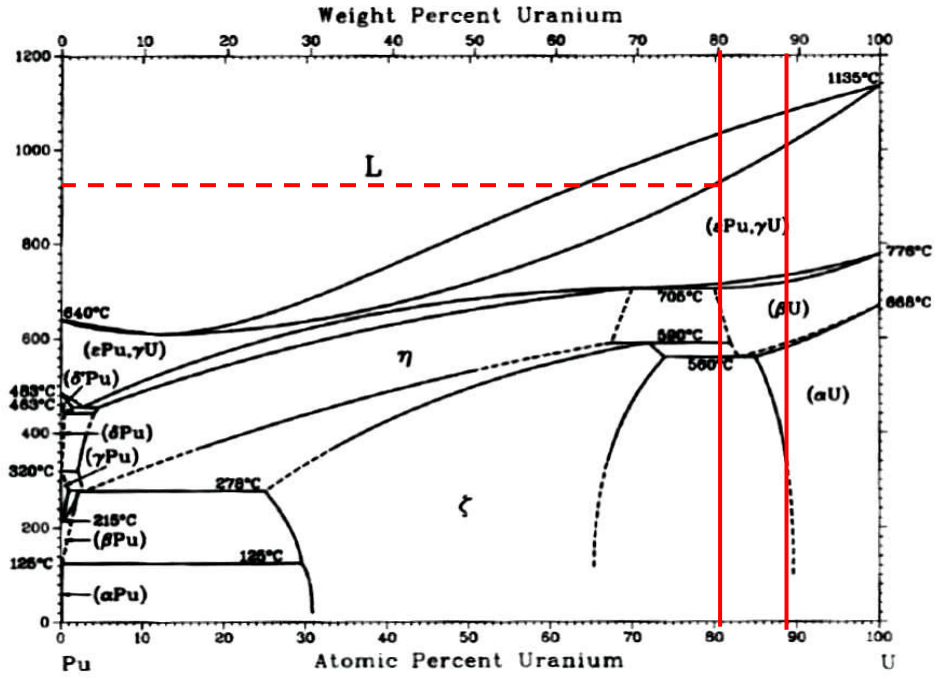

Fig. 5.16. U-Pu phase diagram [18]; the red lines indicate the range of compositions taken in consideration for maximum temperature assessment.

Table 5.1. EPMA results for the fuel phases observed along the radius of the METAPHIX-2 U-Pu-Zr sample.

Phase	r/r_0 (1)	U (wt.%) (2)(3)	Pu (wt.%) (2)(3)	Zr (wt.%) (2)(3)	Phase diagram T (K)	Estimation of phase
Outer fuel	> 0.9	69.54 (2.01)	15.76 (0.41)	7.67 (1.02)	773	$\delta + \alpha + \zeta$
Outer fuel	0.45 – 0.9	62.97 (0.53) 68.59 ((0.55)	17.57 (0.57) 22.24 (0.19)	8.45 (0.11) 10.27(0.10)	773	$\zeta + \delta$
Outer Zr-rich fuel	0.83 – 0.9	42.64 (0.59)	15.89 (0.48)	38.05 (0.37)	773	δ
U-rich Core I	0.45	82.69 (0.06)	14.41 (0.01)	0.28 (0.01)	823	α-U
Crust	0.39 – 0.45	77.75 (0.51) 78.90 (0.66)	17.96 (0.26) 18.58 (0.26)	0.64 (0.16) 1.12(0.22)	823	ζ
Core I	0.05 – 0.39	82.52 (0.93) 85.33 (2.93)	11.51 (2.86) 14.43 (1.22)	0.11(0.02) 0.15 (0.03)	868	β-U+ζ
U-rich Core I	0.33	89.06 (1.04)	8.10 (0.94)	0.14 (0.04)	868	α-U
Core II	0.05 – 0.33	78.36 (0.92) 79.58 (0.86)	17.34 (0.94) 18.41(1.01)	0.25 (0.05) 0.45(0.19)	868	$\zeta + \beta$-U
Pu-rich Core II	0.13 – 0.33	75.90 (0.29) 77.53 (0.86)	21.27 (0.02) 21.66 (0.14)	0.17(0.02) 0.22(0.19)	868	ζ

(1) Relative radius. 0 is the centre and 1 is the surface of the sample.

(2) Range of concentrations measured when applicable.

(3) The uncertainty (2 standard deviations) is shown in parentheses.

5.1.2. U-Pu-Zr-5MA-5RE

EPMA was performed on a sample of U-19Pu-10Zr-5MA-5RE from medium burnup METAPHIX-2. Figs. 5.17 and. 5.18 [19] show relevant macrographs illustrating the morphologies observed. The sample was cut 370 mm from the bottom of the fuel stack; this location corresponds to the highest burnup, ~ 6.5 at.% for this pin.

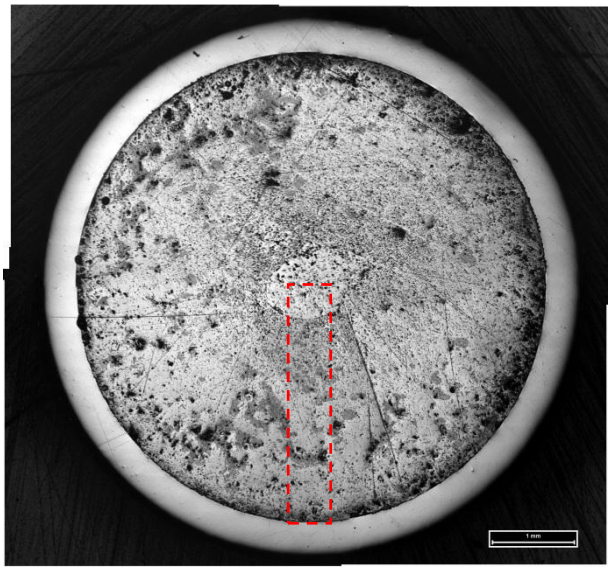

Fig. 5.17. Macrograph of a U-19Pu-10Zr-5MA-5RE metallic fuel sample at 6.5 at.% burnup.

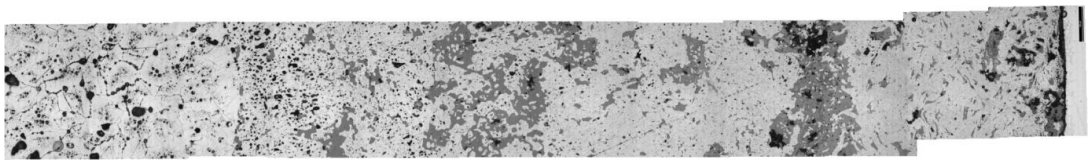

Fig. 5.18. Detailed radial profile from fig. 5.16 of a U-19Pu-10Zr-5MA-5RE metallic fuel sample at 6.5 at.% burnup.

The calculated temperatures at end of irradiation are 873-883 K in the fuel centre and 773-783 K at the fuel-cladding interface, as reported in chapter 2 section 2.2.1. The 2 OM images revealed a 2 regions microstructure along the fuel radius, very similar to that shown in figs. 5.7-5.8, in which the central region appears as a dense phase where no precipitates / secondary phases are visible.

The distribution of the main fuel elements U, Pu, Zr and Np was assessed by X-ray mapping and is shown in fig. 5.19. In fig. 5.20 the results of the quantitative concentration analysis for the three main fuel elements and Np are plotted.

Fig. 5.19 reveals a heterogeneous distribution of the three main fuel elements U, Pu, Zr over the sample radius. The Np X-ray map shows a distribution pattern very similar to Pu and U; Np does not appear to be alloyed with RE or noble metals.

The microstructure observed in the central region of the fuel extends over nearly 500 μm. The U and Pu X-ray maps show that this area is not fully homogeneous in composition, including a major phase and a minor phase with different U/Pu concentration ratios, identified on the ternary phase diagram at 853 K (in O´Boyle [7]) as ζ and δ+γ+ζ, respectively. The Zr concentration in the major phase of this zone (red phase on the U X-ray map) is very low, between 1 and 2 wt.%.

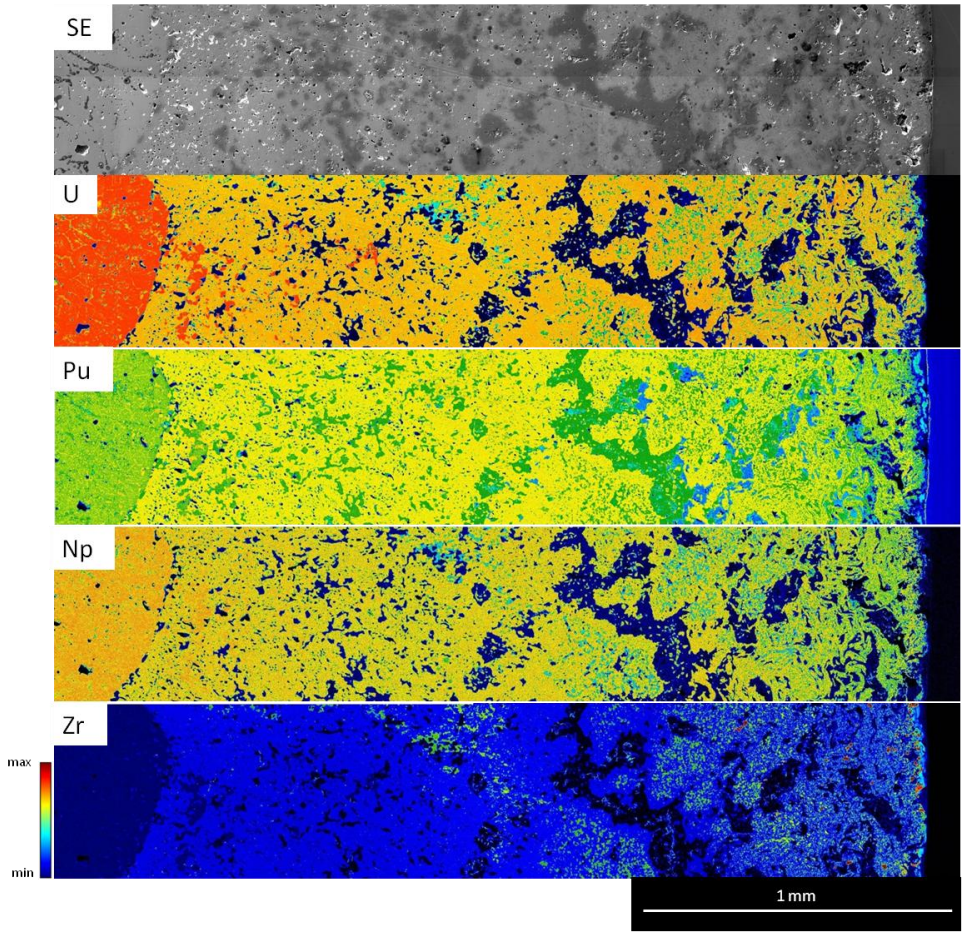

Fig. 5.19. Redistribution of the main fuel elements (U, Pu, Zr) and Np in a METAPHIX-2 U-19Pu-10Zr-5MA-5RE sample obtained by EPMA (qualitative analysis) [19].

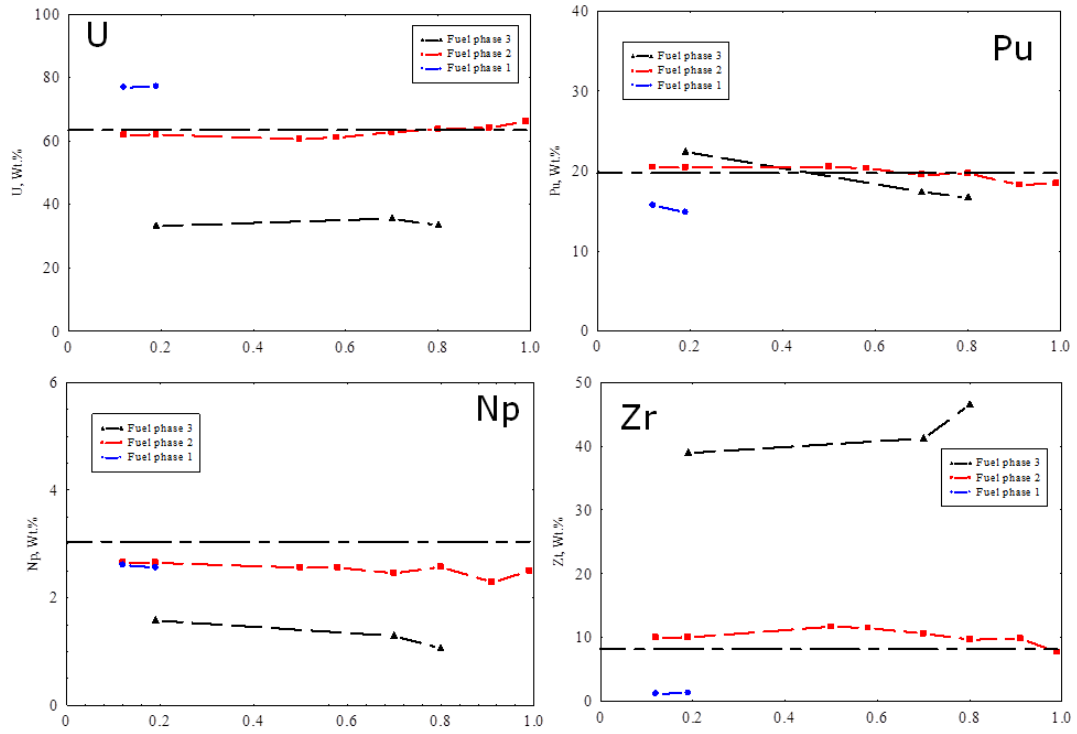

Fig. 5.20. Concentration and redistribution profiles of the main fuel elements (U, Pu, Zr) and Np in the fuel phases observed along the radius of a METAPHIX-2 U-19Pu-10Zr-5MA-5RE sample. The dashed black lines indicate the pre-irradiation composition of the fuel.

In the rest of the sample, the distribution of the three main elements shows steep local variations. A number of local phases, enriched in any one of the fuel elements, are observed at the different radial positions. The Zr X-ray map shows an increase of the overall Zr concentration in the fuel outside the central area, consisting of a matrix phase with ~10 wt% Zr (starting from r/r_0=0.2) and secondary high-Zr phases (starting from r/r_0=0.5).

In the region just outside / across the central area (r/r_0=0.2), 2 phases are identified on the phase diagram at 823 K (O´Boyle [7]), as δ+ζ (major) and ζ (minor).

Fig 5.21 shows quantitative X-ray maps illustrating the change in phases across the central region border (r/r_0=0.2). The dissolution of the high U phase (in red, called fuel minor in table 5.2) to lower concentration (in orange, called fuel minor in table 5.2) is clearly visible.

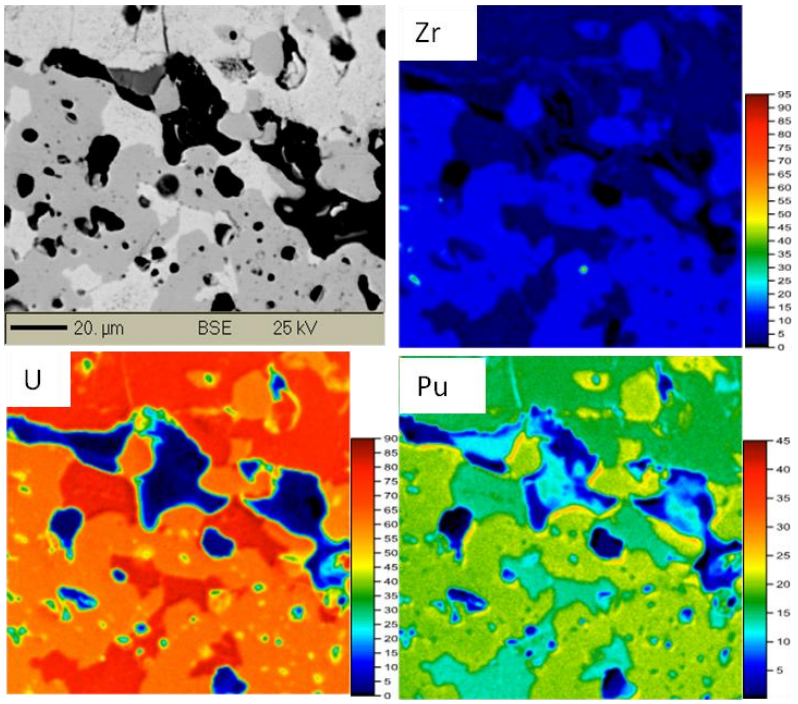

Fig. 5.21. BSE image and large area X-ray mapping for Zr, U and Pu in the region r/r_0=0.2.

From r/r_0=0.3 towards the fuel periphery the U, Pu, Zr elements concentration in the matrix phase are at their nominal values. The major phase is identified on O´Boyle phase diagrams at 823 K and 773 K (from r/r_0=0.7) as δ+ζ. At the periphery of the fuel sample, the major fuel phase is estimated to be δ+ζ (at 773 K) with a small presence of α phase.

From the mid fuel radius to the periphery, a high Zr fuel phase (Zr concentration around 40 wt.%) is formed and identified as a mixture of γ+ζ→δ+η with some possible presence of α (at r/r_0=0.5) and δ (at r/r_0=0.8/0.9) phases.

Table 5.2 reports schematically all the fuel phases identified, their relative radius position and corresponding temperature, the range of composition for the fuel elements measured by point analysis and the corresponding fuel phases.

Table 5.2. EPMA results for the fuel phases observed along the radius of the METAPHIX-2 U-19Pu-10Zr-5MA-5RE sample.

Phase	r/r_0 [1]	U (wt.%) [2][3][4]	Pu (wt.%) [2][3][4]	Zr (wt.%) [2][3]	Phase diagram T (K)	Estimation of phase
Outer fuel	> 0.9	64.19 (4.88) 66.16 (1.46)	16.22 (1.46) 18.45 (0.77)	9.75 (3.51) 7.73 (1.02)	773	ζ + δ
Outer Zr-rich fuel	0.9	33.39	16.68	46.52	773	δ
Fuel	0.9	64.20 (1.51)	18.26 (0.54)	9.82 (2.28)	773	ζ + δ
Zr-rich fuel	0.8 – 0.9	35.48 (1.04)	17.35 (0.34)	41.21 (0.82)	773	δ
Fuel	0.8 – 0.9 0.7 – 0.8 0.6	63.75 (0.41) 62.76 (0.60) 61.10 (0.28)	19.70 (0.22) 19.52 (0.30) 20.33 (0.24)	9.69 (0.52) 10.62 (0.35) 11.50 (0.29)	773 773 823	ζ + δ
Zr-rich fuel	0.5	33.26 (0.70)	22.39 (0.48)	38.94 (0.58)	823	γ+ζ→δ+η
Fuel	0.5	60.56 (0.19)	20.54 (0.23)	11.69 (0.11)	823	ζ + δ
Fuel major	0.2	62.01 (0.62)	20.43 (0.80)	10.05 (0.36)	823	ζ + δ
Fuel minor	0.2	77.23 (1.35)	14.83 (0.91)	1.32 (0.73)	823	ζ
Fuel core minor	0 – 0.1	61.87 (0.40)	20.48 (0.39)	10.01 (0.11)	853	ζ + δ + γ
Fuel core major	0 – 0.1	76.91 (0.60)	15.70 (0.27)	1.21 (0.30)	853	ζ

(1) Relative radius. 0 is the centre and 1 is the surface of the sample.

(2) Range of concentrations measured when applicable.

(3) The uncertainty (2 standard deviations) is shown in parentheses.

(4) Am was added to U. Np was evenly divided between U and Pu with the same motivation discussed in Chapter 4, paragraph 4.3.2.

5.2. Secondary phases

RE elements (especially Nd and Ce) and noble metals (Ru, Rh, Pd) were observed to precipitate as secondary phases and migrate down the temperature radial gradient, to a point where they could possibly reach the cladding. Once contact is made with the cladding, these precipitates can contribute significantly to FCCI, which is a potential cause of concern for the safety of the fuel due to the possibility that they can form low temperature eutectics. The behaviour of these secondary phases is reported in the literature [20, 21].

Scientific effort was made also to understand the possible mechanisms for their transport / migration. Mariani et.al speculated on a liquid-like mechanisms [20] in which the RE are in super-ionic state[1] and they are able to move through the open porosity of the fuel like a liquid and then solidify at the lower temperatures characteristic of the radial periphery of the fuel.

The preferred medium to enable this mechanism is Cs, which is liquid at the reactor temperature. RE have high solubility in Cs [20], so RE can be dissolved in Cs and undergo multiple dissolution and precipitation events while moving towards the cooler region of the fuel. Upon reaching the periphery of the fuel, RE will precipitate when in contact to the excess of liquid Na, since RE have very low solubility in it [22].

For the metallic fuel alloy containing MA and RE, the focus is on MA such as Am and how their behaviour is related to noble metals and RE migration and transport along the fuel radius. There are no experimental data on such elements and just speculations about a potential behaviour similar to RE [21].

Concerning volatile (Xe) or semi-volatile fission products (I or Cs) from metallic fuels relatively few experimental studies were conducted on their behaviour and on their possible chemical forms [23, 24]; volatiles re-distribution along the fuel radius is not known; a significant fraction of Cs is found in the bond sodium [4]. Iodine

[1] At temperatures near liquid phase formation of a metal alloy, the cohesive energy of the metal phase is near collapse. At such temperatures, the bond energy of individual atoms within the metal phase is weak relative to available amount of thermal energy. Consequently, atomic transport through pores, grain boundaries and surfaces of fissures will be rapid [20].

could form stable compounds with the main constituents of the matrix [25]. Recent chemical analysis of the sodium bond from an Integral Fast Reactor fuel pin with 10 at.% burnup revealed a notable iodine deficit [26]. During release experiment iodine was detected as CsI and was thought to have formed in bubbles [24].

In the next sections, the distribution of selected fission products and MA in the basic alloy and in the 5MA-5RE (e.g. Nd, Mo, La, Ru, Xe, Cs, Am) was assessed by X-ray mapping and / or point analysis along the radius.
For the phase identification of the intermetallic compounds containing RE and noble metals, the binary phase diagrams of Okamoto [18] were used.
Some phases in the 5MA-5RE sample could not be identified because too complex or because the relevant phases diagrams do not exist.

5.2.1. Basic alloy U-Pu-Zr

This section will report on the behaviour of RE, noble metals and semi volatile fission products. The experimental data were obtained by EPMA investigations.

Behaviour of Ru

The only occurrence of Ru in the sample is in association with Zr in precipitates, which also include a few wt.% of Mo, Rh and Pd. The precipitates are found in the centre of the fuel (fig. 5.22) and on the outer part of the crust phase (fig. 5.23) where they appear to have "quasi-square" shapes. The latter precipitate compositions include about 50 at.% Zr; a possible compound based on this composition is Zr(Ru, U, Rh, Mo, Pd, Pu), which, similarly to ZrRu, has a simple cubic lattice structure and exists in the Ru-Zr phase diagram [18]. Similar phases were not found in the fuel periphery region during the present observations. Similar ZrRu precipitates were reported by Keiser [27] with additional elements depending on the location in the fuel sample; i.e. including Ni and Pd close to the fuel-cladding interface and containing Mo, Tc, Rh and Pd at various locations in the fuel. Keiser did not report quantitative measurements of the composition of the precipitates so no direct comparison is possible with the measurements reported here.

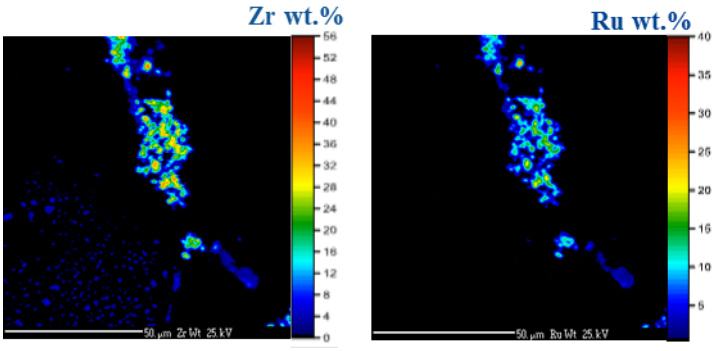

Fig. 5.22. Zr-rich precipitates alloyed with Ru in the fuel central region of a METAPHIX-2 U-Pu-Zr sample (r/r_0=0.13).

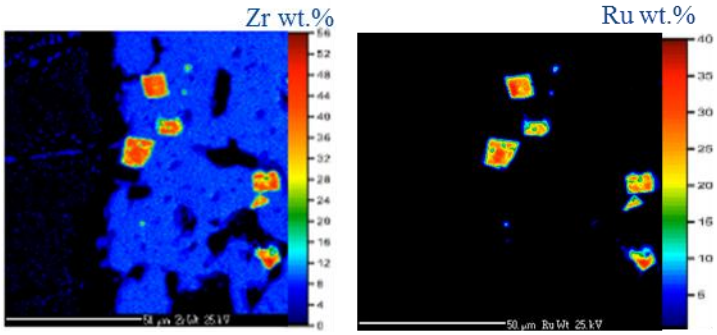

Fig. 5.23. Zr-rich "quasi-square" precipitates at the mid-radius of a METAPHIX-2 U-Pu-Zr sample (r/r_0=0.45).

RE-rich secondary phases

RE-rich phases (mainly Nd, Ce, Pr, La, Y, Gd, Eu), incorporating also noble metals, namely Pd (17-23 wt.%) and Rh (1.6-2.8 wt.%), are observed at different radial locations. Fig. 5.24 shows lanthanum precipitates detected at 2 different locations, in the centre region and at the fuel periphery. From the ratio between RE and noble metals these precipitates are inferred to be of two kinds: $RE_7(Pd,Rh)_3$, found throughout the fuel, and $RE_3(Pd,Rh)_2$ found only at the radial periphery ($r/r_0 > 0.87$). This is in agreement with the fact that the intermetallic compound of the Th_7Fe_3 type structure is found in the Ce-Pd binary system (fig. 5.25). It is worth noting that this is the case also for all other combinations of dominant RE and noble metal except Y-Pd, Eu-Pd and Eu-Rh [18].

At the fuel periphery, the fraction of noble metal elements was slightly higher and the fraction of RE elements was lower compared to the phase observed in the fuel centre. Hence, $RE_3(Pd,Rh)_2$ is considered to be another possible composition for

this phase. An intermetallic compound of similar structure is found in the binary phase diagram for any couple formed with (La, Ce, Nd, Pr, Y, Gd, Eu) and (Pd, Rh), except La-Pd, Nd-Pd, Pr-Pd and Eu-Rh.

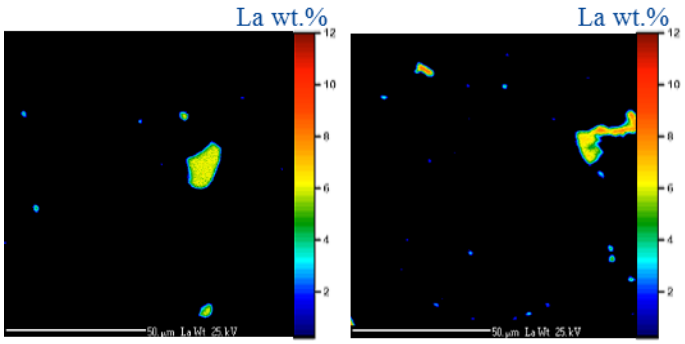

a) **b)**

Fig. 5.24. RE-rich phases in 2 different fuel locations: a) centre of fuel; b) fuel periphery.

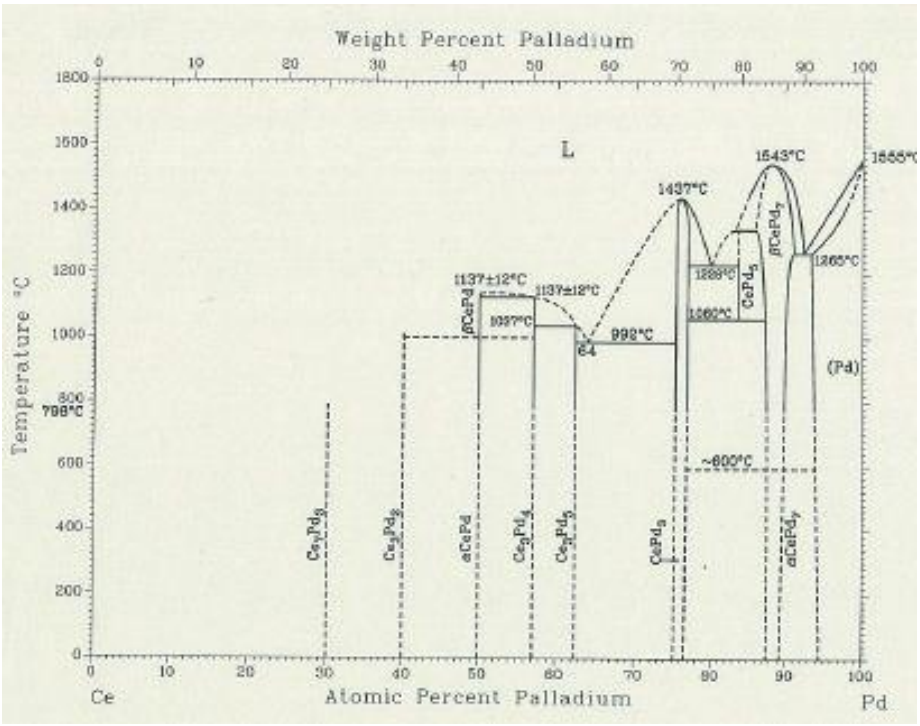

Fig 5.25. Binary phase diagram for Ce-Pd [18].

Volatile and semi volatile fission products: Xe & Cs distribution

Fig 5.26 reports the inhomogeneous distribution of the fission gas Xe remaining in the fuel over the radius of the fuel ingot; the spot density is higher at the periphery of the fuel. Here Xe is associated within Zr particles and in small precipitates. A small number of Xe spots are also found in the central region while no Xe is found in the "crust" region where the matrix phase is particularly dense.

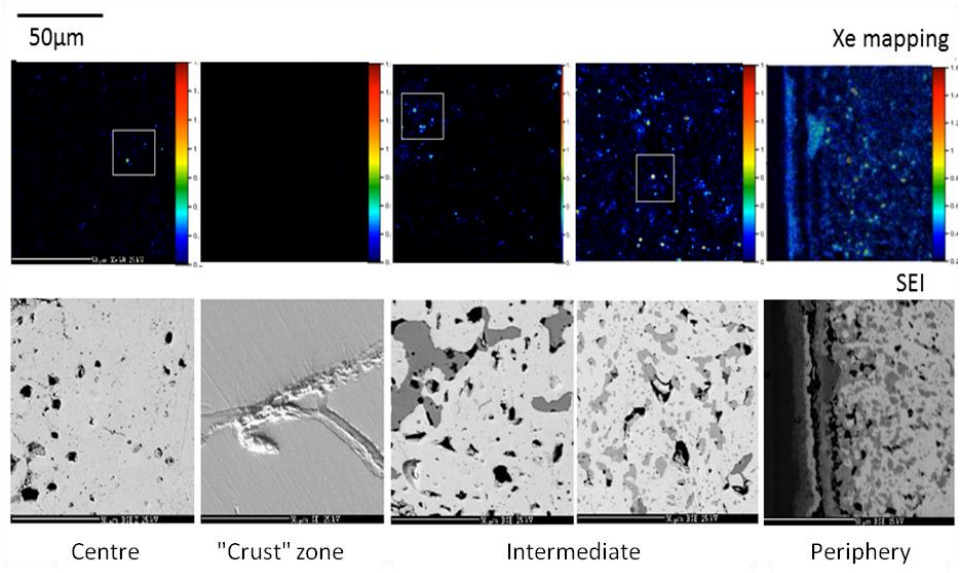

Fig. 5.26. Xe distribution along the fuel radius of a METAPHIX-2 U-Pu-Zr sample.

Cs was also detected in the areas corresponding to the 5 frames of fig. 5.26. Fig. 5.27 shows higher magnification qualitative X-ray maps of Xe and Cs located in the inset of the intermediate region of fig. 5.26 (Xe mapping). These maps indicate an inhomogeneous distribution of Cs similar to that of Xe. However, no systematic association between Xe-rich and Cs-rich spots is observed in the fuel matrix.

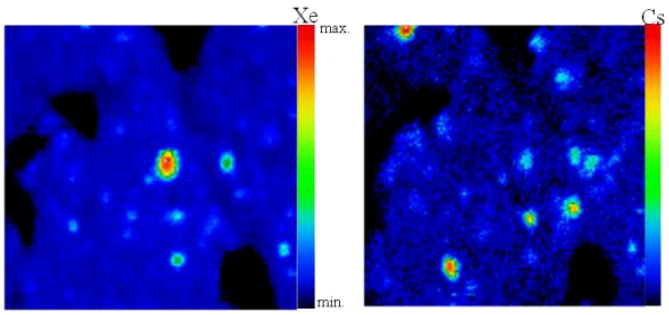

Fig. 5.27. High magnification X-ray maps for Xe and Cs in the intermediate region of fig. 5.25.

5.2.2. U-Pu-Zr-5MA-5RE

In this subsection the focus is on elements of paramount importance such as Am; in particular, it is investigated how its behaviour is related to noble metals and RE migration and transport along the fuel radius.

Figs. 5.28 and 5.29 clearly show that almost no secondary phases are observed in the central region of the fuel. In the rest of the sample, numerous secondary phases different in size and composition are observed. The highest concentration element of the secondary phases is Nd, found with concentrations between 35 and 50 wt.%.

From mid-radius to the periphery, the Nd and Am X-ray maps in fig. 5.28 and the X-ray map for Pd (fig. 5.29) show that two different (RE, Am)-rich phases are present, one associated with noble metals (Pd and Rh) and one without noble metals. Quantitative X-ray maps of the elements present in the secondary phases at $r/r_0=0.7$ (fig. 5.30) describe in more detail this dual behaviour.

It is of interest to notice that noble metals Pd and Rh are segregated in secondary phases only in the part of the fuel between $0.6<r/r0<0.9$, as shown in fig. 5.29 for Pd, in a stripe wide 750 microns. On the other hand, Ru behaves very differently (fig. 5.28) and it is found as precipitate phase only in the periphery at the FCCI region.

Am redistributed with Nd and RE would be a major actor at the FCCI region (to be described later in paragraph 5.3.2). However, it is worth noticing that, similarly to Pd, Am is depleted in a 130-160 μm region before the FCCI, in contrast with the redistribution of Nd.

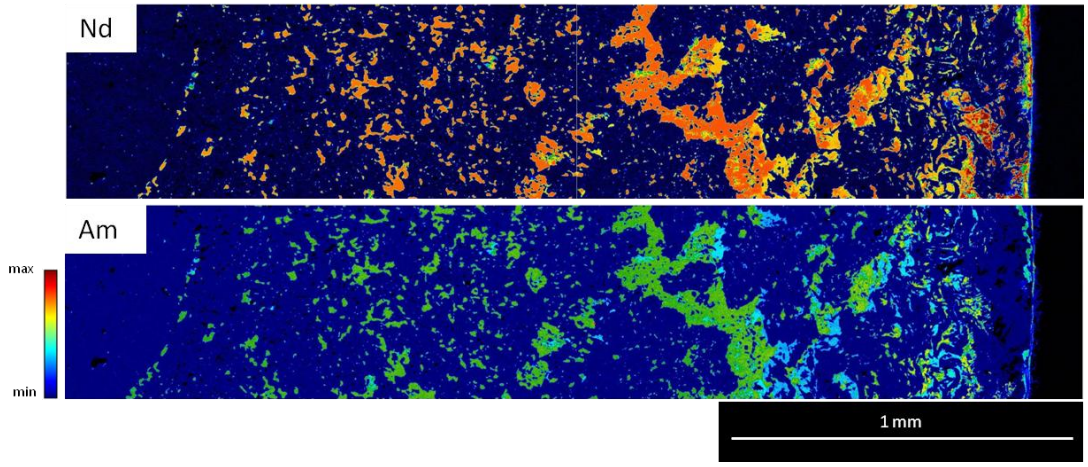

Fig. 5.28. Radial large area qualitative X-ray maps for Nd and Am for a METAPHIX-2 U-19Pu-10Zr-5MA-5RE sample.

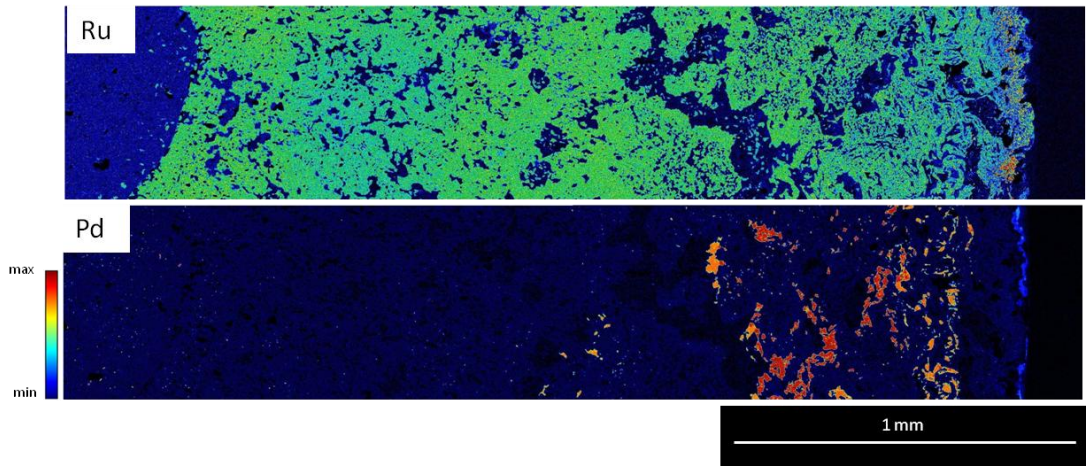

Fig. 5.29. Radial large area qualitative X-ray maps for Ru and Pd for a METAPHIX-2 U-19Pu-10Zr-5MA-5RE sample.

The precipitates that include both noble metals and RE elements, although exhibiting local concentration variations, have phase compositions corresponding to $RE_7(Pd,Rh)_3$, similarly to what is observed for the base alloy fuel. Quantitative point analyses indicate Am concentrations between 10 and 13 wt.%. Cm is also very likely to be present up to 3 wt.%

On the other hand, in the secondary phases depleted in noble metals, Am and Cm have concentrations between 15 and 20 wt.% and around 4 wt.%, respectively.

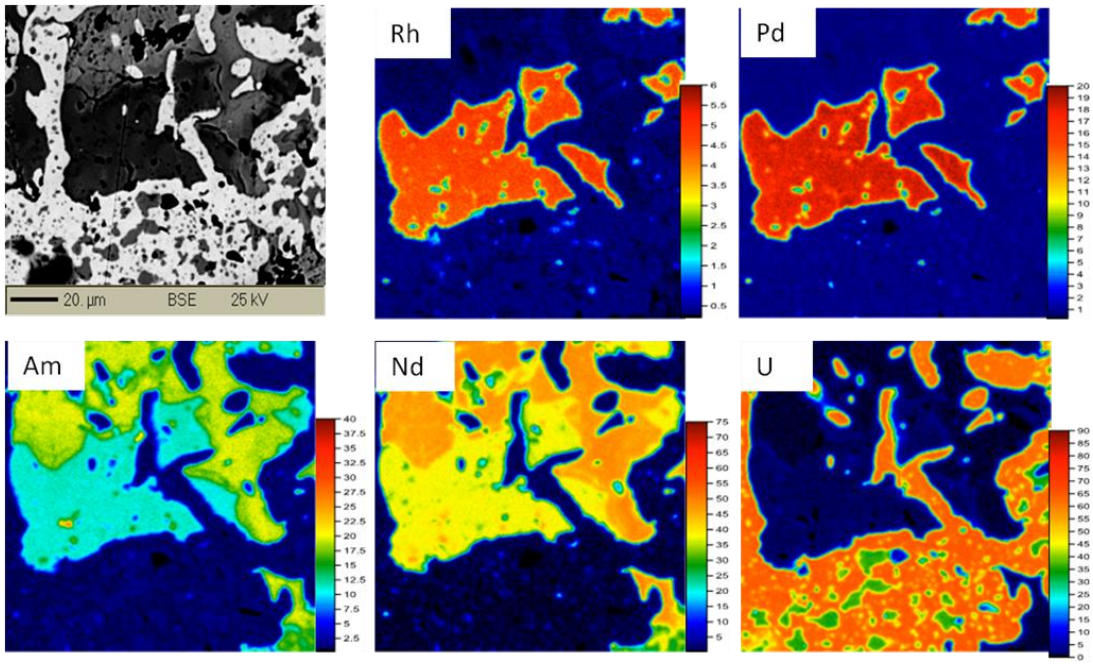

Fig. 5.30. BSE image and quantitative X-ray maps for Rh, Pd, Am, Nd and U in the region r/r_0=0.7.

Volatile fission product Xe distribution

Fig 5.31 reports the distribution of fission gas Xe from r/r_0=0.7 to r/r_0=1. No significant amount of Xe was observed from fuel centre to r/r_0=0.6. Figs. 5.31 and 5.32 suggest that Xe can be associated within Zr particles and in small precipitates, similarly to what was observed in the basic alloy. In the Zr-rich precipitates at the FCCI region (fig. 5.32), the Xe concentration reaches 1-1.3 wt.%.

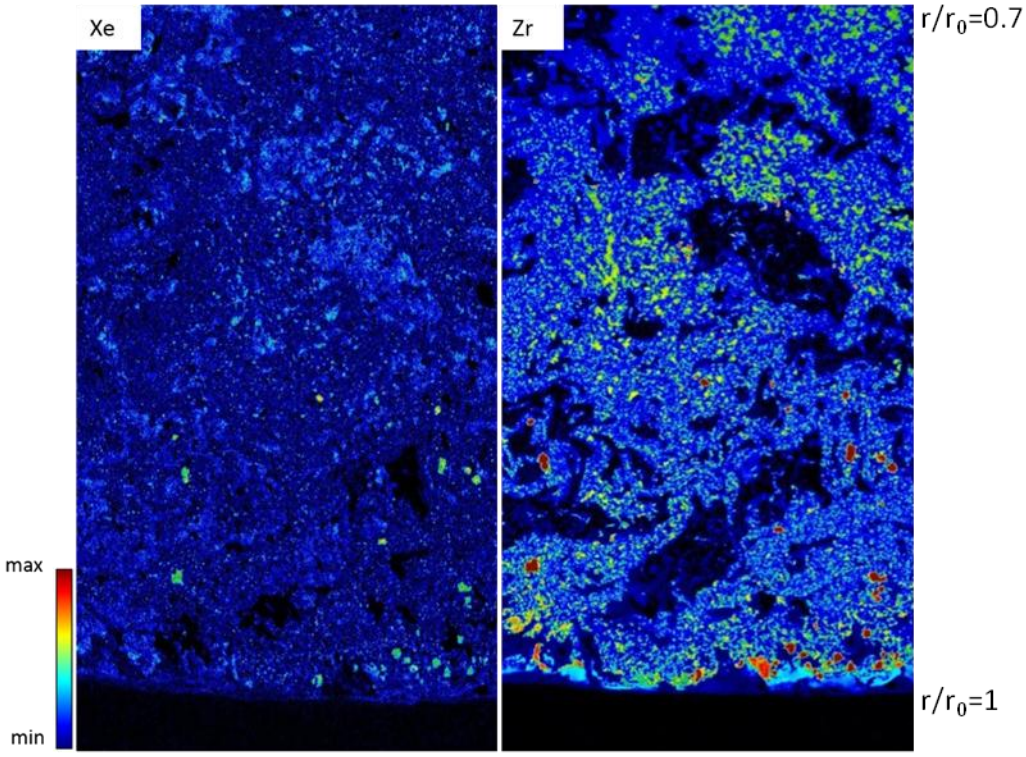

Fig. 5.31. Xe and Zr distribution along the fuel radius from r/r_0=0.7 to r/r_0=1 of a METAPHIX-2 U-19Pu-10Zr-5MA-5RE sample.

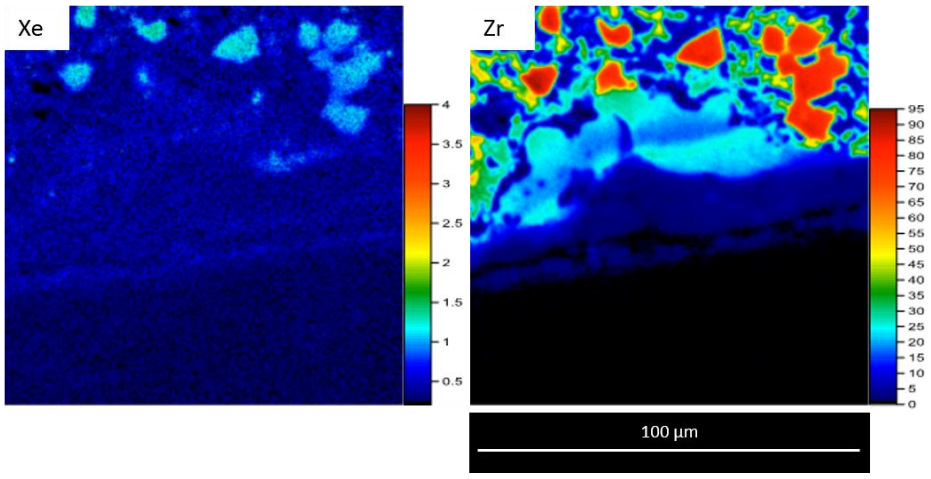

Fig. 5.32. BSE image and quantitative X-ray maps for Xe and Zr in the FCCI region.

5.3. Fuel Cladding Chemical Interaction

One of the main factors that could limit the integrity of the cladding and the possibility to reach higher burnup in metallic fuel is the FCCI.

FCCI is a complex phenomenon, already observed and studied during early irradiation campaigns at EBR-II at Argonne National Laboratory [27] both on U-Zr and U-Pu-Zr alloys and with different cladding material, such as D9, 316 and HT9. FCCI depends in general on 4 factors, temperature, power, burnup and integrity of the Zr rich layer in the periphery of the fuel sample.

The main features representative of the FCCI in U-Pu-Zr are well known and reviewed by Keiser [27, 28]. On the fuel side, interdiffusion of Fe and Ni (when present in the cladding) and formation of second phases preferentially with Zr are usually observed. On the cladding side, there is interdiffusion and agglomeration of RE, U and/or Pu and, in association with changes of the cladding compositions, additional features such as layers enriched in Cr and depleted in Fe/Ni.

Porter and Tsai [29] presented EPMA line scans for FCCI (fig 5.33). Quantitative values were not available. They divided the interaction layer in 2 locations "A" and "B"; "A" is characterized by Ni and Fe loss, "B" is the more "typical" FCCI layer with high concentration of RE fission products and modest levels of Pu and U. The initial interfaces of cladding and fuel are marked as well. Pu is found in the "B" layer, very close to the cladding. However no quantitative data on the amount of Pu are given. Nd and Ce are enriched in the "B" layer. A Ni loss is observed in the "A" layer.

Concerning FCCI in MA bearing metallic fuel, only one experiment was conducted in the past [30]. The fuel composition included 2.1 wt.% of Am and 1.3 wt.% of Np and was irradiated up to 7 at.% burnup. No FCCI was detected.

In the following, the different aspects of FCCI observed in the METAPHIX experiment will be described for both the basic alloy and the fuel containing MA/RE.

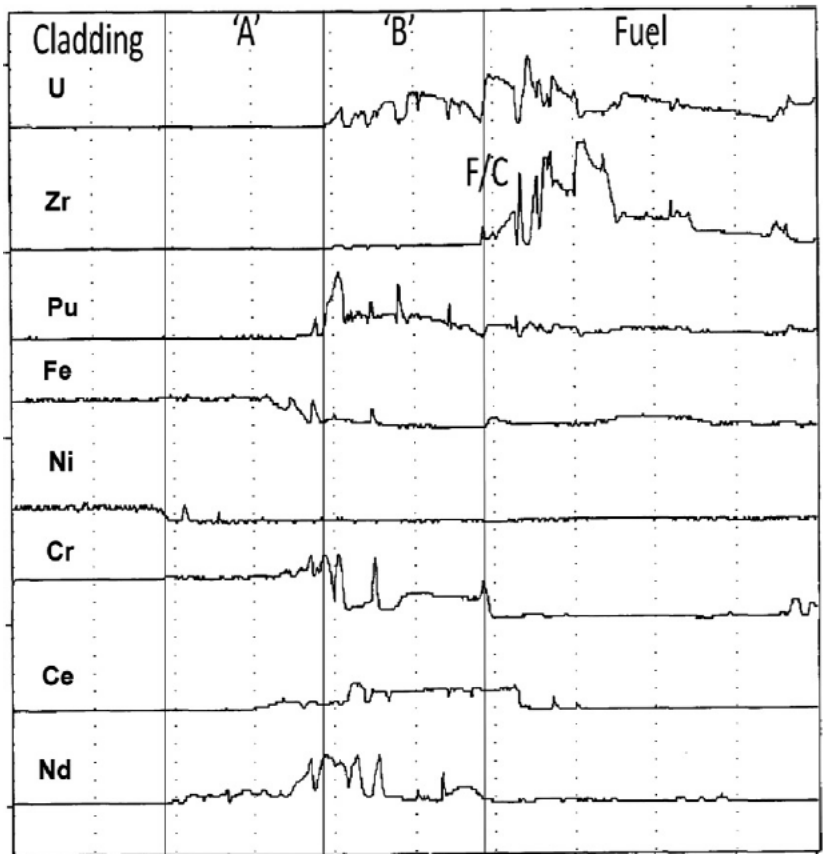

Fig. 5.33. EPMA line scans of FCCI from [29].

5.3.1. Basic alloy U-Pu-Zr

Concerning the U-Pu-Zr basic alloy, OM revealed a wastage layer[2] on the cladding inner surface as shown in fig 5.34.

EPMA quantitative analysis of this region was produced. The investigations included X-ray mapping and quantitative point analysis of more than 15 different elements including cladding and fuel constituents, RE and noble metals.

[2] The wastage layer is defined as the layer of cladding materials attacked by external agents (e.g. RE) resulting in degraded mechanical and chemical properties compared to the not attacked cladding.

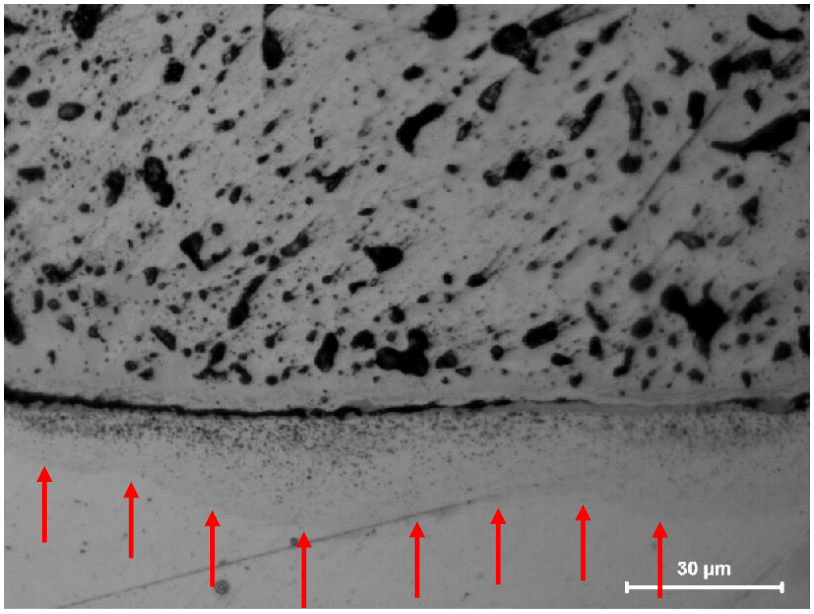

Fig. 5.34. OM image obtained on a, U-Pu-Zr basic alloy, T= 813 K, 6.9 at.% burnup. The red arrows mark the margins of the interaction layer.

Fig. 5.35 shows a higher magnification SE image of the area taken in consideration, between fuel and cladding, along with X-ray maps of the 3 main fuel elements (U, Pu, Zr), the 3 main cladding constituents (Fe, Ni, Cr), Rh (representative for noble metal) and Ce (representative for RE).

From fig 5.35 it is possible to identify several features of interest in this region; the description hereafter is divided in "zones", from fuel side to cladding side.

A schematic representation of the zones identified, highlighting the complexity of this region of the fuel pin, is shown in fig. 5.36. Each observed phase is tentatively labelled for descriptive purpose.

The fuel main phase consists of U, Zr and Pu. Mo, Ru, Rh, Pd, Ce and Nd are included as trace elements. In addition, owing to interdiffusion from the cladding, Fe and Ni are also detected. The diffusion of other cladding elements, such as Cr and Ti, was not observed.

Small particles of precipitate phase (Zr-Ni phase) enriched in Ni (6.7 wt.%) and Fe are visible on the fuel side.

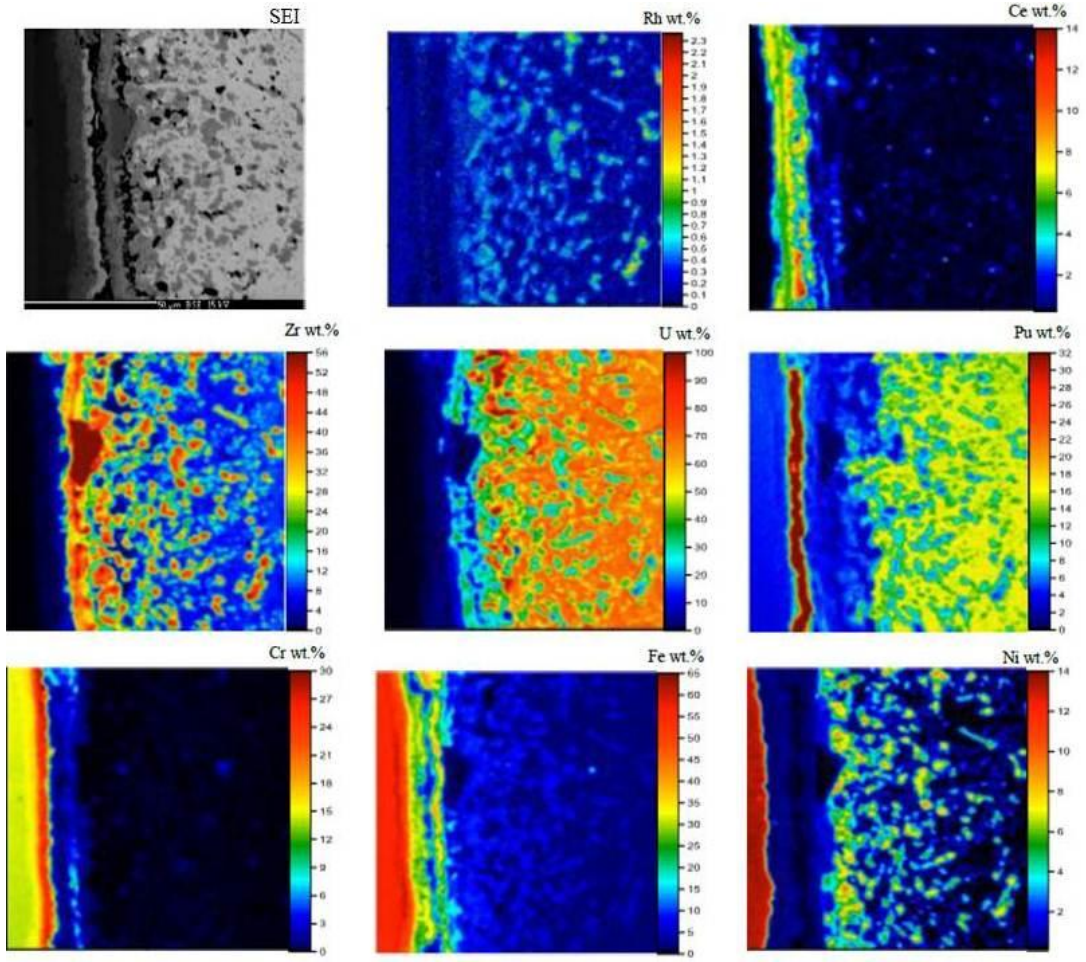

Fig. 5.35. U-Pu-Zr, SE image and quantitative X-ray maps of a FCCI region.

A Pu-free area is observed near the outer surface of the fuel. This fuel region is not homogeneous; it includes discrete precipitates of Zr-Ni and Zr-rich phases. It is estimated that the depletion of Pu in this area is associated with a Pu-rich region formed between the fuel and the inner cladding.

The Zr-rich phase is a layer 5 μm thick; it may correspond to the outer surface of the fuel, i.e. the initial fuel/cladding interface. This phase mainly consists of Zr (33 – 47 wt.%), Fe (18 wt.%), Cr (6 wt.%), U and Pu (15 wt.% and 3 wt.% respectively). Small amounts of RE (less than 4 wt.%) are also included. A dense particle of over 20x10 μm is visible on the SE and AE image in fig 5.35. The Zr X-ray map and the point analysis confirmed that it contains over 80 wt.% Zr. Other elements, originating from fuel, cladding and RE fission products are present as traces. Finding of such a particle was not a single occurrence; similar particles are

present repeatedly along the sample perimeter, very close to the fuel pellet interface. These particles are considered to be remnants of a Zr-layer, possibly originating from the arc-melting stage of the fuel preparation process.

The Pu-rich phase consists of a layer a few μm thick and lays at the cladding inner surface. The small size made the layer difficult to analyse quantitatively, thus a limited number of analysis point are available.

The main constituents of the Pu-rich phase are Fe (29 wt. %) and Pu (up to 57 wt. %) with few at.% of U leading to a composition ratio Fe/(U+Pu) close to 2. The phase Fe_2Pu exists in the Fe-Pu binary phase diagram [18] with a liquidus temperature over 1500K, significantly higher than the estimated temperatures at beginning and end of irradiation, 843K and 743K respectively.

The Cr-rich phase consists of a thin layer 5-8 μm wide formed on the cladding side where the Cr concentration reaches 23 wt.%. In addition to Cr, RE elements (Ce, La, Nd) are also present in significant amount, ~16 wt.%. The point analysis measurements led to the conclusion that the phase composition is $(Fe,Cr)_{17}RE_2$. This intermetallic compound is considered to be one of the main phases formed in the FCCI layer: an intermetallic compound of the same composition was detected in out of pile tests, where a diffusion system of RE alloy and Fe was isothermally annealed [31]. In the $(Fe,Cr)_{17}RE_2$ phase, the Cr content is higher than the initial composition of the cladding. Similar Cr enrichment was already observed in previous irradiation and out of pile experiments [32, 33]. This indicates that reverse diffusion of Cr occurred during the irradiation: Cr diffused from the inner side of the cladding towards the outer side against the Cr concentration gradient. Such behaviour was observed in the ternary diffusion system Cr-Fe-Ce, where Cr exhibited a flux reversal and build up [34]. This phenomenon was explained in [35, 36] with the presence of a zero-flux plane where the interdiffusion flux of a component goes to zero and on either side of the plane occurs a change or reversal in the direction of the interdiffusion flux.

In the cladding region, a distribution average of 0.7 wt% Pu is observed at a distance of around 20 μm from the fuel-cladding initial interface.

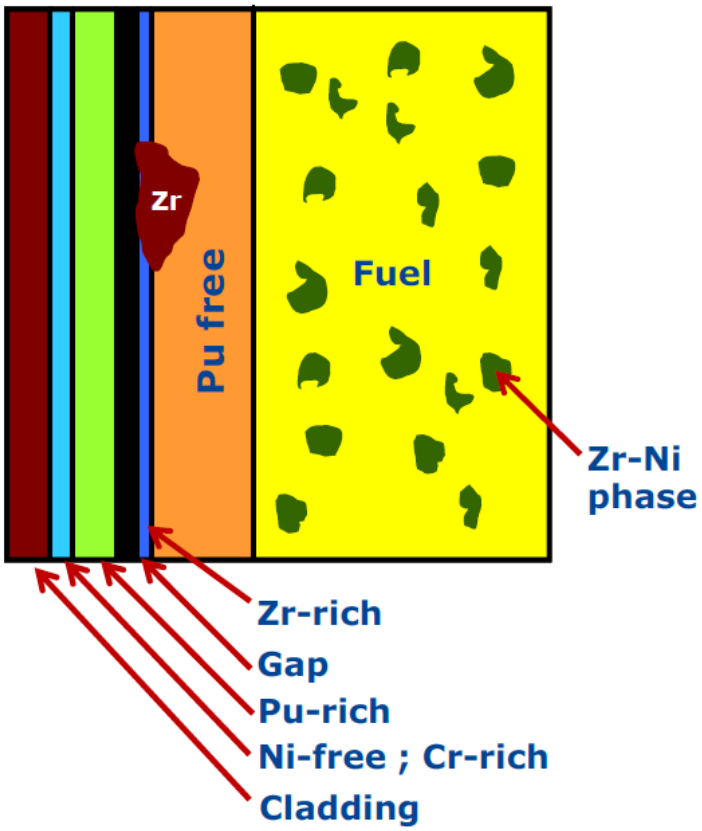

Fig. 5.36. Schematic representation of the different zones at the fuel-cladding interface identified from the EPMA investigations.

5.3.2. MA and RE bearing fuel alloys

The main features of interest of FCCI observed in samples with MA and/or RE are summarized hereafter in figs. 5.37 to 5.40. An interaction zone was identified and is defined in this work as the region across cladding and fuel in which RE and cladding elements (such as Fe, Ni) are mutually interacting and combined.

Zr-rich and RE precipitates are present throughout the interaction zone (fig. 5.37); Ni is detected forming precipitates with Zr; SEM-EDX analysis also confirmed the presence of Fe with U and Pu (fig. 5.38).

On the cladding side of the interaction zone, the morphology of the wastage layer is different from the basic alloys samples. The wastage layer here resembles more an attack along the grain boundaries of the stainless steel. This feature is visible at 2.5 at.% burnup (figs 5.37-5.38) and at ~6.9 at.% burnup (fig. 5.39) as well, and it is independent from the presence or RE.

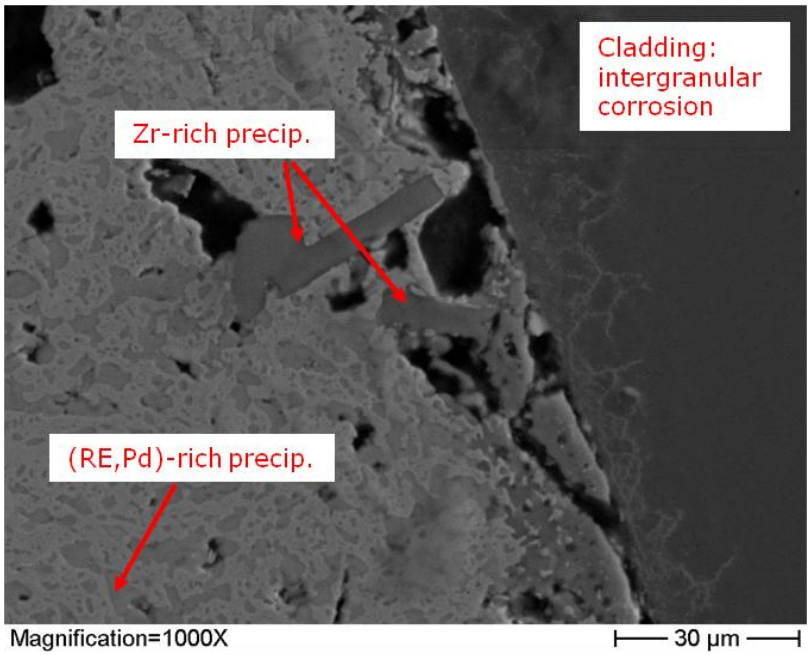

Fig. 5.37. SEM image of U-Pu-Zr + 5MA, T= 803 K , ~2.5 at.% burnup.

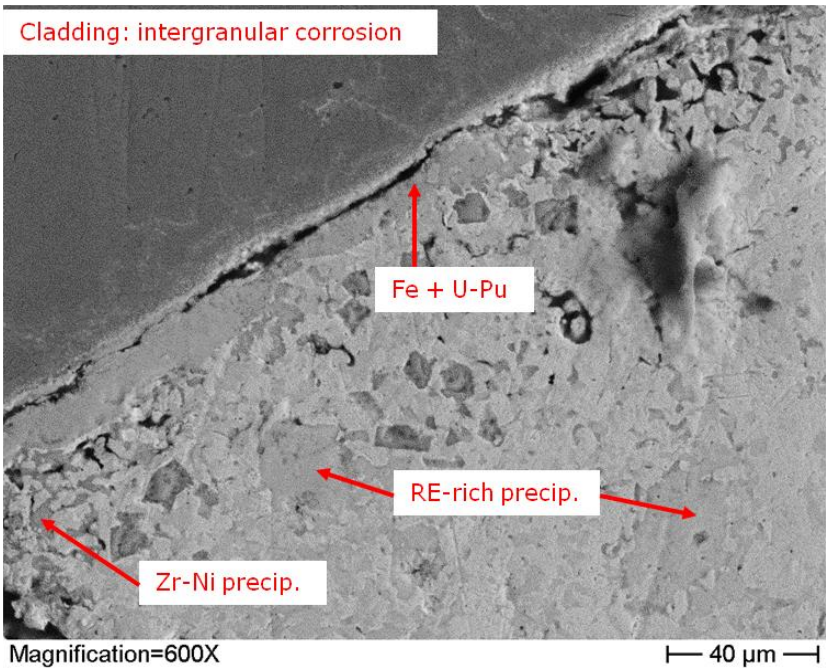

Fig. 5.38. SEM image of U-Pu-Zr + 5MA+5RE , T= 823 K , ~2.5 at.% burnup.

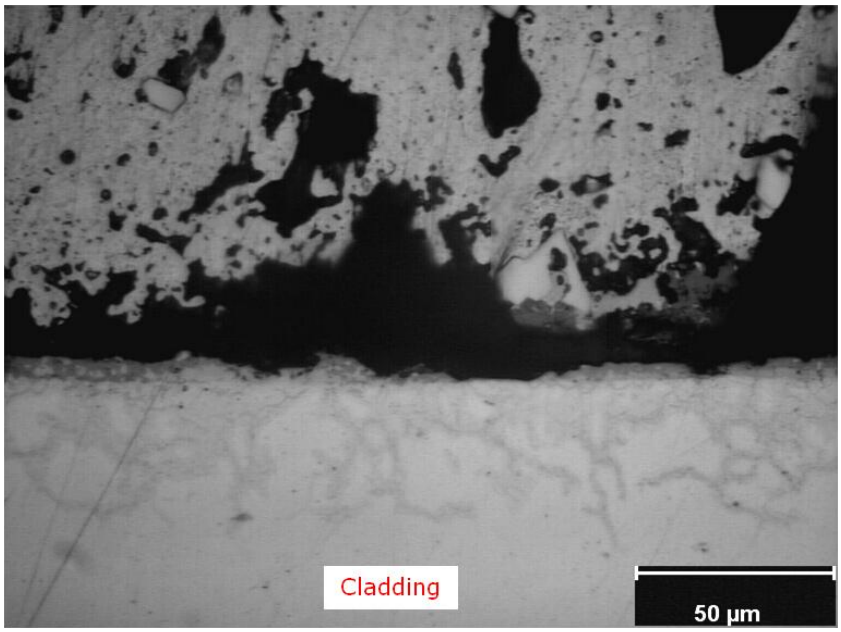

Fig. 5.39. OM image of U-Pu-Zr + 2MA+2RE, T= 783 K , ~6.9 at.% burnup.

SEM-EDX point analysis corresponding of this wastage layer (point 2 in fig. 5.40) revealed the characteristic lines of the actinides (M-lines) and the main peaks of the cladding constituents (Fe, Cr and Ni). On the contrary, in point 1 the EDX analysis did not revealed any characteristic peak for actinides.

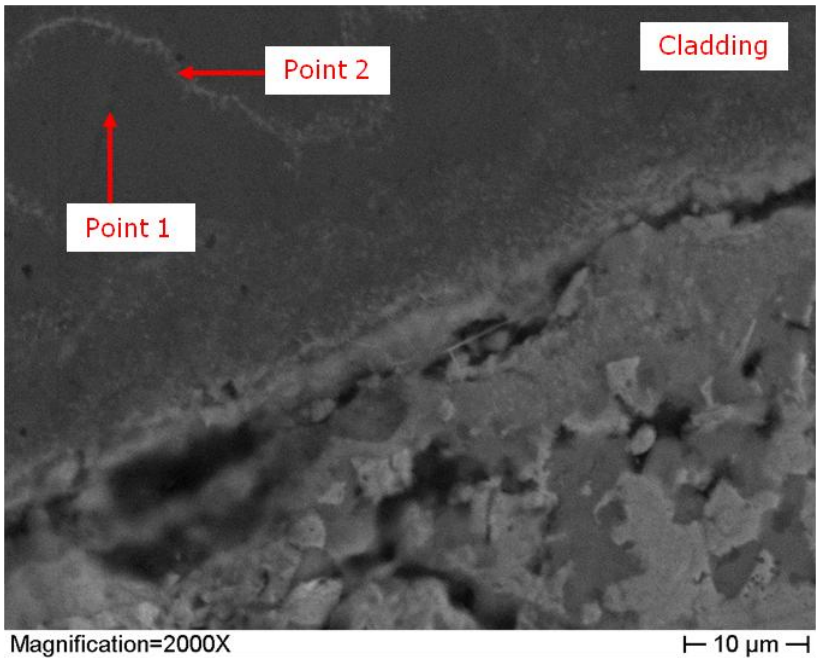

Fig. 5.40. SEM image of U-Pu-Zr + 5MA+5RE, T= 823 K, ~2.5 at.% burnup.

A more exhaustive and quantitative analysis of this phenomena was obtained through EPMA investigations. Fig. 5.41 reveals the presence of an interaction zone inside the cladding where penetration of mainly Sm and Am is observed (see also the line scan profile of fig. 5.42). The cladding corrosion phase is limited to less than 50 micron and appears to be intergranular. Furthermore, the line scan profile of fig. 5.42 reports the evolution inside the cladding wastage of 5 main RE and MA. RE such as Nd and Ce are more abundant at the cladding inner surface; they are also present in small amount inside the intergranular attack phase.

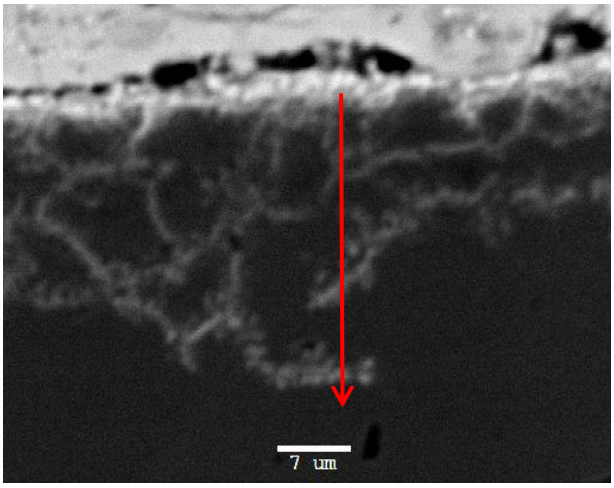

Fig. 5.41. SE image of cladding penetration from RE and Am in a METAPHIX-2 U-19Pu-10Zr-5MA-5RE sample obtained by EPMA.

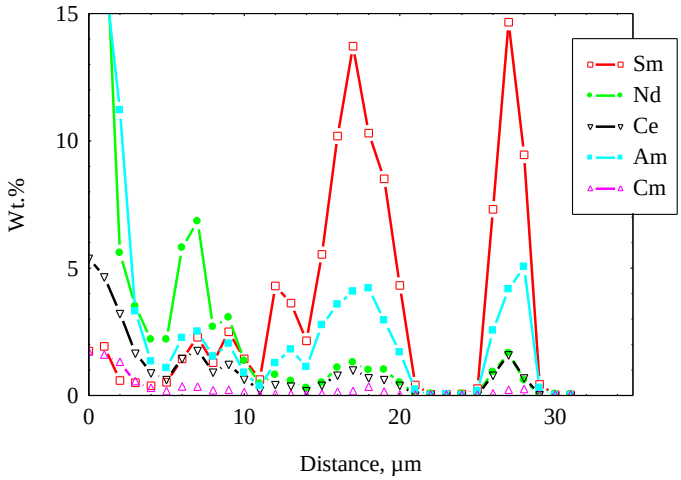

Fig. 5.42. Line scan profile inside the cladding referred to the red arrow in fig. 5.41.

Fig. 5.43 illustrates X-ray maps of the FCCI region in which the 3 main constituents of the fuel, cladding components, MA and RE are displayed.

This FCCI region consists of a precipitate phase enriched in RE and Am. The RE-Am phase is surrounded by the fuel phase containing U, Pu, Zr (also in form of locally enriched particles) and small quantities of Ni and Fe, the latter two elements originating from the cladding.

Am is present in the RE-Am phase in concentrations around 15-17 wt.%, at the inner surface of the cladding. It can be also found locally in Am-rich spot, up to 40%, and then inside the cladding with Sm as shown in fig 5.42. Pu is also present with Am at the inner surface of the cladding.

In the cladding, Ni and Fe are depleted where the interaction of Sm and Am has occurred.

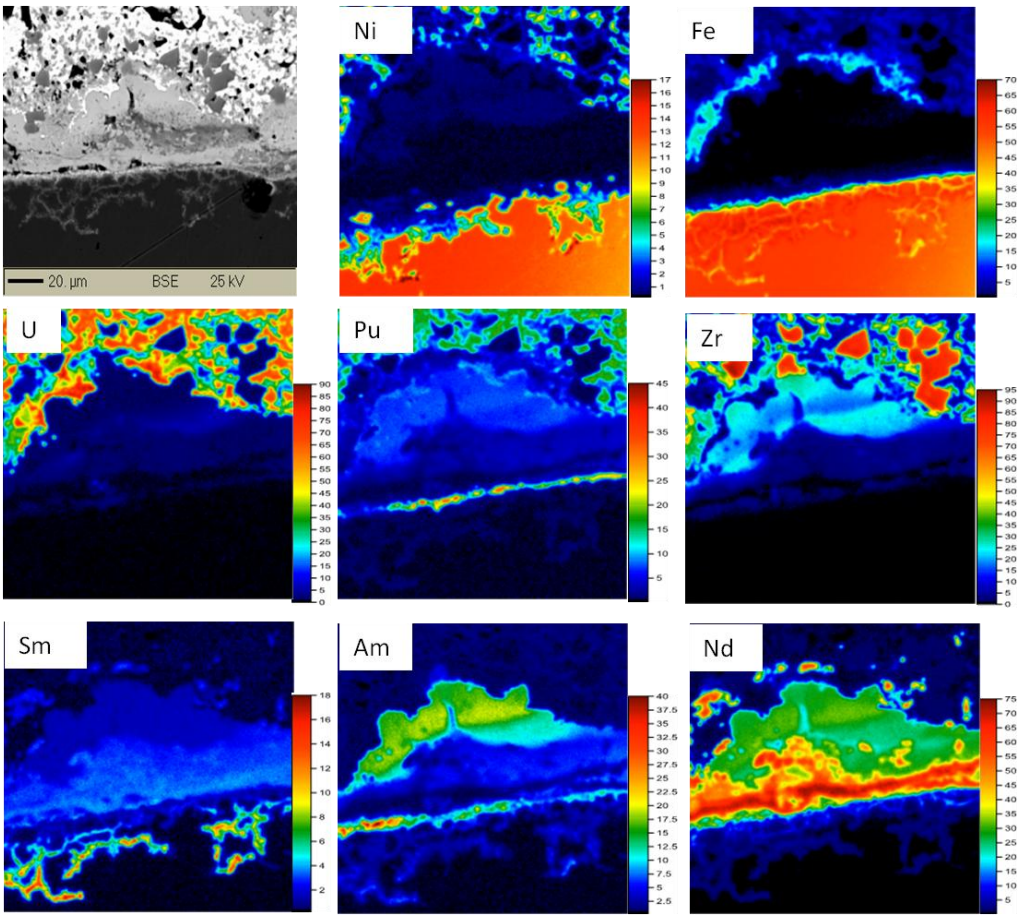

Fig. 5.43. SE image and quantitative X-ray maps of the FCCI region in a METAPHIX-2 U-19Pu-10Zr-5MA-5RE.

The penetration of Ni and Fe inside the fuel is shown fig. 5.44. It is evident that Ni penetrates further inside the fuel matrix confirming earlier observation reported in the literature for such type of cladding with high amount of Ni [27].

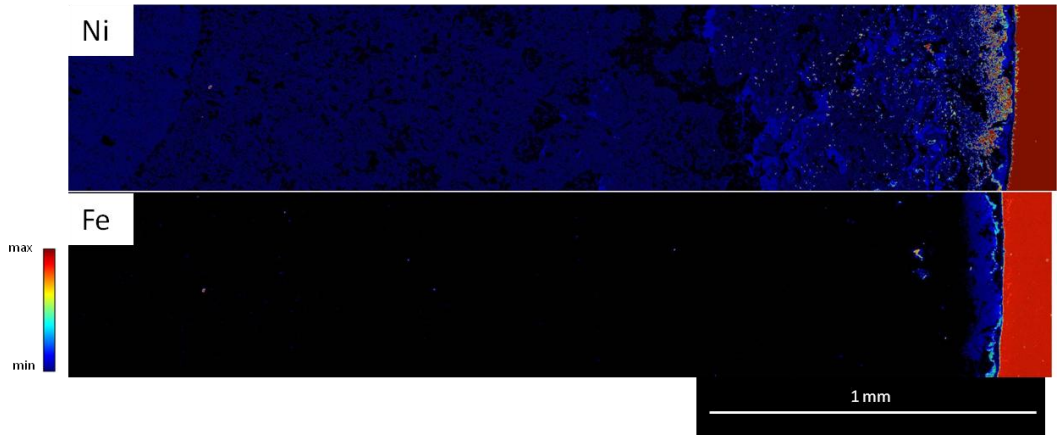

Fig. 5.44. Qualitative radial X-ray maps of Ni and Fe along the fuel radius for a METAPHIX-2 U-19Pu-10Zr-5MA-5RE sample obtained by EPMA.

5.4. Discussion

In the first part of this chapter, experimental investigations of three main aspects of the performance in pile of metallic fuel were presented: redistribution of main elements, secondary phases and FCCI. In the following, the main findings as well as the effect of the addition of RE+MA to the basic alloy fuel will be discussed and summarized.

5.4.1. Redistribution of main fuel elements

The addition of MA or RE affects only to a limited extent the redistribution of the main fuel elements. Np behaves like U and Pu whereas Am, Cm and RE are not included in the matrix and precipitate as segregated phases. This phenomenon is driven mainly by temperature and chemical gradient among the different species. No relevant differences were observed at the microstructure level: both Np bearing U-Pu-Zr and basic alloy fuel samples experienced the same temperature and 2 regions redistribution.

Np is chemically affine with Pu. At such low concentration levels, even without an available quaternary U-Pu-Zr-Np phase diagram, it can be affirmed that this element will not cause significant modification of phase transition temperatures, liquidus and solidus. However, in order to model the redistribution of fuel elements, more research is needed, to properly define the U-Pu-Zr-Np quaternary phase diagram and also to measure diffusion coefficients.

Very similar behaviour was observed by Meyer et al. [30] in a transmutation metallic fuel experiment with small quantities of Am and Np irradiated in EBR-II up to 7.6 % HM burnup and with a peak cladding temperature estimated at 813 K. Fig. 5.45 shows the restructuring of the microstructure in mainly 3 zones and fig. 5.46 presents a WDS line scan describing the redistribution of U, Zr. Pu and Np concentrations are quite constant across the radius.

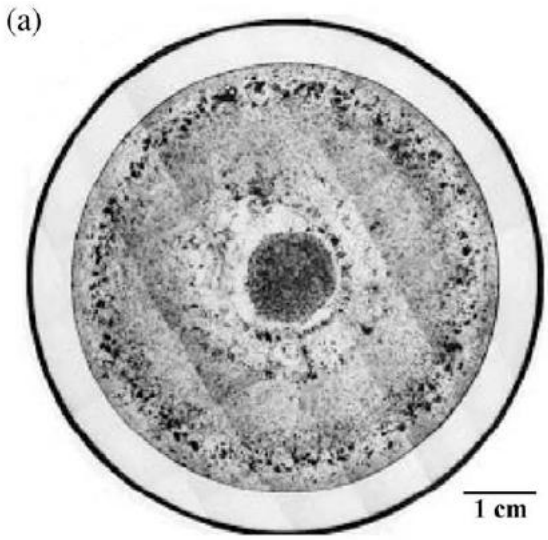

Fig. 5.45. Macrograph taken from the mid-axis of a MA bearing metallic fuel pin irradiated in EBR-II [30].

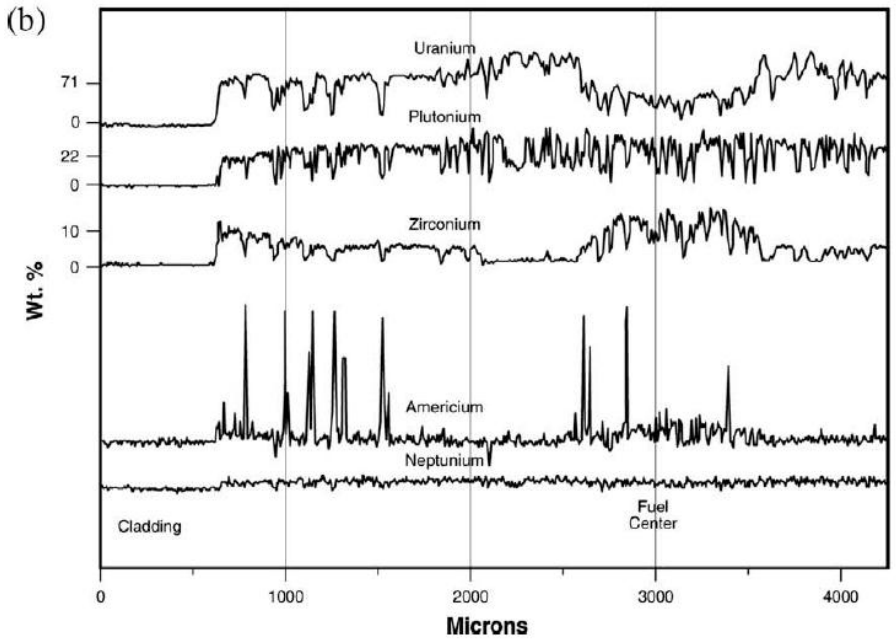

Fig. 5.46. WDS line scans from [30] showing the redistribution of the main constituents and of Np and Am.

5.4.2. Secondary phases

Am, Cm and RE are present as precipitates and secondary phases in the as-cast fuel. During irradiation they combine with noble metals and fission products, adding more complexity to this metallic fuel system.

Compared with the basic alloy, two different (RE, Am)-rich phases are present, one associated with noble metals (Pd and Rh) and one without noble metals. The precipitates that include both noble metals and RE elements have phase compositions corresponding to $RE_7(Pd,Rh)_3$, similarly to what observed in the basic alloy fuel. For the other precipitates it was not possible to infer the exact phase composition due to lack of established phase diagrams.

Furthermore, Pd and Am have a peculiar behaviour at the periphery of fuel radius where they are depleted in a 130-160 μm region before the FCCI, in contrast with the redistribution of other major RE like Nd and Ce. This observation might confirm the behaviour of Pd observed out of pile, namely its ability to immobilize other RE and prevent extensive FCCI, as shown in [20]. However, more studies are needed to better characterize Pd and RE concentration profile along the radius and to understand their interaction and solubility limits.

Ru exhibits a particular behaviour compared to other noble metals. It was possible to observe in the basic alloy that this element precipitates with Zr at centre and mid radius, whereas in the fuel sample with MA+RE Ru is mainly found dissolved in the matrix and precipitates are only visible in the FCCI region.

The differing behaviour described here is not extensively reported in literature: Hofman et al. [37] reported that for a U-19Pu-10Zr fuel sample irradiated at 17 at% burnup RE precipitates are found in 2 distinct phases, one that contains most of the Pd and the other noble metals were concentrated in blocky precipitates throughout the fuel.

5.4.3. Fuel Cladding Chemical Interaction (FCCI)

Regarding FCCI, for the "fuel side" of the interaction zone, no dramatic differences are observed that could be attributed to the presence of RE+MA. In fact, from the SEM/EDX qualitative point analysis it was possible to identity similar behaviour and common features such as Zr precipitates and a Zr-Ni phase.

On the other hand, concerning the "cladding side", OM, SEM and EPMA examinations revealed a different phase configuration at both 2.5 at.% burnup and 6.9 at.% burnup. The configuration observed for the fuel containing MA+RE was characterized by intergranular "attack"; in fact, such attack is only detected in the presence of MA, and appears independent from the presence of RE.

EPMA identified that this penetration is mainly due to Sm and Am. Nd and Ce are also present in small amounts inside the intergranular attack phase.

This behaviour, to the knowledge of the author, has been never observed and studied systematically. A KAERI report [38] just mentions different attack formation between a D9 and HT9 cladding and irradiated metallic fuel, where the attack on the HT9 showed an intergranular aspect. A more detailed discussion is found in a SEM study from Harp et al. [39] where mainly Nd is detected along the grain boundaries of HT9.

Also Hofman et al. [37] report that unlike the uniform diffusion in D9, RE in HT9 diffuse only limitedly over a uniform front, showing penetration rather more along grain boundaries.

There is no PIE data in literature that describes the behaviour of FCCI with Am and RE. The only other fuel transmutation experiment reported in literature does not report about FCCI [30]. Preliminary out of pile studies of diffusion couples seem to confirm that precipitates of lanthanides containing Am penetrate the Zr-layer and interact directly with the cladding [40].

The development of the FCCI layer depends in general on 4 factors: temperature, power, burnup and integrity of the Zr-rich layer in the periphery of the fuel sample. From the results described in this work, it is possible to draw some considerations. As expected, the wastage layer thickness is increasing with the burnup as shown in fig. 5.47. Secondly, it seems there is no correlation between the amount of MA initially present in the fuel and the thickness of the wastage layer (for both burnups studied): the values are quite spread and overlap to each other. The effect of the temperature is considered not influent in this experiment since the range considered for these samples is only 20-40°C at EOI.

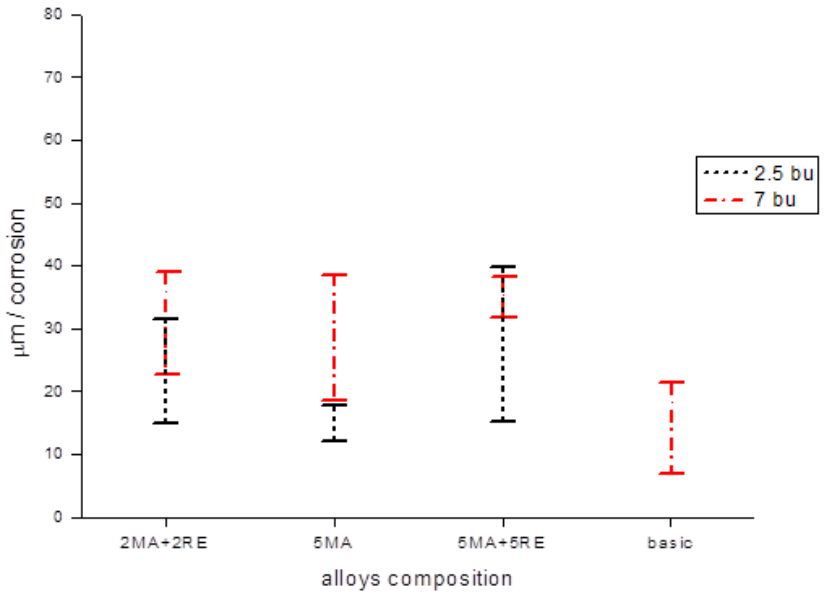

Fig. 5.47. Wastage layer thickness for the different types of metallic alloy and at different burnups.

Wastage layers experimentally measured in this work are in line with the literature. In Porter et al. [41] (fig. 5.48), for U-10Zr and D9 cladding the layer thickness is

reported to be 25-30 µm at temperature of BOI close to those for the fuel samples analysed in this work (813 – 843 K).

Finally, Keiser in [27] presented a variety of experimental results for ternary U-Pu-Zr and D9. However, only one value indicating a wastage layer of 20 µm is reported for a 6 at.% burnup and BOI temperature in the range 813-843 K, which is in line with the results in this work as well.

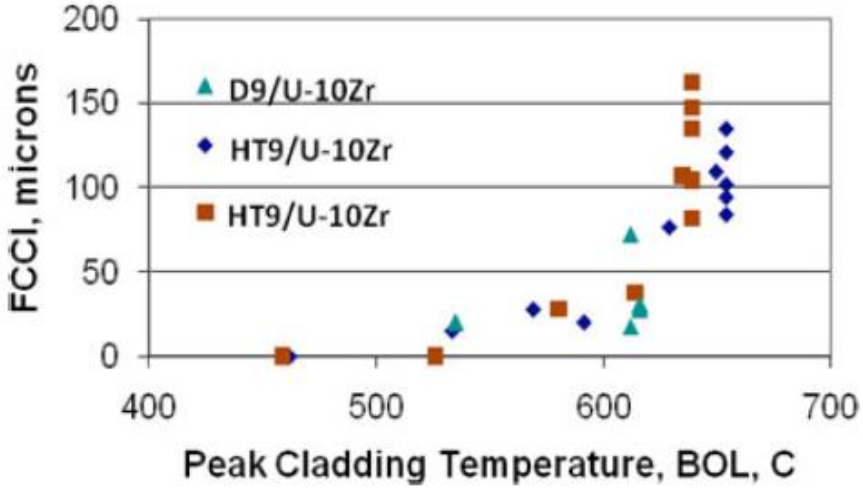

Fig. 5.48. Wastage layer collected from EBR-II U-10Zr fuel experiments with HT9 at 10 at.% burnup and with D9 at burnup ranging from 5.4 to 18.8 at.%. Temperature are calculated at BOI, taken from [41].

5.5. References

[1] G.L. Hofman and L.C. Walters, "Metallic Fast Reactor Fuels", Materials Science and Technology, A Comprehensive Treatment, R.W. Cain, P. Haasen, and E.J. Kramer, Eds., in Nuclear Materials, Vol. 10A, Part 1, B. R. T. Fros, Ed., VCH Verlagsgesellschaft (1994).

[2] T. Ogata, "Metal Fuel", in: Konings R.J.M., (ed.) Comprehensive Nuclear Materials, volume 3, pp. 1-40, (2012), Amsterdam: Elsevier.

[3] Y.S. Kim, G.L. Hofman, S.L. Hayes, Y.H. Sohn, "Constituent redistribution in U-Pu-Zr fuel during irradiation", J. Nucl. Mater, 327 (2004) 27-36.

[4] T. Ogata, Y.S. Kim and A.M. Yacout, "Metal Fuel Performance Modeling and Simulation", in: Konings R.J.M., (ed.) Comprehensive Nuclear Materials, volume 3,pp. 713-753, (2012), Amsterdam: Elsevier.

[5] J. Galloway, C. Unal, N. Carlson, D. Porter, S. Hayes, "Modeling constituent redistribution in U–Pu–Zr metallic fuel using the advanced fuel performance code BISON", J. Nuc. Des., 286 (2015), 1-17.

[6] D.L. Porter, C.E. Lahm, R.G. Pahl, "Fuel constituent redistribution during the early stages of U-Pu-Zr irradiation", Metall. Trans. A, 21A (1990), 1871.

[7] D.R. O'Boyle, A.E. Dwight, "The uranium-plutonium-zirconium system", in: Proc. Fourth Int. Conf. on Pu and Other Actinides, Santa Fe, NM, 1970, p. 720.

[8] H. Ohta, T. Ogata, D. Papaioannou, V.V. Rondinella, M. Masson, JL. Paul, "Irradiation of Minor Actinide–Bearing Uranium-Plutonium-Zirconium Alloys up to ~2.5 at. %, ~7 at. %, and ~10 at. % Burnups", Nuclear Technology, Vol. 190, pp. 36-51, 2015.

[9] S. Bremier, P. Poeml, K. Inagaki, L. Capriotti, D. Papaioannou, V.V. Rondinella, H. Ohta, T. Ogata, "Electron Microprobe Examination of Metallic Fuel for Minor Actinides Transmutation in Fast Reactor", Trans. Am. Nucl. Soc, Vol 109, (2013).

[10] S. Bremier, K. Inagaki, L. Capriotti, P. Poeml, T. Ogata, H. Ohta, V.V. Rondinella, "Electron probe microanalysis of a METAPHIX UPuZr metallic alloy fuel irradiated to 7.0 at.% burn-up", J. Nucl. Mater., 490, 109-119, 2016.

[11] M. Kurata, "Thermodynamic database on U-Pu-Zr alloy and U-Pu-Zr alloy containing minor actinides and rare earths in a temperature gradient", IOP Conf. Series: Mat. Sci. And Eng. 9 (2010), 012022.

[12] H. Ohta, D. Papaioannou, T. Ogata, T. Yokoo, T. Koyama, V. Rondinella, J.-P. Glatz, "Post-irradiation Examinations on Fast Reactor Metal Fuels Containing Minor Actinides - Fission gas release and metallography of ~2.5at.% burnup fuels", Proc. Int. Conf. on Future Nuclear Systems GLOBAL '09, Sept. 6-11, 2009, Paris, France, ANS, paper 9241.

[13] L. Capriotti, S. Bremier, K. Inagaki, P. Pöml, D. Papaioannou, H. Ohta, T. Ogata, V.V. Rondinella, "Characterization of metallic fuel for minor actinides transmutation in fast reactor", Prog. Nucl. Energ. (2016), doi:10.1016/j.pnucene.2016.04.004.

[14] Y.S. Kim, S.L. Hayes, G.L. Hofman, A.M. Yacout, "Modeling of constituent redistribution in U-Pu-Zr metallic fuel", J.Nucl. Mater, 359 (2006), 17-28.

[15] C.T. Walker, P. Knappik, M. Mogensen, "Concerning the development of grain face bubbles and fission gas release in UO2 fuel", J. Nucl. Mater 160 (1988) 10.

[16] D. Yun, A. M. Yacout, M. Stan, T. H. Bauer, A. E. Wright, "Simulation of the impact of 3-D porosity distribution in metallic U–10Zr fuels", J. Nucl. Mater., Vol. 448, (2014) 129.

[17] K. Lassmann, F. Hohlefeld, "The revised urgap model to describe the gap conductance between fuel and cladding", Nucl. Eng. Design, 103 (1987), 215.

[18] H. Okamoto, "Phase diagrams for binary alloys", ASM Inter., Materials Park, OH (1993).

[19] S. Brémier , P. Pöml , L. Capriotti , J. Himbert , V.V. Rondinella , H. Ohta and T. Ogata, "Electron microprobe examination of irradiated metallic fuel containing rare earth and minor actinide elements", Trans. Am. Nucl. Soc, Vol 117, (2017).

[20] R. D. Mariani, D.L. Porter, T.P. O´Holleran, S.L. Hayes, J.R. Kennedy, "Lanthanides in metallic nuclear fuels: Their behaviour and methods for this control", J. Nucl. Mater., 419, 263-271, 2011.

[21] Y.S. Kim, G.L. Hofman, A.M. Yacout, "Migration of minor actinides and lanthanides in fast reactor metallic fuel", J. Nucl. Mater., 392, 164-170, 2009.

[22] J. Isler, J. Zhang, R.Mariani, C. Unal, "Experimental solubility measurements of lanthanides in liquid alkalis", J. Nucl. Mater., 495 (2017), 438-441.

[23] A.W. Castleman, I.N. Tang, "Vaporization of fission products from irradiated uranium-II", J. Inorg. Nucl. Chem, 32, (1970), 1057.

[24] N.R. Chellew, C.C Honesty, R.K. Steunenberg, "Laboratory studies of Iodine behaviour in the EBR-II melt refining process", report ANL-6815 (1964).

[25] E. H. Kim, "A feasibility study of iodine behaviour during pyroprocessing of spent metallic fuel", Proc. 12th IEMPT Prague Sept. 2012.

[26] S. Frank, "Partitioning of Fission Product Iodine During the Electrochemical Treatment of Used EBR-II fuel", Proc. Int. Pyroprocessing Research Conf., 26-29 August, Lake Geneva, Wisconsin, USA, 2012.

[27] D.D. Keiser, "Fuel-Cladding Interaction Layers in Irradiated U-Zr and U-Pu-Zr Fuel Elements", ANL-NT-240, 2006.

[28] D.D. Keiser, "Metal Fuel-Cladding Interactions", in: Konings R.J.M., (ed.) Comprehensive Nuclear Materials, volume 3, pp. 423-441, (2012), Amsterdam: Elsevier.

[29] D.L. Porter, H. Tsai, "Full length U-xPu-10Zr (x = 0, 8, 19 wt.%) fast reactor fuel test in FFTF", J. Nucl. Mater 427 (2012) 46.

[30] Meyer M.K., Hayes S.L., Carmack W.J. and Tsai H., "The EBR-II X501 Minor Actinide Burning Experiment", J. Nucl. Mater., 392 (2009) 176.

[31] K. Inagaki, T. Ogata, "Reaction of lanthanides elements with Fe-Cr alloy", J. Nucl. Mater., 441 (2013) 574.

[32] K. Nakamura, T. Ogata. M. Kurata, A. Itoh, M. Akabori, "Reactions of U-Zr with Fe and Fe-Cr alloy", J. Nucl. Mater., 275, 246 (1999).

[33] D. D. Keiser Jr., M. C. Petri, "Interdiffusion behaviour of U-Pu-Zr fuel versus stainless steel couples", J. Nucl. Mater., 240, 51 (1996).

[34] P. C. Tortorici, M. A. Dayananda, "Interdiffusion of cerium in Fe-base alloys with Ni and Cr", J. Nucl. Mater., 204, 165 (1993).

[35] M. A. Dayananda, C. W. Kim, "Zero flux planes and flux reversals in Cu-Ni-Zn diffusion couples", Metall. Trans. A, 10A, 1333 (1979).

[36] M. A. Dayananda, "An analysis of concentration profiles for fluxes, diffusion depths, and zero flux planes in multicomponent diffusion", Metall. Trans. A, 14A, 1851 (1983).

[37] G. L. Hofman, L. C. Walters, T. H. Bauer, “Metallic Fast Reactor Fuels”, Progress in Nuclear Energy, 31, 83-110, 1997.

[38] Experimental Specifications of Eutectic Reaction between Metallic Fuel and HT-9, Tech. Rep. KAERI/TR-1139/98, KAERI, 1998.

[39] J. M. Harp, D. L. Porter, B. D. Miller, T. L. Trowbridge, W. J. Carmack, "Scanning electron microscopy examination of a Fast Flux Test Facility irradiated U-10Zr fuel cross section clad with HT-9", J. Nucl. Mater., 494, 227-239, 2017.

[40] Transmutation Fuels Campaign FY-09 Accomplishments Report, INL/EXT-09-16834, page 17, 2009.

[41] D. L. Porter, C. B. Hilton, “Extending sodium fast reactor driver fuel use to higher temperatures”, Nucl. Tech., 173, 219-225, 2011.

Chapter 6

Conclusion and future work

6.1 Summary of the results

The METAPHIX project is a collaboration between the Central Research Institute of Electric Power Industry (Japan) and the European Commission, Joint Research Centre Karlsruhe (Germany), with the support of CEA (France), investigating safety and performance of a closed fuel cycle option based on fast reactor metal alloy fuels containing MA. The aim of the project is to investigate the behaviour of this type of fuel under irradiation and assess its viability in terms of fuel behaviour: safety, application of all fuel cycle steps including fuel synthesis, irradiation, pyroprocessing (and eventually re-preparation for new irradiation), and transmutation effectiveness.
This research work is dedicated to understand the behaviour of this fuel system during irradiation by performing PIE which take advantage of advanced characterization techniques such as scanning electron microscopy (SEM) and electron probe micro analysis (EPMA). In parallel, a series of measurements on un-irradiated archive fuel samples was performed to complement the PIE work and the data collected at the time of fuel preparation.

The characterization of as-prepared metallic alloy U-19Pu-10Zr-2MA-2RE was performed using EPMA and XRD. The results indicate that the fuel matrix is composed mainly of U-Pu-Zr-Np and reveal two different phases where the concentration of U and Zr vary inversely. The crystalline structure was identified by XRD as a mix of U-Pu ζ and $\delta - UZr_2$. Am is found alloyed in the matrix in small

concentrations whereas the majority of Am is found in secondary phases that are present throughout the fuel and contain RE as well. No major alterations were detected after storing the as-prepared fuel samples for more than 20 years.
This characterization completes the data acquired at the time of preparation applying state of art techniques to this unique metallic system that result in more accurate measurements. The main features of this metallic alloy are in good agreement with the available literature.

The metallic fuel under irradiation is a complex system characterized by many phenomena such as redistribution of main fuel elements, formation of secondary phases and fuel chemical interaction with cladding (FCCI). Those phenomena are influenced by many factors, the most important being burnup, temperature radial profile and chemistry change along the radius. The system grows in complexity when MA and/or RE are added in the synthesis of the fuel. Very few studies have been performed on such alloys and this project is unique due to the addition of Cm and the variety of alloys irradiated (2MA-2RE, 5MA-5RE, 5MA, basic alloy).
In this work, the behaviour of metallic fuel with MA and/or RE is analyzed and compared with that of basic alloy. The redistribution of the main fuel elements is driven mainly by temperature and chemical gradient and is affected only partially by the addition of MA and RE. While Am, Cm and RE are not included in the fuel matrix and precipitate as segregated phases, Np behaves like U and Pu. There are no relevant differences in microstructure comparing Np-bearing U-Pu-Zr matrix and basic alloy.
Regarding Am, Cm and RE precipitates, during irradiation they combine with noble metals and fission products as well. Two different (RE, Am)-rich phases are present, one associated with noble metals (Pd and Rh) and one without noble metals. The precipitates that include both noble metals and rare earth elements have phase compositions corresponding to $RE_7(Pd,Rh)_3$, similarly to what observed in the basic alloy fuel. It was not possible to infer the possible phase composition of the other precipitates due to the lack of phase diagrams. It is worth mentioning that Pd and Am have a peculiar behaviour at the periphery of fuel radius where they are

depleted in a 130-160 μm thick region before the FCCI, in contrast with the redistribution of other major RE like Nd and Ce; this aspect has never been reported. Concerning the redistribution of Ru, it was possible to observe in the basic alloy that this element precipitates with Zr at fuel centre and mid radius, while in the fuel sample with MA+RE, Ru precipitates are only visible in the FCCI region. These different behaviours can be related to thermo-chemical aspects and affinity of the different elements and solubility limit in the U-Pu-Zr matrix.

Finally, concerning FCCI it can be argued that for the "fuel side" of the interaction zone no dramatic differences are identified compared with the basic alloy. On the other hand, concerning the "cladding side", PIE examinations reveal a different phase configuration on the inner cladding side at both 2.5 at.% burnup and at 7 at.% burnup. This formation is characterized by intergranular "attack", and is associated with the presence of MA, appearing independent from the presence of RE. Quantitative analysis identified that this intergranular penetration is mainly due to Sm and Am; also Nd and Ce are present in small amount inside the intergranular attack phase.

This behaviour, to the knowledge of the author, has been never observed and studied systematically and there is no PIE data in literature that describe the behaviour of FCCI with Am (Cm) and RE, as discussed in paragraph 5.4.3.

6.2 Outcome

This experimental work directly shed light on two fundamental questions and challenges regarding the behaviour of metallic fuel with addition of MA, the knowledge gap associated with it and more in general about its safety (cfr. Chapter 1, paragraph 1.1.2):

- Metal fuel properties must not be seriously degraded by the addition of the MA compared to the U-Pu-Zr system performance.

- Demonstration of an acceptable level of fuel-cladding-chemical interaction (FCCI) with fuel that includes rare earth impurities and MA fuel constituents over the lifetime of the fuel up to its burnup limit, e.g. ~20 at.%.

The old and new set of characterization data on the as-prepared metallic alloy clearly affirm that the addition of MA and RE (up to 5 wt.%) does not degrade properties such as phase transition temperatures and thermal conductivity. The microstructure of these alloys presents unique characteristics such as Am-RE precipitates and Np fully soluble in the matrix of U-Pu-Zr. As seen in Chapter 4 these features associated with the presence of MA do not change dramatically the microstructure and crystalline structure of this alloy as measured in the present work and as reported by the literature.

The characterization data obtained here are very useful to describe and understand the behaviour during irradiation. For instance, the results show that Am (and most probably also Cm) segregated in secondary phases will perform much like a rare earth element (confirming thermo-chemistry calculation) and will migrate towards the periphery of the fuel.

Regarding the performance under irradiation, the data analysed for low (2.5 at.%) and medium (7 at.%) burnup are exceptional regarding the type of alloys irradiated and they show a benign outlook in term of safety operation. The fuel pins did not fail. Non-destructive examination (e.g. gamma spectroscopy and profilometry) as well as fission gas release are in line with historical data on base alloy fuel.

The microstructure (restructuring), the thermo-chemical behaviour (redistribution) and the phase formation and evolution in the fuel are not affected by adding MA. There is a high number of secondary phases where MA and RE are present; many of them could not be identified due to lack of relevant phase diagrams in the literature. Finally, although not altering the benign assessment in terms of fuel pin safety during irradiation, Am seems to play an important role in the development of peculiar FCCI attack modes inside the cladding. This behaviour is reported in this work for the first time ever and it has to be studied in particular to understand how the cladding is affected by this attack at burnup higher than 7 at%.

6.2. Recommendation for future works

The behaviour under irradiation of metallic fuel system with MA and RE leaves open very interesting scientific questions.

Concerning the finding about the intergranular attack of the cladding by Am and Sm, TEM studies would be important to investigate the microstructure of the affected region and micro- or nano-indentation would shed light on the mechanical properties of the affected cladding.

More quantitative data (such as what can be provided by EPMA and SEM) at lower and higher burnups (METAPHIX-1 and METAPHIX-3) are definitely needed to put the findings of this work into the context of evolving properties during extended irradiation, in particular to have a comprehensive picture of FCCI evolution, redistribution, secondary phases and how they evolve with burnup.

As discussed briefly in chapter 5, very few studies have been done on volatile and semi-volatile fission products: It would be worth to consider complementing EPMA measurements with e.g. SIMS analyses able to measure elements present in very small quantities like I (Iodine).

Following the same thoughts, Knudsen cell measurements would be of paramount importance in view of potential future licensing of this fuel, for the determination of how volatile and semi-volatile species react at higher temperatures and to determine source terms for potential accident conditions.